Universidade de Aveiro
2004
Departamento de Física
Departamento de Engenharia Mecânica

Victor Fernando Santos Neto

Investigação das propriedades de filmes de diamante depositados por TMCVD

"Investigation on the film properties of advanced diamond coatings deposited using time-modulated CVD"

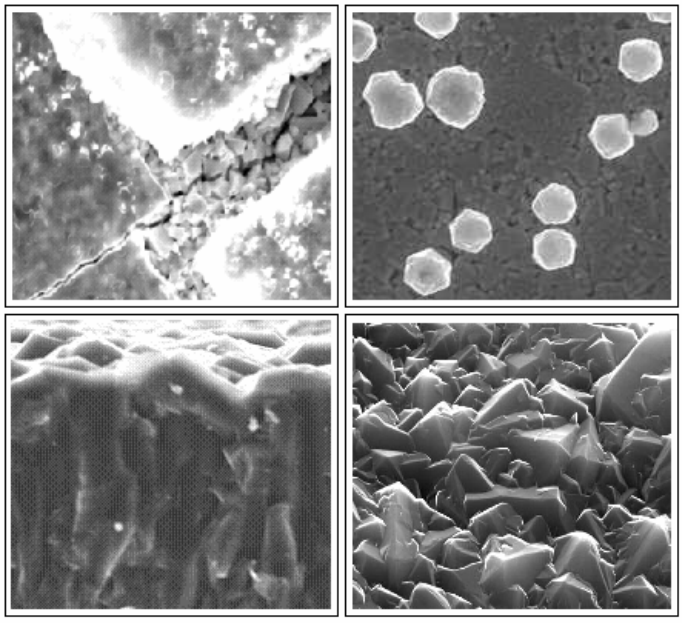

Universidade de Aveiro
2004
Departamento de Física
Departamento de Engenharia Mecânica

Victor Fernando Santos Neto

Investigação das propriedades de filmes de diamante depositados por TMCVD

"Investigation on the film properties of advanced diamond coatings deposited using time-modulated CVD"

Dissertação apresentada à Universidade de Aveiro para cumprimento dos requisitos necessários à obtenção do grau de Mestre em Física Aplicada, realizada sob a orientação científica do Doutor Luís M. Cadillon Martins Costa, Professor Auxiliar do Departamento de Física da Universidade de Aveiro e do Doutor Nasar Ali, Professor Auxiliar Convidado do Departamento de Engenharia Mecânica da Universidade de Aveiro

o júri

presidente

Prof. Dr. João Lemos Pinto
professor catedrático do Departamento de Física da Universidade de Aveiro

vogais

Prof.ª Dr.ª Maria de Fátima Guimarães Cerqueira
professora auxiliar no Departamento de Física da Universidade do Minho

Prof. Dr. Luís M. Cadillon M. Costa
professor auxiliar do Departamento de Física da Universidade de Aveiro

Prof. Dr. Nasar Ali
professor auxiliar convidado do Departamento de Engenharia Mecânica da Universidade de Aveiro

agradecimentos

Este trabalho foi efectuado sob a supervisão do Professor Doutor Luís Cadillon, do Departamento de Física e do Professor Doutor Nasar Ali, do Departamento de Engenharia Mecânica. Agradeço as suas incansáveis e valiosas orientações. Através das nossas discussões, recebi inúmeros comentários que podem ser encontrados ao longo desta tese. Neste sentido, esta tese também é deles.

Devo especial gratidão ao Professor Doutor José Grácio, por me ter motivado à iniciação dos estudos de pós-graduação.

Ao meus mais directos colegas - Gil Cabral; Yasmeen Kousar; Doutor Qi H. Fan; Doutor Tainben Huang e Doutora Elby Titus, dos quais obtive bastante apoio e encorajamento.

Ao pessoal técnico – Doutor Luís Augusto Lopes (Departamento de Cerâmica e Vidro) pelo apoio na Microscopia Electrónica, ao Doutor Jorge Soares e ao Eng.º Jorge Monteiro (Departamento de Física), pelo apoio aos estudos de Raman e caracterização eléctrica, respectivamente. À Doutora Rosário Soares (Laboratório Central de Analises) pela ajuda nas análises de Raios X, ao Eng.º Pedro Reis (Departamento de Engenharia Mecânica) pelo apoio nos estudos de rugosidade, ao pessoal da secretaria do Departamento de Engenharia Mecânica – Sr. Ventura, D. Cecília e D. Isabel pelo apoio logístico incansável e a um número de outras pessoas a quem estou profundamente agradecido pela ajuda recebida.

A todos os meus amigos da universidade mais próximos, os quais ajudaram a criar um ambiente de trabalho inspirador.

Um agradecimento especial à minha mulher, Raquel, aos meus pais e família, pelo muito apoio e encorajamento.

Finalmente, gostaria também de agradecer ao júri pelo seu tempo e paciência para rever esta tese.

Victor F. Neto

Aveiro
Março 2004

resumo

O diamante possui um conjunto de propriedades que tornam a sua aplicação na industria e no mercado de consumo, altamente apetecível.

O interesse em revestimentos de diamante disparou após o desenvolvimento da tecnologia de deposição química na fase de vapor [*Chemical Vapor Deposition (CVD)*], a qual possibilitou o revestimento de uma série de materiais diferentes. Contudo, a dificuldade de depositar diamante de elevada qualidade é tão grande como a grandeza das suas propriedades.

Os filmes de diamante depositados utilizando sistemas convencionais de CVD, onde o metano e o hidrogénio são utilizados como precursores, tende a apresentar elevadas rugosidades superficiais, devido principalmente ao crescimento colunar dos cristais e ao não crescimento homogéneo. Uma das grandes limitações de aplicação é mesmo a elevada rugosidade dos filmes, não permitindo a sua utilização maciça nos campos da micro electrónica e biomedicina, por exemplo.

Investigadores do Centro de Tecnologia Mecânica e Automação, da Universidade de Aveiro, desenvolveram um processo de deposição por modulação temporal do hidrocarboneto precursor [*Time-modulated CVD (TMCVD)*], dando origem a filmes nanocristalinos de baixa rugosidade, mais duro e de melhor qualidade.

O processo chave da tecnologia TMCVD é a modulação temporal do metano durante o crescimento do filme. No método convencional, o CH_4 é mantido a um fluxo constante ao longo do crescimento. No TMCVD, é esperado que ocorra nucleações de segunda ordem, com o aumento da concentração de metano no precursor.

É dado assim origem a um filme crescido por multicamadas, que envolve uma nucleação inicial, seguido de uma fase de crescimento e de uma nova nucleação, podendo o processo ser continuado de forma cíclica.

A caracterização dos filmes crescidos por TMCVD, pode abrir as portas para uma série de aplicações até agora barrada pelas limitações dos filmes convencionais, tais como ferramentas de cirurgia, implantes humanos, por exemplo válvulas cardíacas.

Neste trabalho, foi efectuado estudos comparativos das propriedades de filmes convencionais e modelados. As propriedades eléctricas de filmes convencionais e modelados foram também estudas. No entanto será necessário proceder a mais investigação, para uma total compreensão das consequências do novo processo de deposição proposto. Métodos de optimização foram também aplicados.

abstract

Diamond has many extreme properties that make it suitable for many industrial and consumer applications.

The interest in diamond coatings boosted ever since the realization that diamond films can be deposited onto a range of materials using a process called Chemical Vapor Deposition (CVD). However, the difficulty in depositing truly superior diamond coatings is nearly as extreme as the material's outstanding properties.

Diamond films deposited using conventional CVD systems, where methane and hydrogen are used as the precursor gases, tend to exhibit high surface roughness mainly due to the columnar growth of the non-orientated polycrystalline diamond films. One of the major limitations of the wide scale use of diamond coatings has been the high roughness of the films. As a result, this has severely hampered diamond coatings' widespread use in microelectronics, biomedical, and optical applications.

At the "Centre for Mechanical Technology and Automation", University of Aveiro, the researchers have developed a novel time-modulated CVD (TMCVD) process for producing smooth/nano-crystalline, harder and better quality diamond films.

The key distinctive feature of the TMCVD process is that it modulates methane flow during film growth. In conventional diamond CVD, the CH_4 flow is generally kept constant for the complete growth process. In TMCVD, it is expected that secondary nucleation processes occur during the high/low CH_4 pulse cycles.

This can effectively result in the formation of a diamond film involving nucleation stage, diamond growth, and secondary nucleation, and the cycle is repeated.

The successful and effective characterization of the time-modulated films can see such film coatings used in a number of new and interesting applications, such as surgical tools, human implants, e.g. heart valves.

In this work, we perform comparative studies of the properties of conventional and time-modulated films. Electrical properties are also investigated in conventional and modulated films, although further research is needed to fully understand the consequences of the new proposed deposition process. Optimization methods are also performed.

preface

Após estas primeira páginas em português, por obrigação protocolar, o trabalho será apresentado em inglês, por forma a humildemente, servir de apoio a uma comunidade cientifica mais alargada. Obrigado pela compreensão.

Diamond's extreme properties make it a potential material for a variety of important applications, which increased significantly ever since the realization that diamond films can be deposited onto a range of materials using a process called Chemical Vapor Deposition (CVD).

Each of the potential uses require that diamond properties are optimized, such as: hardness, surface smoothness, electrical conductivity, etc. This optimization can only be achieved by operating on the microstructure, because one obviously cannot change diamond's molecular structure or its composition.

It was with this in mind, that researchers at the Centre for Mechanical Technology and Automation (TEMA) proposed a new process to control the microstructure of diamond polycrystalline coatings. This new process consists of modulating hydrocarbon precursor flow throughout the deposition process (*Time-Modulated CVD – TMCVD*), promoting the occurrence of secondary nucleation. This deposition process leads to the microstructure modifications, leading to the alteration of some of the film properties.

The principal aims of the current project are: understand the behavior of the physical properties of time-modulated diamond coatings in comparison with conventional diamond films; and establish a relationship between changes in film properties with different CH_4 pulse duty cycles.

The introductory chapter (*Chapter I*) reports the theoretical aspects of CVD diamond technology.

An important chapter is the description of the preliminary work done to test the TMCVD technological process (*Chapter II*). In this chapter, the potentials of TMCVD and time-modulated films are reported.

Chapter III, describes the *state-of-the-art* relating to the mechanical and electrical properties on conventional diamond CVD.

Chapter IV presents the characterization techniques used to investigate the films properties, conventional and modulated. The main techniques used were: scanning electronic microscopy to investigate the films morphology and structure; surface profilometery to investigate the surface smoothness; Raman spectroscopy to evaluate the films quality in terms of sp^3/sp^2 contents; hardness test; electrical conductivity and other electric properties; and some other complementary analyses such as X-ray diffraction to complement information.

Chapter V is the prime chapter of this dissertation. The chapter reports the optimization of the hot-filament CVD system. The second and fundamental step is to attempt to optimize the modulation process and to understand the growth mechanism that governs the process. Special focus has been on comparing the properties of conventional and time-modulated films. During this investigation, it was established that the deposition temperature in TMCVD was a crucial factor in the new modulated process. Electrical properties are also investigated in conventional and modulated films, although further research is needed to fully understand the consequences of the new proposed deposition process. Finally, some not fully developed applications of the newly developed coating process have been outlined. The surface engineering of small dental tools and heart valves components have been considered.

Further work is required in order to understand fully the mechanisms involved during diamond TMCVD process.

This thesis has been written in a clear and transparent style, coherent with the new trends in scientific report writing. The author hopes this has been achieved, however, if the objective has not been met then please accept sincerely my apologies.

Victor F. Neto

Aveiro
March 2004

TABLE OF CONTENTS

FIGURES LIST

TABLES LIST

List of symbols

Abbreviations

AC	Alternating Current
AES	Auger Electron Spectroscopy
CVD	Chemical Vapor Deposition
DC	Direct Current
DLC	Diamond Like Carbon
EDS	Energy Dispersive X-Ray Spectroscopy
FSND	Free-Standing Nanodiamond
FWHM	Full Width at Half-Maximum
HFCVD	Hot Filament CVD
HPHT	High Pressure High Temperature
HVD	Artificial Heart Valve Disks
LTIC	Low-Temperature Isotropic Carbon
MWCVD	Microwave Plasma CVD
PVD	Physical Vapor Deposition
PyC	pyrolytic-carbon
Ra	Surface roughness coefficient
RFCVD	Radio Frequency CVD
sccm	Standard Cubic Centimeters per Minute (flow unit)
SEM	Scanning Electron Microscopy
TMCVD	Time Modulated CVD
XRD	X-Ray Diffraction
WDS	Wavelength Dispersive Spectroscopy

Chemical Compounds

Al	Aluminum
Ar	Argon
CH_4	Methane
CH_3	Methyl
CN	Carbon Nitride
Co	Cobalt
Cr	Chromium
H	Atomic hydrogen
H_2	Hydrogen
O_2	Oxygen
Ta	Tantalum
TBOT	Titania Butoxide
Ti	Titanium
TiC	Titanium Carbide
TiN	Titanium Nitride
TiO	Titanium Oxide
V	Vanadium
WC-Co	Tungsten Carbide – Cobalt (*hard metal*)

Roman letters

A	Area
C	Capacity
E	Electric field
E	Energy
F	Applied force
F	Helmholtz free energy
g	Gravity acceleration
h	Thickness
H	Magnetic field
HV	Vickers hardness
I	Intensity
N	Number of Particles
P	Pressure
P_c	Crystal pressure
P_v	Vapor pressure
Q	Quality
Q_c	Capacitor charge
r	Radius

R	Resistance	U	Electrical potential
T	Temperature	Y	Young modulus
V	Volume		

Greek letters

α_p	Molecule polarization	σ_d	Charge density
σ_s	Stress	λ	Thermal conductivity
α_g	Growth parameter	μ_e	Dipolar momentum
∂	Partial derivate symbol	ν	Poisson ratio
ε	Permittivity	μ	Chemical potential
σ_t	Surface tension of a crystal	ω	Angular frequency
σ	Conductivity		

Unit conversions

Pressure	1 Torr = 133.3224 Pascal 1 Torr = 1.333224 milibar
Flow	1 sccm = 1 milliliter/minute
Temperature	0ºC (degrees Celsius) = 273.15 K (Kelvin)
Energy	1 eV = 1.6022 x 10^{-19}J 1 cm^{-1} ≈ 8 meV

CHAPTER I

INTRODUCTION

"Diamonds are forever…"

1. The mineral

The mere mention of the word “DIAMOND” fills the mind with a panoply of concepts and images. Diamond is a mineral and a natural crystalline substance, which appears from the transformation of carbon when placed in high-temperature and high-pressure environment. It is something superb, the peerless "king of gems" that glitters, dazzles, and symbolizes purity and strength. Diamond is indomitable, the hardest surface known to mankind.

On nature, the geologic conditions to achieve those conditions are not that rare. The penetration of the oceanic crust on the terrestrial mantel, which results in the continental drift, is one of the forms. As the oceanic crust enters the subduction zone, it will take with her sedimentary rocks, rich in carbon (limestone’s, per example). With dept, the temperature and pressure will rise, transforming carbon to graphite in a first stage and to diamond in a second stage. Volcano phenomena are responsible for the transportation to the earth surface afterwards.

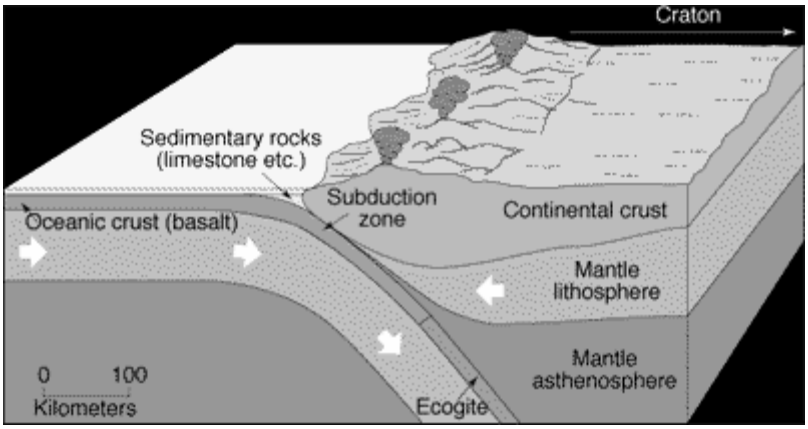

Figure 1 - Dynamic of earth’s crust that levees to the formation of mineral diamond [1]

The tectonic plates drift is also responsible for the production of diamond. The continental collisions involve large amounts of energy, providing the necessary energy for the creation of diamond crystals. This phenomenon was observed in Kazakhstan.

The impact of extraterrestrial objects of considerable mass with Earth, also leads to the release of great amounts of energy, being another way of production of diamond crystals.

Sometimes, meteors transport with them diamond crystals that created from the impacts with other celestial bodies. Traces of nanocrystals of diamond, older than the solar system were already found, being the result, probably of the explosion of red giants, supplying radiation to methane clouds.

The conditions that lead to the transformation of carbon into diamond, creates in fact an atomic structure of carbon with one of the highest packing factors.

The word “diamond” results from a Greek adjective “adamas”, used to describe a very hard substance. In fact, diamond is the hardest known mineral, being the top of the Mohs scale.

Table 1 - Bulk diamond properties [2]

Property	Value	Unit
Hardness	10 $x10^3$	kg/mm^2
Stress	>1.2	GPa
Compression	>110	GPa
Sound velocity	18 $x10^3$	m/s
Density	3.52	g/cm^3
Young Modulus	1.22$x10^3$	GPa
Poisson Coefficient	0.2	Dimensionless
Thermal expansion coefficient	11$x10^{-7}$	/K
Thermal Conductivity	20.0	W/cm-K
Thermal shock parameter	30x106	W/m
Debye temperature	2 200	K
Optical refraction Index @ 591 nm	2.41	Dimensionless
Optical Transmissibility (from nm to IR)	225	Dimensionless
Lost tangent @ 40 Hz	6 $x10^{-4}$	Dimensionless
Dielectric constant	5.7	Dimensionless
Dielectric Force	10$x10^6$	V/cm
Electronic mobility	2 200	cm^2/V-s
Vacancy mobility	1 600	cm^2/V-s
Electronic saturation velocity	27$x10^6$	cm/s
Vacancy saturation velocity	10$x10^6$	cm/s
Work function	Small and negative	On surface {111}
Energy gap	5.45	eV
Resistivity	10^{13} - 10^{16}	Ohm-cm

2. Industrial usage

The exceptional combination of mechanical, thermal, chemical and optical properties of diamond make this material an ideal choice for numerous applications in which materials are required to operate in severe environments exposed to abrasion or chemical attack, or in situations requiring the dissipation of extreme levels of power. Diamond, as a single crystal, is widely used as a gem stone and in jewelry.

The price and the need to obtain crystals adaptable to several application fields (tribology, electronic, optical, etc.) give rise to an effort to reproduce nature in a laboratory environment.

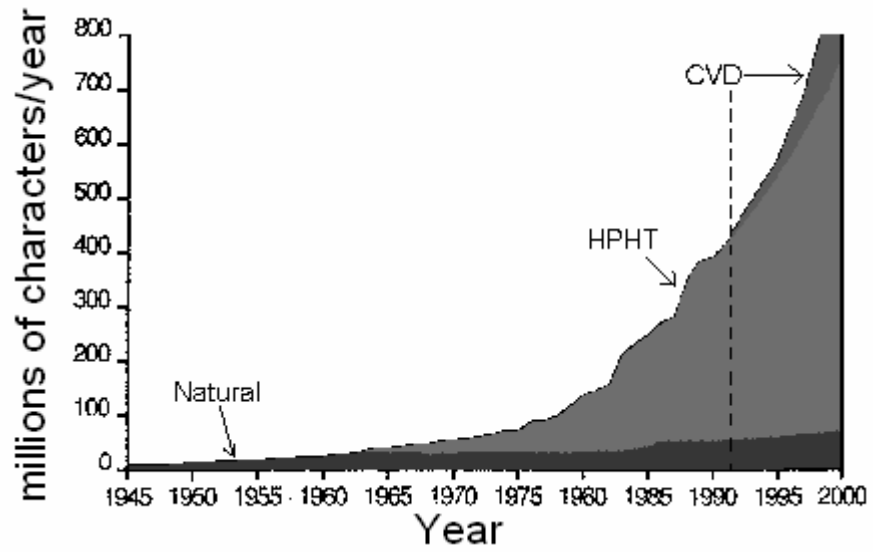

Figure 2 - Industrial usage of diamond [2]

The first successful way used to obtain synthetic diamond was reproducing what nature does – high pressure and high temperature (HPHT), and it was done by General Electric Company (GEC), in 1959, using pressures in the range of 50 to 100 kbar and temperatures from 1800 to 2300 K. This development lead to an exponential increase in diamond industrial usage.

Although, the industry that HPHT diamond supplied was almost strictly cutting and wear tools, one can see in figure 2 that the consumption of this artificial type of diamond developed exponentially, since its initial years.

In the 1970-80's, Chemical Vapor Deposition of polycrystalline diamond films came to light, leading to a reasonable growth rate of crystals, from a precursor mixture of methane in a hydrogen rich atmosphere. CVD diamond has very similar properties to the ones of natural diamond and can be used in several fields of materials engineering, namely electronics, optics, mechanics and tribology.

Almost everyday, new applications for CVD diamond films appear. Diamond coated cantilevers as an alternative for metal coated ones, to improve stability, for example in Scanning Capacitance Microscopy [3], output windows for thermonuclear reactors [4], radiation detectors in hot and/or high radiation dose environments [5]. Cutting tools for civil engineering applications [6] and for hard material machining [7].

Diamond has also potential biomedical applications, and fulfils the main requisites for use in human implants: biocompatibility and chemical stability. Carbon is one of the main components of the human body, and diamond is chemically stable in both basic and acid environments. The extreme hardness and low friction coefficient of diamond are also desirable properties of diamond when considered to be used in hip prosthesis. In this regard, there has been several attempts to apply CVD diamond in ceramics teeth implants [8], hip-joint prosthesis domes [9], dental burs [10], artificial hearth valves [11].

3. CVD of diamond film

Thermodynamically, crystal growth process is a matter of chemical potential equilibrium between two systems: the environment in the reactor chamber and the crystallites.

Chemical potential governs the flow of particles between the systems, just as the temperature governs the flow energy. If two systems have different chemical potential particles will flow from the system at the higher chemical potential to the system at lower chemical potential. As an example, this is what happens with batteries – electrons flow from one terminal to the other, in spite of the potential difference.

Chemical potential, μ, is a function of the system temperature, T, volume, V, and number of particles, N, and is defined as:

$$\mu(T,V,N) \equiv (\partial F/\partial N)_{T,V} \quad (1)$$

where F is the Helmholtz free energy [12,13].

Applying the chemical potential concept [14], with the Laplace equation:

$$P_c - P_v = 2\sigma_t/r \quad (2)$$

where σ_t is the surface tension of the crystal and r is the body radius (considering a crystal with a shape similar to a droplet) and the product $2\sigma_t/r$ is know as the Laplace pressure, and with the Thomson-Gibbs equation:

$$\mu_v - \mu_c = 2\sigma_t V_c/r \quad (3)$$

we can say that volume, V_c, is gained when transferring n atoms or molecules from the supersaturated ambient phase (vapour), with higher chemical potential, μ_v, to the crystal phase with lower bulk chemical potential, μ_c:

$$(P_c - P_v)\, V_c = n\, (\mu_v - \mu_c) \quad (4)$$

where P_v is the vapour pressure and P_c is the crystal pressure.

The crystal shape is due to the equilibrium of a small crystal with its ambient phase, that leads to the formation of a particular shape which is the most favorable from a thermodynamic point of view, this is, when the work to form such crystal is at a minimum [14].

The surface requires a work equal to $\sigma_t.S$, where S is the crystal surface, to create a new phase-dividing surface.

The volume part depends on the crystal volume or the atoms transferred. At a constant volume, the surface part depends only on the crystal shape, tending for a minimum of surface energy or an equilibrium shape. Then the conditions for a minimum Gibbs free energy, change with the crystal formation at a constant volume.

If instead a crystal, we have a liquid droplet, the equilibrium shape would be evidently a sphere. In the case of a crystal, equilibrium shape is not that simple, due to the

different crystallographic orientations and different specific surface energies. This means that the surface energy depends on the crystallographic orientation and in that sense it is anisotropic.

Although, as Gibbs first noticed, the formation of a new phase requires, as a necessary prerequisite, the appearance of small clusters of building units (atoms or molecules) in the volume of the supersaturated ambient phase.

In any thermodynamic system, even stable ones, local deviations from the normal state (fluctuations) should have place, which are less probable in the sense that they increase the thermodynamic potential of the system. If we consider a homogeneous molecular system, there are always small fluctuations of the density in the sense of small molecular aggregates, which are well compatible with the given state of aggregation. Such density fluctuations can be called “homophase” fluctuations. On the other hand, there might be the so-called “heterophase” fluctuations that could lead to visible transition to another state of aggregation. Their concentration should increase considerably near the phase equilibrium, determined by the equality of chemical potentials. If the initial bulk phase is the stable one, these density fluctuations are “lifeless” in the way that they grow to negligible sizes and decay without revealing a tendency to unlimited growth. If, however, the initial phase is unstable, the tendency to growth prevails after exceeding a certain critical size.

It is just these density fluctuations or clusters that are called the critical nuclei of the new phase. In order to form such clusters, some free energy should be expected. In other words, the system should overcome an activation barrier whose height is given by the work of formation of the critical nuclei.

Coming back to synthesized diamond, the first experiments at low pressure conditions dates back to the 50’s, but it’s not until the 70’s that the deposition in metastable conditions turns to be economically viable, with the work of Deryagin e Fedoseev (in 1976), Spitsyn et al. (in 1981), Fedoseev et al. (in 1984), DeVries (in 1987), Angus (in 1989) among others [2]. They finally achieved a reasonable growth rate, many time larger than the 0.01 μm/hour reported by Spitsyn and Deryagin from the Physics and Chemistry Institute of Moscow, in 1956 and by Eversole from the Union Carbide Corporation (USA), in 1962.

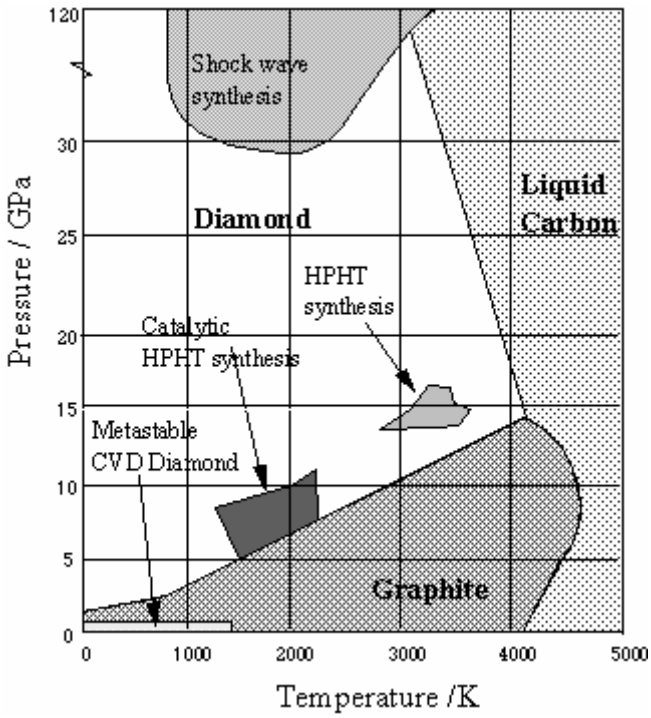

Figure 3 - Carbon phase diagram [15]

Although the mechanism of crystal nucleation and growth presented is valid, if we attend in figure 3, it would be expected that graphite, instead of diamond, should be deposited at this pressure and temperature conditions.

Growth of diamond from vapor phase, in non-diamond substrates, at reasonable growth rates, was achieved mainly due to the development of CVD thermal or plasma assisted methods, in which small amounts of hydrocarbon is introduced (normally methane) in excess hydrogen atmosphere.

Thermal or plasma energy was the key factor to promote the fluctuations of the density to achieve small aggregates and to promote the thermodynamic environment to lead to crystal growth.

But the superequilibrium concentration of atomic hydrogen also has a positive effect on diamond growth [16]. It is accepted that the growth of diamond crystals at these conditions, from gas phase, is not because just of one simple step process, but due to several stages and phenomenon's [17,18]:

1 – Activation of the gas mixture
2 – Transport of the active gas to the substrate
3 – sp^2 and sp^3 simultaneous deposition
4 – Dissolution of the deposited sp^2 carbon in the gas phase (etching) or its conversion to sp^3

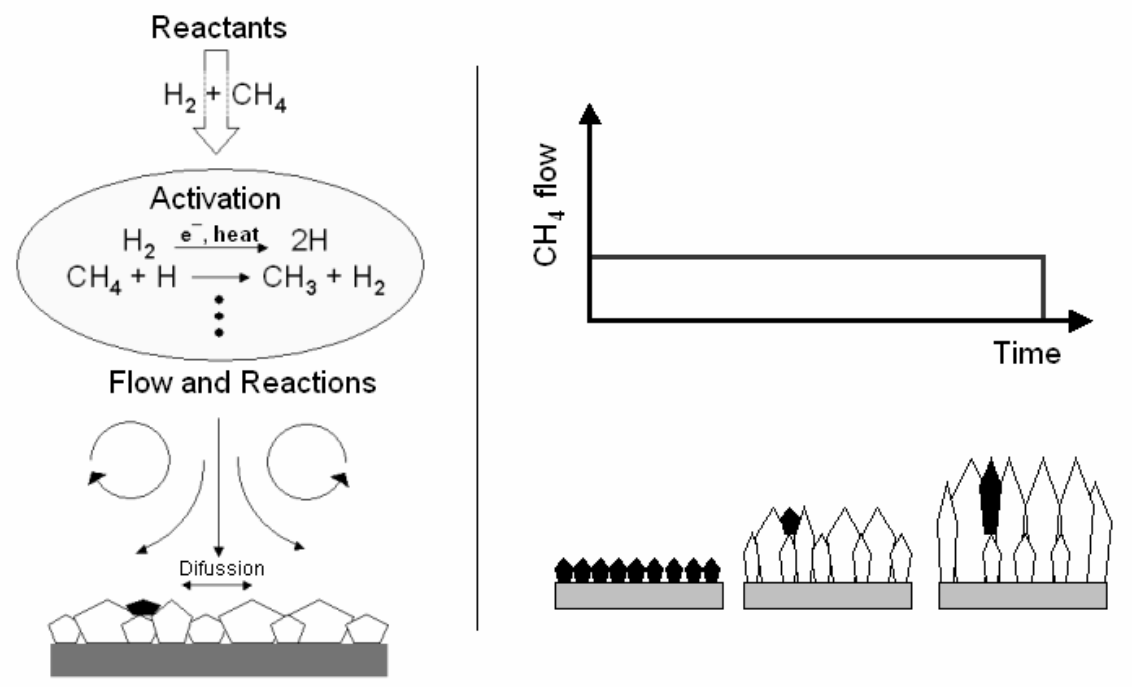

Figure 4 - Reactions inside the CVD chamber

With time, the crystals (often referred to as grains or crystallites) will grow normally in a columnar growth mode (figure 4).

Let's consider the growth of a {111} site represented in figure 5. In this site there is only one available connection in tetrahedral carbon to connect to a C_xH_y gas specimen. Figure 5(a) shows a surface of 6 hydrogen atoms surrounding a radical. A similar picture is presented in (b), but one of the hydrogen atoms is missing, giving place to a new radical. In (c) and (d) CH_2 and CH_3 radicals replace the hydrogen atoms. Figure 5(e) shows the adjoining methyl radicals. Finally, (f) illustrates a possible formation in a {111} surface.

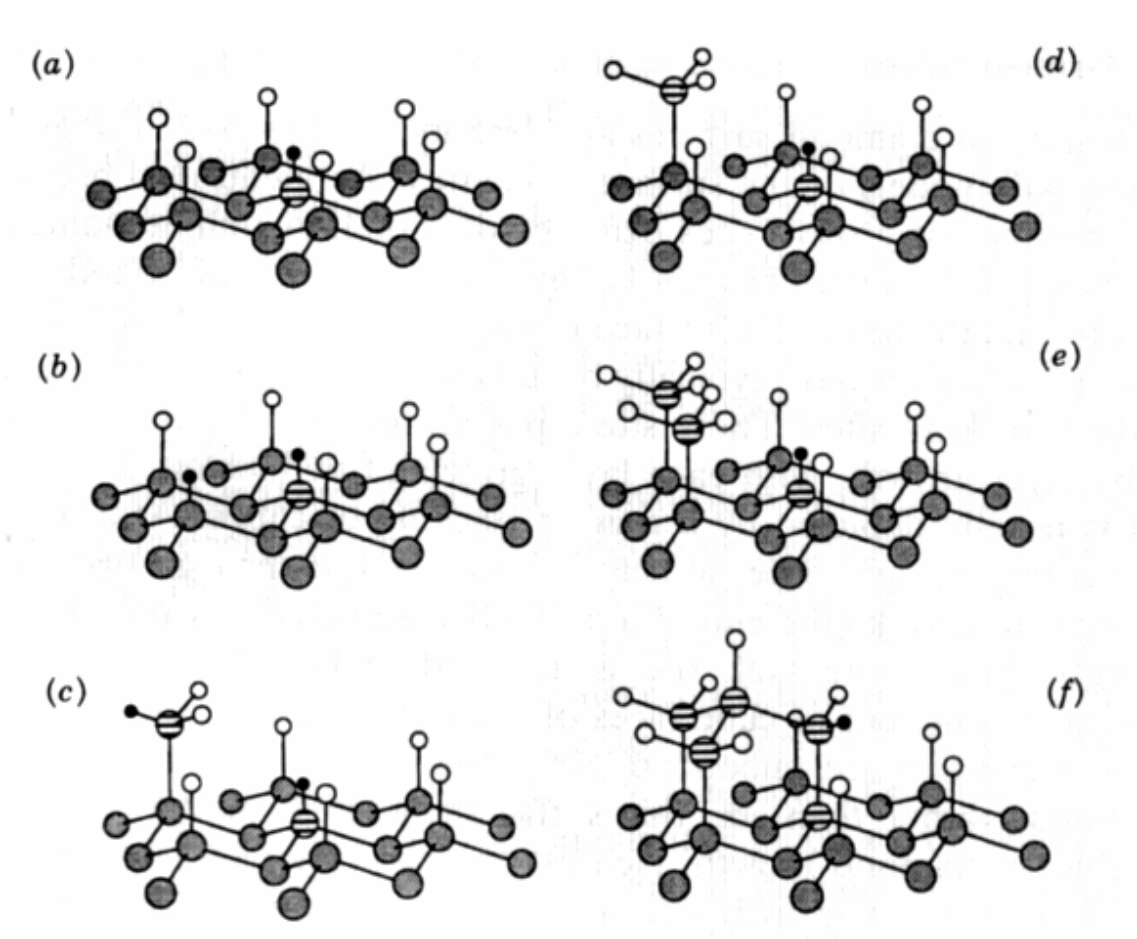

Figure 5 - Illustration of the {111} grow site. Big dark and hatched circles represent carbon atoms; small white circles represent hydrogen; and small dark circles represent radicals [2]

In order to understand why different crystal shapes can be achieved when deposition conditions are altered, it is important to note that the crystal growth can be understood as a result of the competition between differently oriented grains [19].

The model of evolutionary selection of specific crystallite orientations, as described by Van der Drift, is based on two assumptions: (i) the absence of secondary nucleation; (ii) and a crystallite morphology which is independent of the crystallite orientation. The latter condition is fulfilled for large surface diffusion, which ensures that growth on particular surfaces does not depend on the orientation of the surface relative to the incoming flux of growth species. Since the shape of isolated crystals at the beginning of the film growth process usually does not depend on the crystal orientation, the assumption of a large surface diffusion is very reasonable.

The basic parameter, which determines the film texture, is the direction of fastest growth. The growth of a polycrystalline diamond film starts from distinct nucleation sites. As individual randomly oriented nuclei grow larger, their diameters equal the average distance between the nucleation sites and they begin to form a continuous film. The subsequent film growth is dominated by competitive growth between differently oriented grains. With increasing film thickness, more and more grains are

overgrown and buried by adjacent grains. Only those crystals with the direction of fastest growth perpendicular to the surface will survive. The result is a pronounced fiber texture where the fiber axis equals the direction of fastest growth and the degree of texturing increases with increasing film thickness.

For isolated untwinned crystals the direction of fastest growth is parallel to the largest diameter of the crystallite. The relative growth rates on {100} and {111} faces determine the crystal shape. This can be expressed by a growth parameter:

$$\alpha_g = 3^{1/2} V_{100} / V_{111} \quad (5)$$

where V_{100} and V_{111} are the growth rates on the {100} and {111} faces respectively. The dependence of the crystal shape is shown in figure 6. For $\alpha_g \leq 1$, idiomorphous crystals grow in the form of cubes, for $1 < \alpha_g < 3$ in the form of cubo-octahedra and for $\alpha_g \geq 3$ in the form of octahedra. The arrows shown in figure 6, indicate the direction of the largest diameter of the crystals. When α is varied from 1 to 3, the largest diameter and therefore the direction of fastest growth varies from {111} over {110} to {100}.

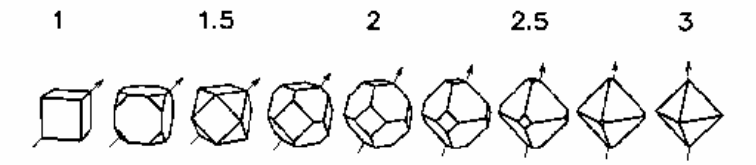

Figure 6 - Idiomorphic crystal shapes for different values of the growth parameter, α_g. The arrows indicate the largest diameter, i.e. the direction of fastest growth [19]

4. Deposition Methods

There are numerous ways to deposit diamond films onto a range of substrate. However, the most successful and widely used technique is CVD.

Cataloging the systems by energy source, we can divide reactors in thermal systems (hot filament, electron beam or laser), plasma assisted (DC and RF plasma or microwave plasma) and even combustion flame CVD systems.

Discussing other methods of diamond deposition, such as PVD methods, is beyond the scope of this thesis. However, in this thesis the traditional HFCVD and MPCVD systems used for diamond CVD will be described.

4.1 Hot Filament CVD

The hot filament assisted CVD system was first proposed by Matsumoto et al. in 1982 [2,20]. In this method, diamond particles are deposited on a heated holder, from a mixture of methane and hydrogen, activated by the heat of the incandescent filament, placed near the sample to be coated.

The substrate temperature is normally in the range of 600 to 900ºC. This can be a disadvantage if low melting materials are to be used, like Teflon as substrates. The filament temperature must be about 2000 to 2500ºC to achieve the gas activation, and

the pressure inside the deposition chamber must be around 10 to 100 Torr. Normal CH_4/H_2 rates, to deposit good quality diamond, are 1 to 2 %, considering a hydrogen flow of 100 to 400 sccm [2,23].

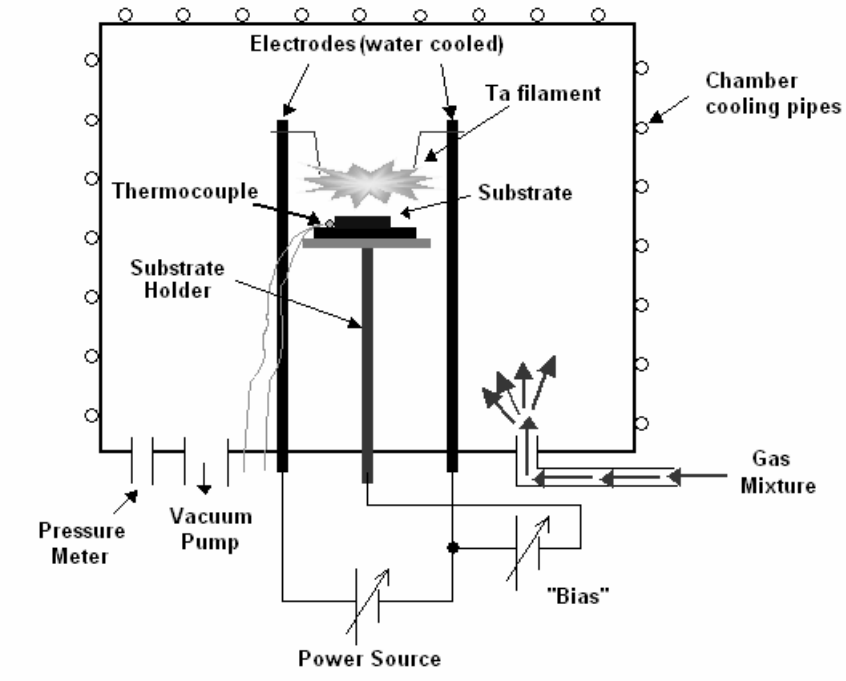

Figure 7 - HFCVD system description

The deposition area in these types of systems can go from a small 5x5 mm^2 sample, to industrial applications with 1 m^2, depending on the arrangement of the filament and system configuration [20].

Generally, the filament material displays weaker stability and frequently metal contamination of the coating occurs [21]. However, prior to diamond CVD, the filament can be pre-carburized in a CH_4 rich environment for up to 30 minutes.

The growth rates obtainable from this technique is also a disadvantage when compared with other deposition systems. The typical grow rate for HFCVD is 1 μm/hour, although there are reports of growing rates of around 10 μm/hour, using organic compounds with high methyl concentration, such as acetone, ethanol, methanol [20] or even through graphite etching [22]. There is also some work done with the assistance of a bias source, mainly to increase the nucleation density in the beginning of the deposition process.

The great advantage of this process is the prize of such equipment, representing a much reduced investment than most of other methods. A second advantage is the ability of scaling up this type of equipment, to industrial usage.

4.2 Microwave Plasma CVD

Microwave plasma assisted CVD is a widely used system for growing diamond films. In this system the source of energy for gas activation comes from a microwave magnetron generator, normally with a frequency of 2.45 GHz.

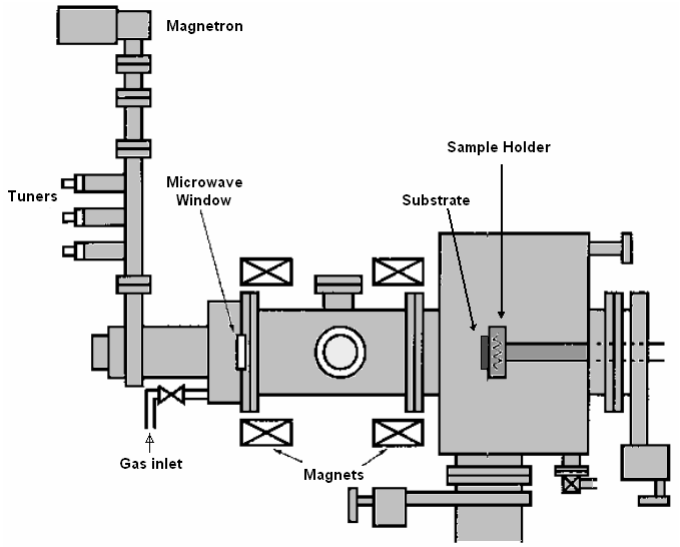

Figure 8 - Microwave CVD system

Microwave CVD gives good film uniformity, quality, homogeneity and process stability.

The growth rate of this kind of systems are in the rage of 1 to 10 μm. The substrate temperature is approx. the same as in other equipments, ranging from 600 to 1100 ºC. Inside chamber pressure is also in the range of 10 to 100 Torr and gas rates 1 to 2%, but the total gas flow is normally larger than in HFCVD, for example, ranging from 100 to 1000 sccm [2,23].

MPCVD systems can coat areas in the region of 30 cm^2.

But the principal disadvantage of a MWCVD system is its prize, mainly due to the complexity of the magnetron and of the waveguides.

CHAPTER II

TIME-MODULATED CVD DIAMOND PROCESS

In many surface engineering deposition techniques, modulation of deposition parameters is commonly used to promote special characteristic or properties.

Some applications of CVD diamond could be improved if one could control, for instance, grain size, surface roughness or internal stress.

It is known that the longer the deposition time is the thicker the film and the bigger the grain size is, promoting a higher roughness, as seen in figure 9 and figure 10.

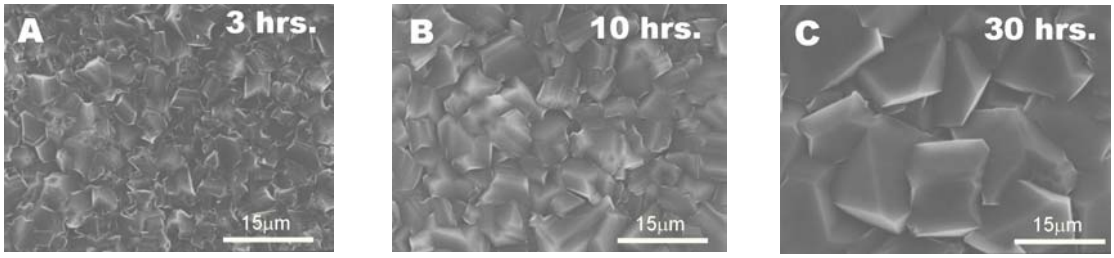

Figure 9 - SEM pictures of three different samples deposited for 3, 10 and 30 hours

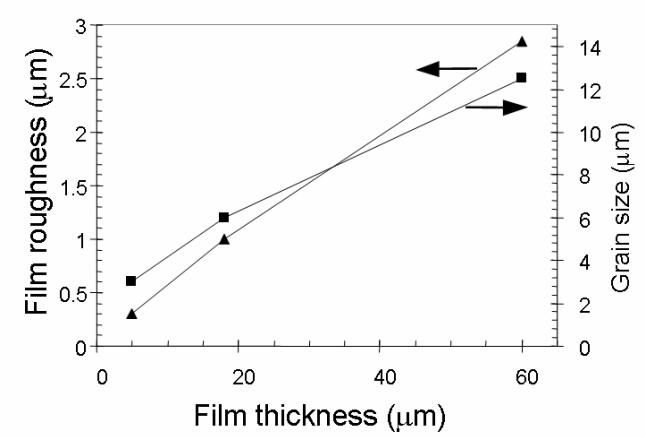

Figure 10 - Film roughness and grain size dependence of the film thickness

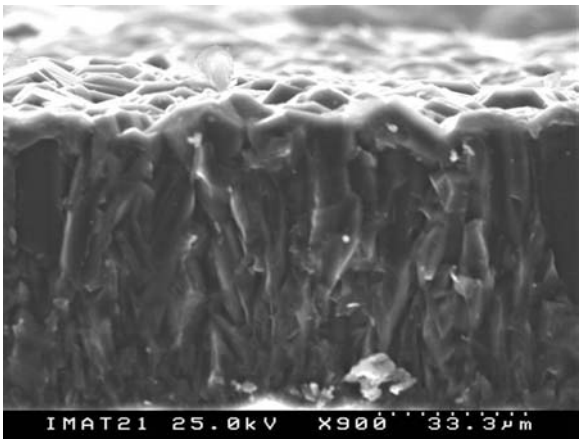

Figure 11 - Cross-section SEM picture

Due to the columnar growth mode of the crystals, as shown in figure 11, the thicker the film is the bigger the internal stress is, promoting film cracks or other deformation.

In the other hand, as it can be seen in the Raman spectra in figure 12, as the deposition time increases (from a to c) the diamond peak scatters more efficiently. This is due to the better defined diamond crystals and to the lack of impurities, etched by the atomic hydrogen.

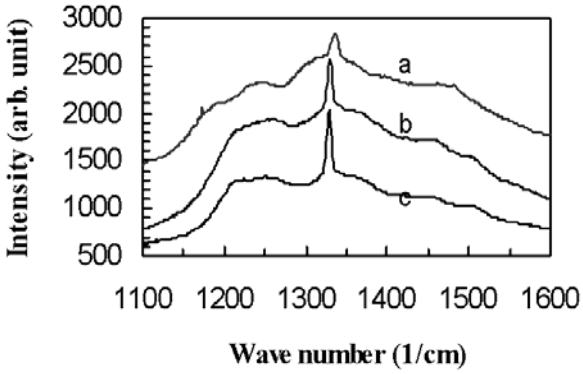

Figure 12 - Raman evolution with deposition time

The films properties can not truly be controlled, having in mind many possible applications, such as in biomechanical require prefect homogeneous film, normally with very low roughness.

One possible way to pass this contrariety could be by the deposition of multi-layer type diamond film structure. For that, one should be able to promote secondary nucleation during the film growth, in order mainly to decrease radically the film roughness, without sacrificing film quality.

In figure 13(a), it is seen that the higher the concentration of methane, the higher the nucleation density of diamond crystallites.

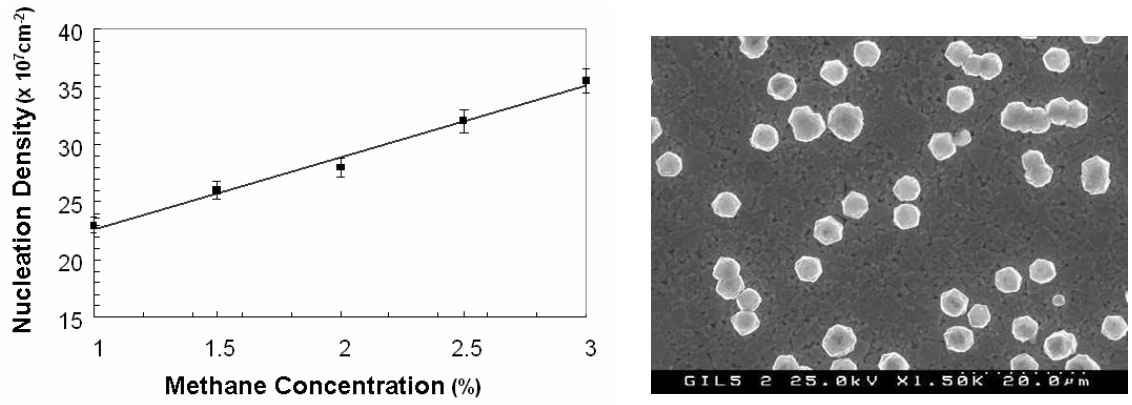

(a) (b)

Figure 13 - (a) Nucleation density vs Methane Concentration, (b) SEM of nucleation stage

But a deposition at a high methane concentration promotes bigger incorporation of amorphous and graphite components in the film, and reduces drastically the diamond quality, as observed in figure 14. As reported in the previous chapter, low concentration of hydrocarbon gas, releases a bigger amount of atomic hydrogen to etch impurities (mainly graphite-like).

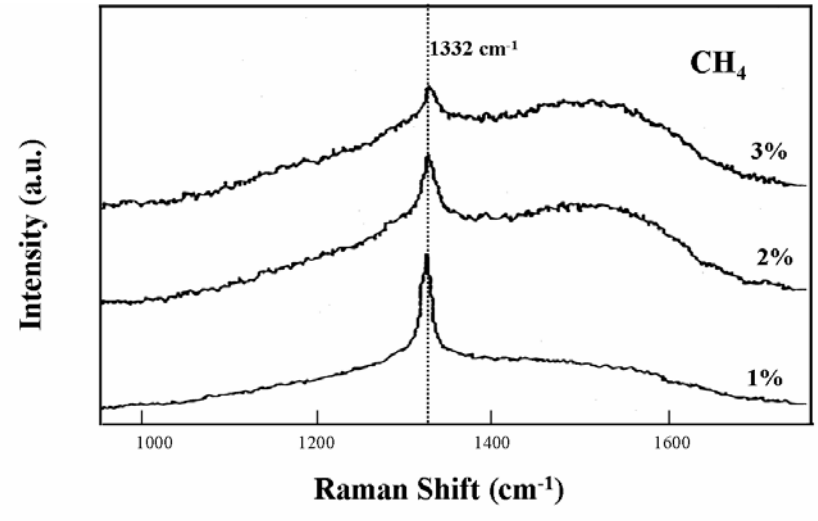

Figure 14 - Raman spectrum for different CH_4 concentrations

It can be deduced that the nucleation stage should be carried out at high methane concentration and the growth stage should be conducted under low methane concentration.

Theoretically, the solution should be the conjugation of this to attributes, as presented in figure 15.

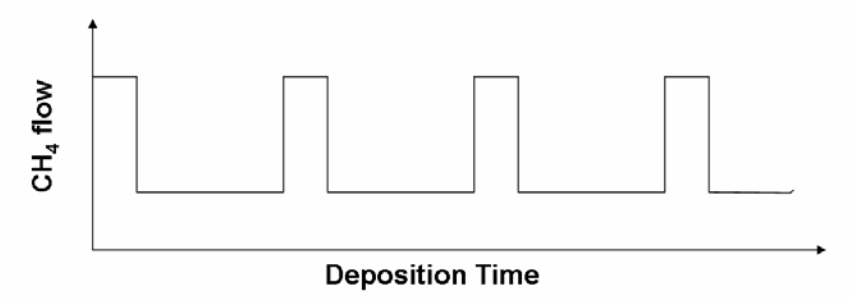

Figure 15 - Methane time modulation

In other words, it consists on pulsing the hydrocarbon gas, at different flow rates for varying time durations into the vacuum reactor during the CVD process, promoting 2.º , 3.º, … nucleation processes.

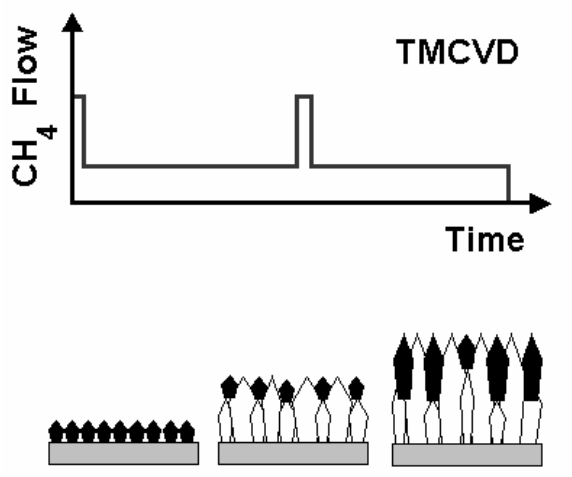

Figure 16 - Proposed TMCVD mechanism

An interesting calculation to do, in respect to the time-modulation process, is to determine the residence time of the gas particle in the reaction chamber, i.e. the time that the system need to renew the gas inside it.

Let's consider that the total volume of the chamber is approximately 5 liters. Now let's also consider that the gas flow to the system at 150 sccm, and that the deposition pressure is of 30 Torr (typically).

By Boyle law, we know that the volume (V) of a given mass of gas, at constant temperature is inversely proportional to its pressure (P), i.e. PV = constant. Although this is true only for an ideal gas, we can hypothesize that the gas mixture in the CVD chamber – due to the low pressure - behaves like an ideal gas.

So,

$$V_1 P_1 = V_2 P_2 \tag{6}$$

where V_1 and P_1 are the volume per minute and pressure of the gas entering the system as measured by mass low controller (i.e. cm^3/min at standard conditions, that

means at 1 atm) and V_2 and P_2 are the volume per unit time (cm^3/min or mL/min) and pressure of the gas mixture inside the system.

$$V_2 = \frac{150 \times 760}{30} = 3000\text{mL/min} = 3.0\text{L/min} \quad (7)$$

Knowing that the system volume is ~ 5 liters, the gas residence time, t, will be given by:

$$\text{t} = \frac{V_T}{V_2} = \frac{5.0}{3.0} = 1.67\,\text{min} = 100\,\text{sec} \quad (8)$$

This calculation means that 100 sec is the minimum modulation time to have effect in the deposition process.

Preliminary results presented by Q.H. Fan [24] and N. Ali [25], showed that this theoretical model can be experimentally applied, by the deposition of thin polycrystalline diamond films, using both conventional CVD and TMCVD processes, as shown in figure 17.

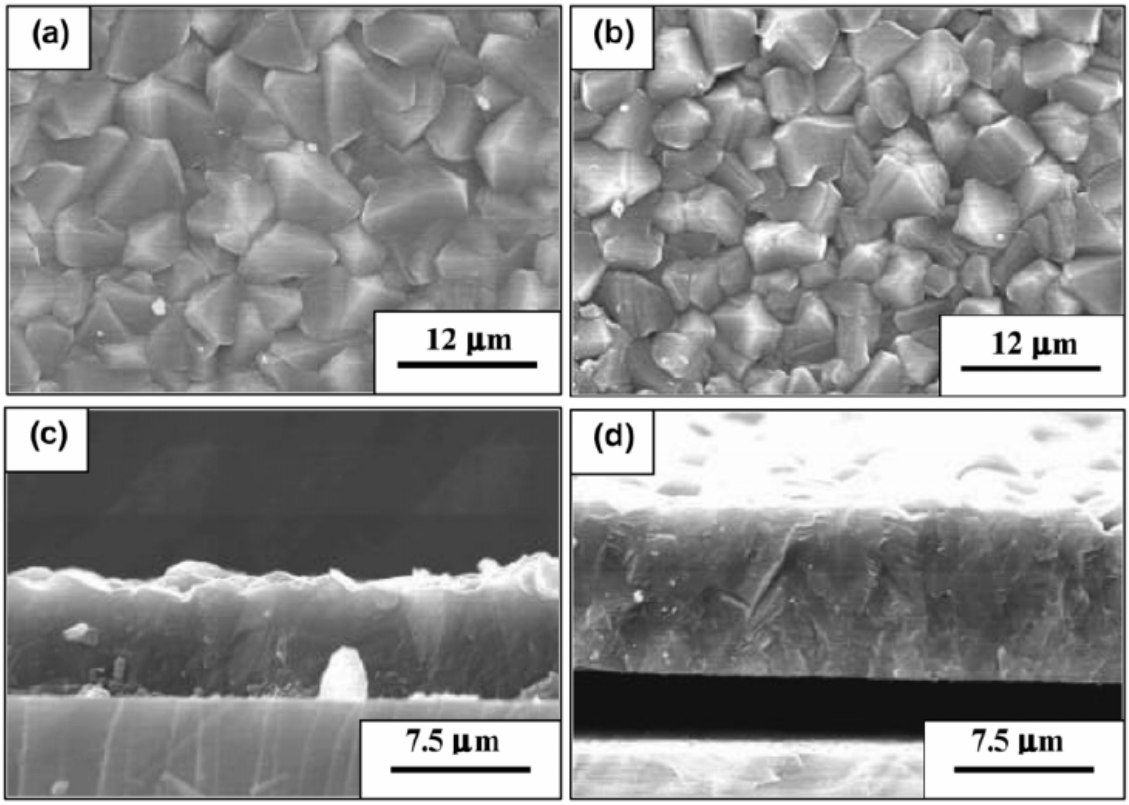

Figure 17 - SEM images of as-grown film surfaces (a, b) and their profiles (c, d).The films were grown using conventional CVD (a, c) and TMCVD (b, d)

Films grown using conventional CVD produced films which displayed columnar growth. It was found that diamond crystallite size increased with film thickness. Furthermore, the coating surface roughness increased with film thickness. Higher methane concentrations increased the nucleation density. However, the quality of the as-grown films decreased during growth under increased methane concentrations.

The TMCVD process promotes secondary nucleation to occur on the existing grains as a result of pulsing methane at different concentrations. Films grown using the TMCVD method were smoother and were grown at higher growth rates than those grown via conventional CVD.

One of the objectives of this thesis is to continue working on the TMCVD process, in order to control more accurately the film microstructure and surface roughness and to investigate further the possible changes in the physical properties of the deposited films grown using this novel method.

CHAPTER III

CVD DIAMOND PROPERTIES

Natural and synthetic single crystal diamond properties have been studied for a long time and are well reported in the literature [2,16,17,26,27].

Polycrystalline CVD diamond films are relatively new. So much is under investigation and still needs to be done. The properties of single crystal diamond (natural or synthetic) depend on the crystal orientation, and the defects and impurities incorporated in the crystal. The properties of polycrystalline materials are not only dependent in the orientation, form, structure, impurities and defects of the individual crystals but also on the material at/or between the individual crystal boundaries.

Morphology, is defined as the internal and external form and structure of a diamond material and is a consequence of the basic diamond cubic crystal structure and the process and parameters that created it.

The morphology of diamond materials is especially important because first, so many mechanical, physical and chemical properties of diamond single crystals are strongly depends on it; and second, once the diamond material is created, it is difficult to significantly modify its structure, defects or impurities by practical processes.

Polycrystalline diamond films consist of many small crystals grown together to form a film, as reported in previous sections. The crystallites may be of various degrees of perfection, size and shape as determined by growth conditions. They may have random orientations or they can be more or less aligned with respect to each other and the substrate. The boundaries between the crystals are imperfect because of misalignment of adjacent grains and because they may contain impurities or high concentration of crystal defects or non-diamond carbon. Although the grain boundaries are usually mechanically strong, they are discontinuities in the structure and will affect bulk properties, especially those which depend on the crystal perfection such as thermal conductivity and carrier lifetime in electronic devices. They also affect chemical, mechanical, and other physical properties.

Oxidation rates for polycrystalline diamond films are dependent on the crystallite faces exposed, so generally they are much higher than for single crystal films [28]. Grain boundaries present less perfect material and can include non-diamond carbon. Etch rates for polycrystalline films may be 100 times the rate for single crystal {100} faces, especially if the films consist of small highly defective crystals i.e. microcrystalline diamond films. A polycrystalline {100} textured film with well developed relatively large columnar crystals can resist oxidation of individual crystallites but fall apart due to rapid oxidation of the grain boundaries between the individual crystals. This example clearly demonstrates the significance of the less perfect diamond at grain boundaries.

1. Thermal Properties

Thermal conductivity is very sensitive to the crystal structure. Figure 18 shows that growth conditions change film structure and can produce very large changes in thermal conductivity. The more perfect film – those with a higher intensity 1332 cm^{-1} Raman spectroscopy lines, offer much better thermal conductivity.

Figure 18 also display typical thermal conductivity for diamond type IIb, type I, gold (Ag) and copper (Cu).

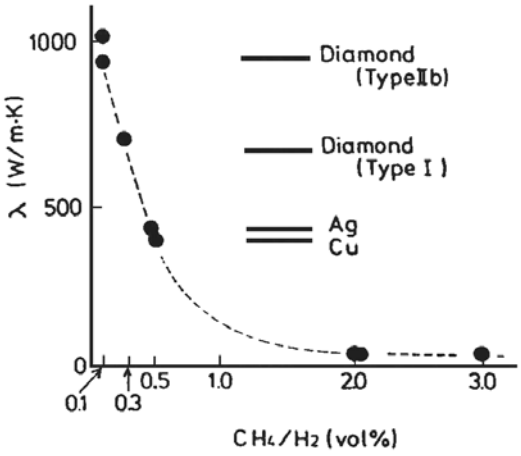

Figure 18 - Thermal conductivity variation with different methane concentration [28]

2. Mechanical Properties

Most of mechanical properties investigations in polycrystalline diamond date from the 90's.

The elastic modulus and hardness can also be decreased by the presence of grain boundaries and highly defective diamond crystal structure, with fracture toughness may increase.

N. Savvides and T. J. Bell [29], measured the hardness, H, and Young's modulus, Y, of a polycrystalline diamond film from force-displacement curves obtained using an ultra low load micro hardness instrument. The response of the diamond film shows nearly complete elastic behavior, and showed that its hardness (80–100GPa) and modulus (500–533GPa) are comparable with those of natural {001} diamond (H=56–102GPa; Y=1050GPa).

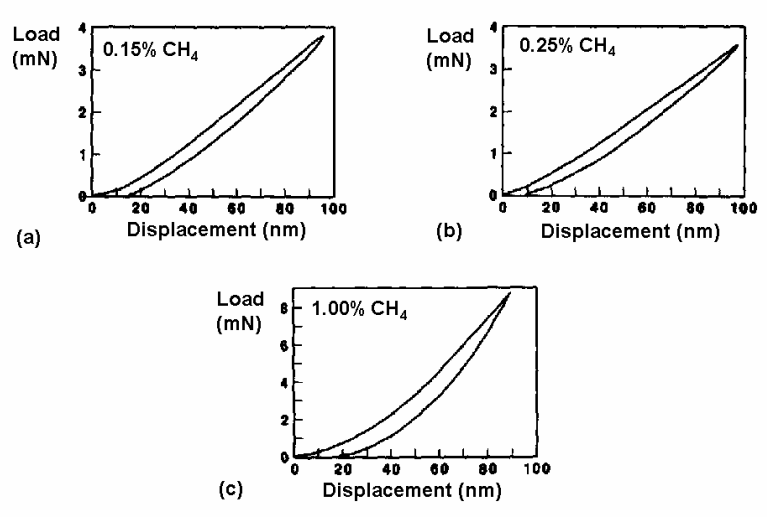

Figure 19 – Load-displacement curves for three different CH_4 concentrations [30]

C. V. Cooper and C. P. Beetz, Jr. [30], investigated diamond films, ranging in thickness from 5 to 20 μm, grown on Si {100} and polycrystalline Si_3N_4 substrates using hot-filament chemical vapor deposition. The concentration of methane in flowing hydrogen was varied over the range 0.15—1.0 vol.% at a constant flow rate of 100 sccm. They also used ultra low-load indentation equipment on polished diamond surfaces, establishing an inverse relation between hardness and methane concentration, with hardnesses ranging from 110 to 180 GPa. They also reported evidence of the outstanding quality of the film deposited using the most dilute mixture of methane in hydrogen, by offering an indentation load—deflection curve that exhibits substantially reduced hysteresis, indicating essentially elastic deformation.

F. Szuecs et al [31], studied the dependence of the Young's modulus with film thickness and temperature. As it can be observed from figure 20, there is no significant dependence of the film thickness.

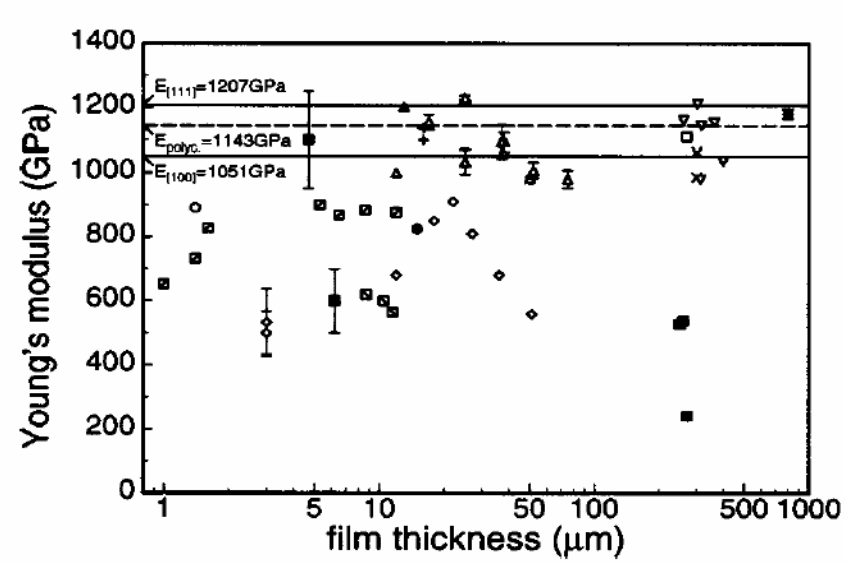

Figure 20 - Experimentally obtained Young's modulus of several polycrystalline CVD diamond films as a function of film thickness [31]

In what matters the temperature dependence, the Young's modulus decreases linearly with increasing temperature. The temperature coefficient in the range -150 to 700 °C is -1.027×10^{-4} K^{-1}. At higher temperatures an irreversible decline in Young's modulus can be observed under air, which can be explained by material loss due to oxidation.

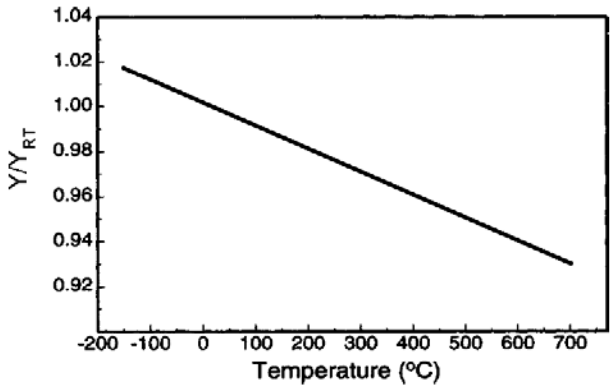

Figure 21 - Relative Young modulus fluctuation with temperature [31]

Mark A. Prelas et al. [28] presented a compilation of several works done between 1989 and 1994, where it could be found hardness of diamond film coating ranging from 31 to 111 GPa. Nowadays it is reported hardness values of 180 GPa. In addition the report presented Young's Modulus with values from 250 to 1079 GPa, a Poisson's Ratio from 0.07 to 0.29, Bulk Modulus from 380 to 500 GPa and a density of 3.5 g/cm^3.

Table 2 - Mechanical parameters of CVD diamond and natural diamond [2,26,28,31]

	CVD Diamond	Natural Diamond
Hardness (GPa)	31 – 180	~ 100
Young's Modulus (GPa)	250 – 1079	~ 1200
Poisson's Ratio	0.07 – 0.29	0.2
Density (g/cm^3)	3.5	3.52

3. Electrical Properties

The potential application of diamond, due to its properties, in electronic devices is enormous, but the concretization of that potential is very discrete.

Natural diamond posses a combination of properties, that result in the best Johnson and Keves merit figure. Johnson and Keves merit figure was developed to compare electric properties with thermal properties, so we can evaluate its power transport capability.

As already mentioned, morphology, crystal size, crystal orientation, film quality, surface roughness and coating adhesion, are critical in determining the suitability of the coating being used for a particular application, namely in electronic devices. It is reported that structural defects, non-diamond phases (film quality), grain boundary network and film thickness [32-35], influence the electronic properties.

Careful control of the deposition parameters, produces diamond films that exhibit different morphologies, preferred orientations and consequently with different electrical properties. The conductivity of oriented polycrystalline films is normally lower than that of non-oriented [36], as a consequence of the large number of grain boundaries accompanied by non-diamond phases in the non textured films. A. Ibarra et al. [37] observed that the dielectric properties are dominated by the same mechanism in a wide frequency range, and that the temperature dependence is very small. Electrical properties is also influenced by the presence of hydrogen in the film, due to the hydrogen rich atmosphere in the grown stage. Annealed and non-annealed samples display different characteristics [38,39].

The recent advances in CVD technique make it possible, to some extent, to obtain polycrystalline films with desired orientation of the crystallites, thus making it possible to control the electrical properties with good reproducibility.

The resistivity of a conventional non-doped CVD diamond film is around 10^6 Ω.cm, a much lower value than the 10^{13} to 10^{16} Ω.cm presented by natural diamond. This phenomenon may occur due to the defects passivation by hydrogen. If the material is submitted to a thermal treatment, resistivity rises, if the material is submitted to a hydrogen plasma (atomic hydrogen) resistivity decreases.

Nitrogen and boron are the only doping elements that affect significantly electric conductivity of diamond, either natural or synthetic. The resistance also depends on the doping concentration, as can be seen in figure 22.

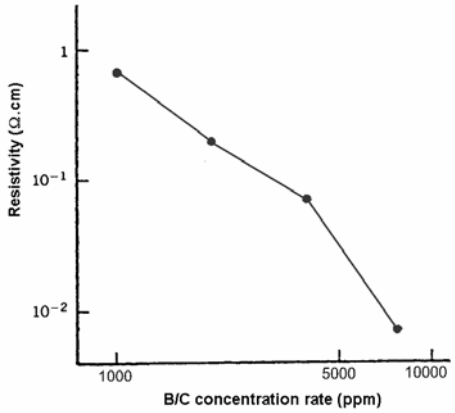

Figure 22 - Resistivity as a function of Boron concentration [2]

The charge mobility in CVD polycrystalline diamonds is similar to natural diamond type IIa (natural diamonds with a very low concentration of nitrogen).

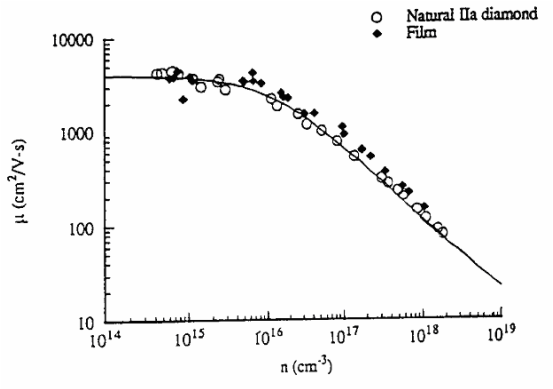

Figure 23 - Mobility as a function of transporters [2,28]

It can be seen that after an initial platform, figure 23, the mobility decreases significantly with the increase of the number of transporters. This is due to the electrons –holes scattering.

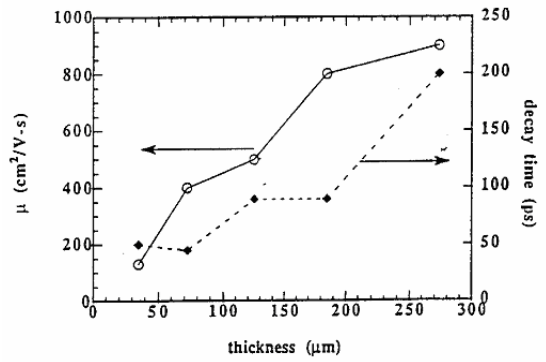

Figure 24 – Mobility and decay time as a result of different film thickness [2,28]

The proportional dependency of the charge mobility and the decay time with the film thickness can also be observed. Thicker films present coarser grains, so the boundary volume will be inferior.

An important issue in electronic application is the electric contacts with the material. Metal-semiconductor contacts can be classified as ohmic or Schottky contacts, depending on the work function (needed energy to remove one electron from Fermi level to vacuum) of the metal and the semiconductor.

Ohmic contacts present an interfacial discrete resistance/impedance. Schottky are rectifier contacts, this is, electrons are blocked when passing from the contact material to the semiconductor material, the conduction is only allowed from the semiconductor to the contact. This is the case when contacts are made of aluminum, gold or silver [18].

Electric contacts cannot be transposed, when studying an electronic device. So what maters is the ensemble properties and not the isolated properties of the material.

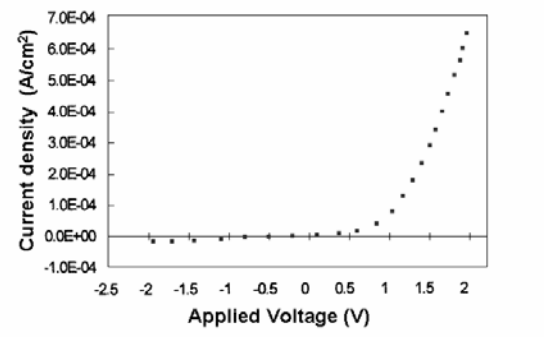

Figure 25 - Current density as function of applied voltage in a polycrystalline diamond with a Schottky contact [18]

From figure 25, we can observe the expected behavior of a Schottky contact device. For negative voltage, electric current is residually negative. For positive voltage, the device is ohmic, presenting a resistance of ~10kΩ, for the exposed example.

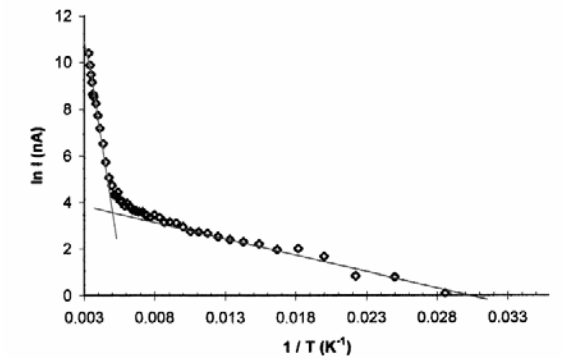

Figure 26 - Electric Current as a function of temperature (Arrenhius Plot) [18]

Figure 26 shows the Neper logarithm of electric current as a function of the inverse temperature – the so called Arrenhius Plot. In this figure one can observe two different types of dependency. At low temperatures, it's the "Nearest Neighbor Hopping" that dominates the electric conductivity. At high temperatures, it's the ionization processes that dominate.

If we apply an AC signal, the materials response will be obviously different. Nath et al. [32] stated that the electrical transport in undoped CVD diamond films, occurs predominantly on grain boundaries. They observed that the conductivity becomes nearly independent of temperature at the high frequency end. In the low temperature limit the conductivity followed a power law dependence with frequency, with a slightly increasing exponent of 0.88 (figure 27). They interpret the frequency dependent conductivity in polycrystalline diamond films as a single conductivity mechanism.

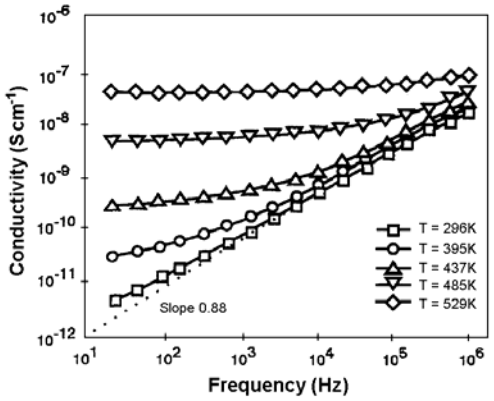

Figure 27 - Frequency and temperature dependence of conductivity [32]

The contrasting explanation of thermal emission of carriers from traps is deduced by other authors, from a small bump in the frequency dependent curves of their diamond films. This bump may be possibly related to the diamond-silicon interface of their samples [40].

Although, considering the different structures of the samples and measurement temperatures used, it is difficult to select one explanation over the other. Nath et al. [32] also reports the variation in quality of CVD diamond prepared by different methods and conditions effects the electrical properties.

Ibarra et al. [37] measured the dielectric properties of CVD diamond in a wide frequency (more than 10 orders of magnitude) and temperature range and reported that the results indicate that dielectric properties are dominated by the same mechanism over the whole frequency range, and that the temperature dependencies are very small.

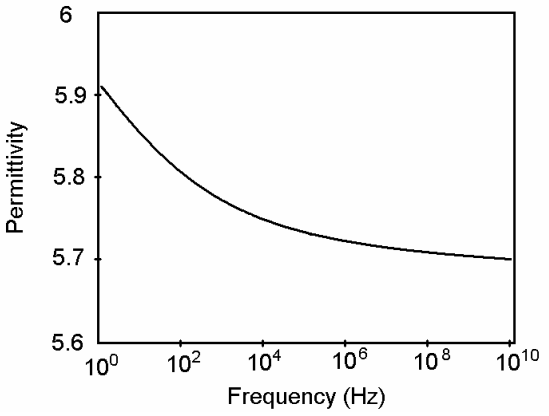

Figure 28 - Room temperature frequency dependence of permittivity for CVD diamond [37]

CHAPTER IV

CHARACTERIZATION TECHNIQUES

The characterization of thin film coatings is extremely important in trying to assess the range of properties of the film coating. Nowadays, an abundance of different types of characterization techniques are available to seek such properties, even some time different techniques can be used to study the same parameter. Nevertheless, one must comprehend the individual characteristics and limitations of each technique.

In this chapter, we will introduce some of the common characterization techniques, used in the evaluation of diamond CVD films, namely scanning electronic microscopy (SEM), surface roughness, Raman spectroscopy, film micro-hardness and dielectric properties determination by LCR equipment.

1. Scanning Electronic Microscopy

Electronic microscopy analyzing techniques are a result of the bombardment of specimens with high-energy beam and the interaction of the beam with the specimens matter [41-43].

Although the creation and transport of the electron beam to the sample is not a simple issue, the detection and interpretation of the different signals that result from the interaction of the beam with the specimen, is quite complex. The first equipment to work with electron beams dates the early 50's – the electron prove microanalysis (EPM), just a few years after the first commercial X-ray spectrometer came to existence.

The first remark of scanning electronic microscopy is attributed to Oatley, in the late 50's, but the first high-performance equipment dates the 70-decade. In these days the evolution of such techniques made it possible to have pictures in the nanoscale range and a set of different signal interpretation, like EDS (energy dispersive X-Ray spectroscopy), AES (auger electron spectroscopy), Cathodeluminescence and WDS (wavelength dispersive spectroscopy).

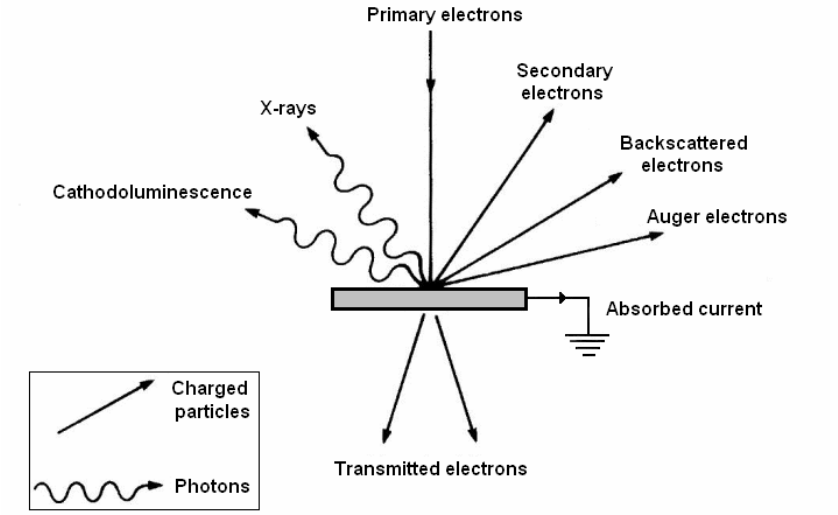

Figure 29 – Emission of electrons and photons as a result of the bombardment of a sample with an electron beam

As can be observed from figure 29, the bombardment of a sample with a electron beam produces different emission electrons and photons, such as:

- secondary electrons;
- backscattered electrons;
- transmitted electrons;
- X-ray photons;
- Auger electrons;
- Cathodoluminescence;
- and residual current.

To produce SEM images, secondary and backscattered electrons are used. Secondary electrons result from inelastic collisions from of the primary electron beam with the sample, freeing electrons from the near-surface region that will interact with ionized electron neighbors, creating an emitted current – the secondary electrons.

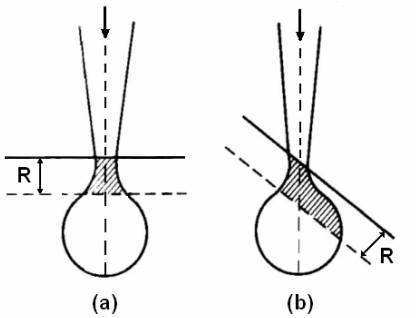

Figure 30 - Thickness of the sample that generates the secondary electrons. (b) A common technique to acquire better quality images is to till the sample

Crystallite size and morphology of the CVD diamond films presented in this work was investigated by SEM pictures acquired in a Hitachi 4100 SEM system. Magnification of samples topology ranges from 30x to 300 000x. Besides providing higher magnification than optical microscopy, SEM also has a greater depth of field.

Sample preparation is important and necessary for SEM. In order to avoid charge effect, the diamond surface was coated with conducting carbon prior to SEM analysis. The carbon coating, although, can be a disadvantage if one would like to perform EDS analyses of the sample.

2. Surface profilometery

Surface profilometery measures the films average roughness. Roughness is the arithmetic average of the absolute values of the measured profile height deviations taken within the sampling length and, ensured from the graphical centerline. Ra is expressed, normally, in micrometers. Stylus type profilometers are designed to respond only to irregularity spacing less than a given value, called the cutoff. In other words, all irregularities having a spacing less than the value of the cutoff are included in a measurement.

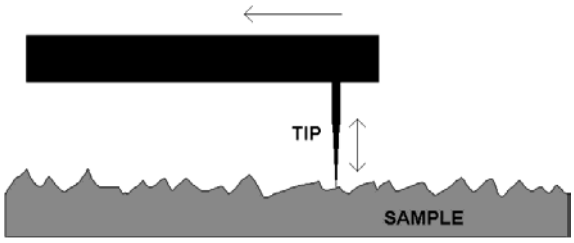

Figure 31 - Profilometery scheme

Surface profilometery was conducted in a Hommelwerke T1000 (Japan) surface profiler.

3. Raman spectroscopy

Raman spectroscopy is, in sort words, a characterization technique based in the light dispersion phenomenon [43-45], discovered in 1928 by India's physicist Chandrasekhara Venkata Raman.

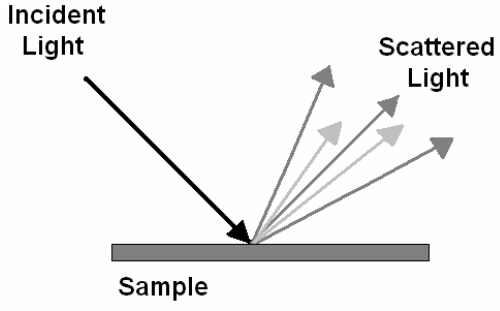

Figure 32 - Scattered light as a result of the interaction of light with a sample

The bigger part of light is scattered by the effect of an elastic collision with the sample, know as Rayleigh dispersion and doesn't have any variation in frequency terms. A small part of light suffers an inelastic collision due to the momentum variation of the molecules, as can be seen in figure 33.

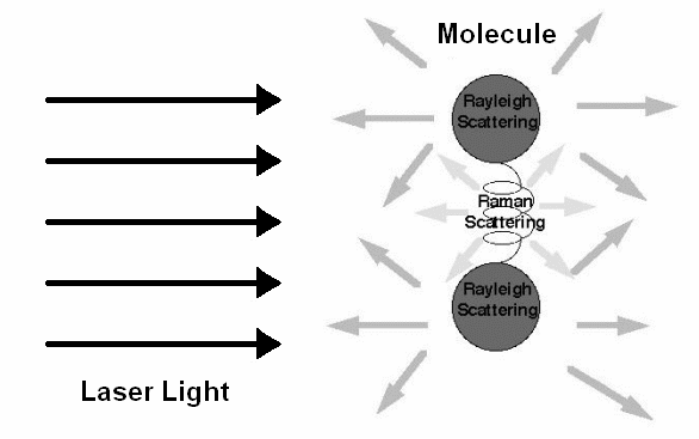

Figure 33 - Rayleigh and Raman scattering of the laser light

Let's take in consideration the case of a diatomic molecule. Let's consider the incident electromagnetic wave:

$$E = E_0 \cos(\omega_0 t) \tag{9}$$

This electric field will promote the vibration of the molecule, inducing a dipolar momentum, μ_e, in the form:

$$\mu_e = \alpha_p E_0 \cos(\omega_o t) \tag{10}$$

Where α_p is the molecule polarizability and in general a function of the atomic separation.

If x is the extra dislocation of the molecule atoms, we can expand the polarizability by a Taylor expansion development, around x_0

$$\alpha_p(x) = \alpha_{p0} + (\partial\alpha_p/\partial x).\ x + \ldots \tag{11}$$

α_{p0} is the polarizability in the average x position. The molecule will vibrate also in it's natural resonant frequency, ω_m, then we will have:

$$x = a \cos(\omega_m t) \tag{12}$$

Combining equations (10), (11) and (12), we have:

$$\begin{aligned} \mu_e &= \alpha_{p0} E_0 \cos(\omega_0 t) + (\partial\alpha_p/\partial x).(a \cos(\omega_m t)).(E_0 \cos(\omega_m t)) + \ldots \\ &= \alpha_{p0} E_0 \cos(\omega_0 t) + \tfrac{1}{2} (\partial\alpha_p/\partial x).aE_0.\{\cos((\omega_0-\omega_m).t) + \cos((\omega_0+\omega_m).t)\} + \ldots \end{aligned} \tag{13}$$

We will have then the emission of three different frequencies: the Rayleigh emission with a frequency equal to $[\omega_0]$, and the two Raman frequencies – Stokes emission: $[\omega_0-\omega_m]$ and anti-Stokes emission: $[\omega_0+\omega_m]$.

A different way to understand the Raman Effect is by a quantum energy scheme shown in figure 34. The exchange of energy from the incident phonons to the molecule isn't big enough to transport the system to the excited state, so a virtual state "quasi-excited", between the fundamental and excited state, is formed, giving place in the decay to the Stoke or Anti-Stokes emission.

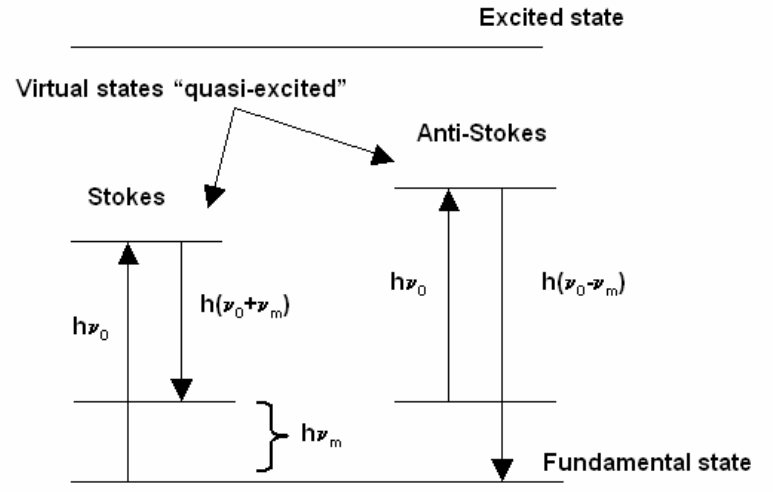

Figure 34 - Quantum representation of energy exchange in the Raman phenomenon

The variation of the radiation energy can be read as the difference between the incident energy (E_i) and the energy reflected by Raman Effect (E_s). This difference is the so-called "Raman Shift", that common Raman systems measure, coupled with the radiation intensity, which is proportional to the incident intensity, to the dispersed frequency and first of all depends greatly on the molecules being illuminated.

Different molecules scatter more effectively at different energy, so we can identify the molecules present in a sample by identifying the scattered peaks or bands. As demonstrated in chapter II, diamond films incorporate large amounts of graphite and amorphous carbon. Diamond crystals present a Raman peak at 1332 cm^{-1} and graphite and amorphous carbon present a Raman band from 1360 cm^{-1} to 1550 cm^{-1}.

L. Pereira [18] presented a resumed table of the most significant scattering reported in literature.

Table 3 - Raman scattering of carbon materials [18]

Scattering Band (cm^{-1})	Scattering source
1140	Nanocrystalline diamond
1140 and 1490	Diamond precursors (sp^2 disordered carbon)
1150 and 1470	Nanocrystalline diamond
1350 and 1590	Microcrystalline graphite (D and G bands)
1350 and 1600	Carbon with a high disordered order
1355 and 1580	Diamond Like Carbon (DLC)
1357 and 1580 (large bands)	Vitreous carbon

(continues)

(continuation)

Scattering Band (cm^{-1})	Scattering source
1560 and 1610	Amorphous carbon duplet
1350, 1580 and 1620	Microcrystalline graphite
1200 (large bands)	Graphite phonons from the K zone boundary
1326	Hexagonal diamond
1331 - 1336	Natural Diamond
1333 - 1345	Polycrystalline diamond
1357	Polycrystalline graphite
1360	Disordered graphite
1380	CH_3 group phase deformation vibrations
1400 - 1470	CH_2 and CH_3 group anti-phase deformation vibrations
1450 – 1550 (large bands)	Amorphous carbon or DLC
1480	sp^2 amorphous phase structures
1500 (large bands)	Amorphous carbon
1510 - 1560	Bridged graphite or diamond
1550 (large bands)	Carbon without no diamond structure
1560	Graphite (G band)
1560 (large bands)	Carbon phases with inclusions of structures similar to graphite (graphite like carbon)
1580	Graphite (crystalline, hexagonal crystalline and natural)
1581	Graphite (crystalline and hexagonal crystalline)
1613	Microcrystalline graphite (D' band)

So, it is possible to get qualitative information of the purity of the deposit films from the disconvolution of the total spectrum. Disconvolution is normally possible by Lorentzian and/or Gaussian functions.

A semi-quantitative measure of the quality of the diamond film [46] can be calculated from the following formula:

$$Q = \frac{I_d}{I_{glc} + I_d} \tag{14}$$

where Q is the quality factor of the diamond film, I_d is the intensity of the diamond peak, and I_{glc} is the intensity of the graphite-like carbon peak. It is worth noting that pure diamond has a quality factor, Q, value of 1.

Raman spectroscopy analysis was a crucial tool for the present work in determining the quality of the deposited films. The analyses were preformed in a Renishaw 2000 micro-Raman system (VS-Schwenningen, South Germany) with a 514 nm He-Ne laser.

Raman spectra can also be used to characterize the stress levels in the films [23]. A general model was developed from the investigation of residual biaxial stress in diamond films by Raman spectroscopy, which describes quantitatively the relations between singlet or doublet phonon scattering and the biaxial stress σ_s, measured in GPa, as follows:

$$\sigma_s = -1.08(\nu_s - \nu_0) \text{ for singlet phonon} \quad (15)$$

$$\sigma_s = -0.384(\nu_d - \nu_0) \text{ for double phonon} \quad (16)$$

where ν_0 = 1332 cm^{-1}, ν_s is the observed maximum of the singlet in the spectrum, and ν_d the maximum of the doublet. In the case when the splitting of the Raman line is not so obvious, the observed peak position ν_m is assumed to be located at the center between the singlet ν_s and the doublet ν_d, i.e., ν_m = ½ (ν_s + ν_d). From equations (15) and (16) we obtain:

$$\sigma_s = -0.567(\nu_m - \nu_0) \quad (17)$$

Thus, the stress in the diamond films is proportional to the Raman peak shift.

It is known that the stress in the diamond film consists of thermal stress σ_s^{th} and intrinsic stress σ_s^{in}, i.e.,

$$\sigma_s = \sigma_s^{th} + \sigma_s^{in} \quad (18)$$

Fan et al. [47] discussed thermal stress in terms of thermal mismatch between diamond and substrate material. This stress can be expressed as

$$\sigma_s^{th} = \frac{Y}{1-\upsilon}\int_{Ts}^{Td}(\alpha_f - \alpha_s)dT \quad (19)$$

Where Y and ν are the Young's modulus (1143 GPa) and Poisson's ratio (0.07) for diamond, T_d and T_s are deposition temperature and sample temperature at the end of the cooling procedure. α_f and α_s are temperature dependent thermal expansion coefficients of diamond and substrate material, respectively.

For diamond deposition on copper at 600ºC, the compressive thermal stress obtained was $\sigma_s^{th} \approx$ -8.78 GPa.

Considering that the spectral Raman resolution is 1 cm^{-1}, a Raman shift ranging from 1331.5 to 1332.5 cm^{-1} is regarded as 1332 cm^{-1} in the measurement. Thus, the biaxial intrinsic stress σ_{in}, even though in tension, is only 0.284 at maximum, corresponding to a 0.5 cm^{-1} shift, from equation (14). According to equation (18), the residual stress for the example given above, is still about -8.496 GPa in compression.

Raman can also provide some useful information about the stress variation along the depth of the film, as shown in [47].

From Airy stress equation:

$$\frac{\partial^4 \phi}{\partial x^4} + 2\frac{\partial^4 \phi}{\partial x^2 + \partial y^2} + \frac{\partial^4 \phi}{\partial y^4} = 0 \tag{20}$$

applied to a real sample condition, combining with equation 17, we can obtain the Raman shift, τ, contributed by s layer at a depth y of the film:

$$\tau = 1332 - \frac{1}{0.568}\frac{\sigma_s}{h} y \tag{21}$$

were h is the thickness of the diamond film and σ_s is the stress at the film-substrate interface (y=h), assumed to be uniform. Note that σ_s is negative for compressive stress and positive for tension stress.

On the other hand, the absorption loss δI is proportional to the thickness δy of a material that the electromagnetic wave penetrates:

$$\delta I = - \eta I \delta y \tag{22}$$

where η is the loss factor and I the signal intensity at depth y. The loss factor includes the intensity loss of both the incident light and Raman signal. It's value depends on the material and its structure, as well as the laser source. According to equation 22, we find

$$I = I_0 e^{-\eta y} \tag{23}$$

With I_0 being the intensity of the Raman signal, coming from the surface layer. Equation (23) shows that the intensity of the Raman signal is in a great manner due to the top layers of the film.

If we use a Lorentzian function to simulate the Raman spectra of different "layers", it is found:

$$I_y = \frac{I_0 e^{-\eta y} \psi^2}{(\xi - \tau)^2 + \psi^2} \tag{24}$$

where I_y is the intensity of Raman signal coming from a depth of y microns, ψ the full width at half-maximum (FWHM), ξ the laser wave number and τ the peak center that can be obtained from equation (21). Then the total intensity is the sum of all I_y.

4. Micro-hardness test

Hardness tests are frequently used in metallurgic industry to control the quality of materials and processes. The physical concept of hardness is associated with the penetration resistivity or to the permanent deformation of the surface.

When interested in evaluating the penetration hardness, the most common methods used are Brinell, Vickers and Rockwell.

Coating adhesion was assessed using indentation methods Rockwell C or Brinell indentation, with different imposed loads to characterize the coating adhesion strength.

Brinell hardness test consists in the penetration of the material with a steel or hard metal sphere, applying a controlled force in a period of time. Rockwell is normally used to acquire higher values of hardness, in an accurate way, something that Brinell method fails to do.

In the present work, Vickers hardness test method was used to assess the hardness properties of the films samples. Vickers tests involve penetrating the material surface with an indenter, a quadrangular pyramid instead of a sphere. This quadrangular pyramid is made out of diamond and has an angle between faces of 136º.

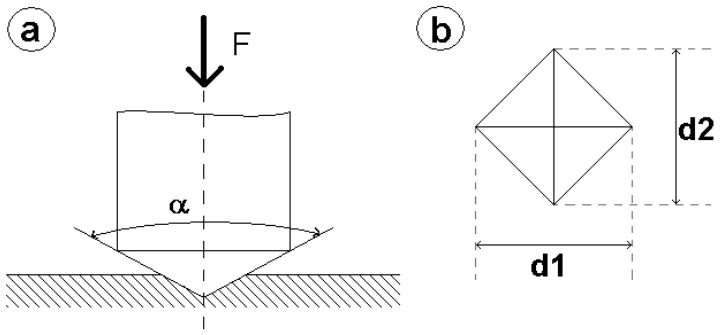

Figure 35 - (a) Vickers diamond penetrator and (b) penetration mark in the material surface

The value of hardness given by this method is proportional to the coefficient of the applied force and the impressed lateral area, represented in figure 35(b). This can be expressed mathematically by the expression [48]:

$$HV = \frac{1}{g}\frac{F}{A} \tag{25}$$

Where, g is the gravity acceleration in $m.s^{-2}$ and *F* is the applied force in Newton. Considering the average diagonal length d1 and d2, of the impressed lozenge, the contact area will be:

$$A = \frac{d^2}{2.sen\left(\frac{136º}{2}\right)} = \frac{d^2}{1.854} \tag{26}$$

So Vickers Hardness will be given by the mathematical expression:

$$HV \cong 0.102\frac{2.F.\sin\left(136º/2\right)}{d^2} = 0.1891\frac{F}{d^2} \tag{27}$$

By the norm NP 711-1:1990, Vickers hardness is designated with the symbol HV after the hardness value and the value of the used force expressed in kgf and duration time in seconds.

According to the NP 711-1:1990 norm, the deposit films were studied with an applied force of 500gf (~ 5N) for 20 seconds. Because diamond films had a low roughness, there was no special need of sample preparation before testing.

The Vickers hardness of the coatings was measured using a Micro-hardness tester, Shimadzu HMV-2000 (Kyoto, Japan).

5. Electric properties

Dielectric functions, f(t) in time domain and $\chi(\omega)$ in frequency domain, represent the simple way to get information about the dielectric properties of a material. However, there are several possibilities to present data, depending on the nature of the response, one needs to study. As an example, it can be an advantage to represent conductivity dependency of the frequency $\sigma(\omega)$, instead of the dielectric loss; or $\varepsilon'(\omega)$ instead of $\chi'(\omega)$ [49,50].

Dielectric data has a distinct characteristic from major physic parameters related to steady state situation. They involve time or frequency variables, and in the same time they involve also temperature, pressure or composition. This means that we are dealing with a big number of different information, which needs extra care in the interpretation and presentation of results.

Also, when one passes from a theoretical ideal material to a real material, uniformity is almost a utopia. There are always parasitic components lurking in the shadow waiting for the unwary. Unwanted resistance in capacitors, unwanted capacity in inductors and unwanted induction in resistors.

Let's take the electric permittivity, for example. The permittivity of a dielectric pure material is given by the product of the vacuum permittivity by the relative permittivity of the material ($\varepsilon=\varepsilon_o\varepsilon_r$). The majority of real materials present a resistivity and capacity component at the same time, so total or complex electric permittivity will be:

$$\varepsilon^* = \varepsilon' - i\varepsilon'' \tag{28}$$

where ε' is the real component and is related to capacity, and ε'' is associated with the imaginary part and related with the resistivity of the sample.

To better understand this concept, let's look to Ampere's Law in it's differential form in vacuum:

$$\begin{aligned} & rot\vec{H} = \vec{J} + \varepsilon_o \frac{d\vec{E}}{dt} \Leftrightarrow \\ & \Leftrightarrow rot\vec{H} = \sigma\vec{E} + \varepsilon_o i\varpi\vec{E} \\ & \Leftrightarrow rot\vec{H} = i\varpi\vec{E}\left(\varepsilon_o - i\frac{\sigma}{\varpi}\right) \end{aligned} \tag{29}$$

If instead, we are in the presence of a material, we can make the correspondence of the real part to ε' and the imaginary component to ε'', this is:

$$\varepsilon'' = \frac{\sigma}{\varpi\varepsilon_o} \tag{30}$$

So we can rewrite Ampere's Law as:

$$rot\vec{H} = i\varpi\vec{E}\left(\varepsilon' - i\varepsilon''\right) \Leftrightarrow$$
$$\Leftrightarrow rot\vec{H} = iw\varepsilon^{*}\vec{E} \quad (31)$$

that turns to be a generic form of the fourth Maxwell equation.

The permittivity of a given material is not constant, except for a discrete values of frequency. This phenomenon is associated to the polarization of the electric dipoles, witch depend on the relaxation frequency of each material.

Relaxation frequency, or other electric properties can be measured assuming that the material is a dielectric of a capacitor in a controlled environment – a cryostat, for instance.

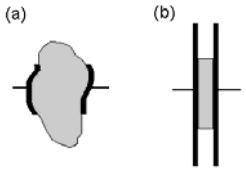

Figure 36 – (a) Representation of a general configuration of a dielectric body with two metallic contacts and (b) a coplanar body [50]

The idea of the sample being the dielectric of a capacitor is illustrated in figure 36, and we can define the capacity of this sample as the rate between the charge, Q_c, in the capacitor plates and the applied potential, U:

$$C = \frac{dQ_c}{dU} \quad (32)$$

This expression is completely general, independent of the shape, homogeneity and linearity of the studied material. Although it can be used a sample like the one presented in figure 36(a), it is convenient to use well defined geometry samples, like the one illustrated in figure 36(b). Even using this shape, it is convenient that the plates have lateral dimensions much bigger than the sample's thickness, d, so that the fringing effect is minimal.

From this presuppose (Area>>d^2), assuming that the dielectric is homogeneous, the contact between the electrodes and the sample is efficient and the material has a linear response relatively to the amplitude of applied potential, we can write an expression for the electric field: E=U/d, an expression for the total charge: Q_c=A.σ_d, where σ_d is the charge density, and assume a equivalent circuit for the case represented in figure 36.

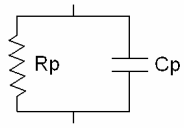

Figure 37 - Equivalent circuit of sample represented in figure 36

The dielectric induction, D, represents the charge induced in the electrodes by the field E, so we can have:

$$Q_c = A\sigma_d = AD = A\varepsilon_0\varepsilon' E = \varepsilon_0\varepsilon'\frac{A.U}{d} \tag{33}$$

from here we can deduce an expression for the capacity:

$$C = \frac{\varepsilon_0\varepsilon' A}{d} \tag{34}$$

The resistive part is deduced from the conductivity expression:

$$R = \frac{d}{\sigma A} \tag{35}$$

that combined with equation (30), turns to be:

$$R = \frac{d}{\varepsilon_0\varepsilon'' \omega A} \tag{36}$$

We can also rewrite equations (34) and (36) as:

$$\varepsilon' = \frac{d}{A}\frac{C}{\varepsilon_o} \tag{37}$$

$$\varepsilon'' = \frac{d}{A}\frac{1}{\varepsilon_o \omega R} \tag{38}$$

or in a conductivity form, knowing that:

$$\sigma^* = i\omega\varepsilon_0\varepsilon^* \tag{39}$$

$$\sigma' = \frac{d}{A}\frac{1}{R} \tag{40}$$

$$\sigma'' = \frac{d}{A}\omega.C \tag{41}$$

Experimentally, one just needs to measure accurately R and C, in a highly controlled atmosphere. For that propose, a LCR equipment was used with a frequency range from 75 kHz to 30MHz and a bath cryostat.

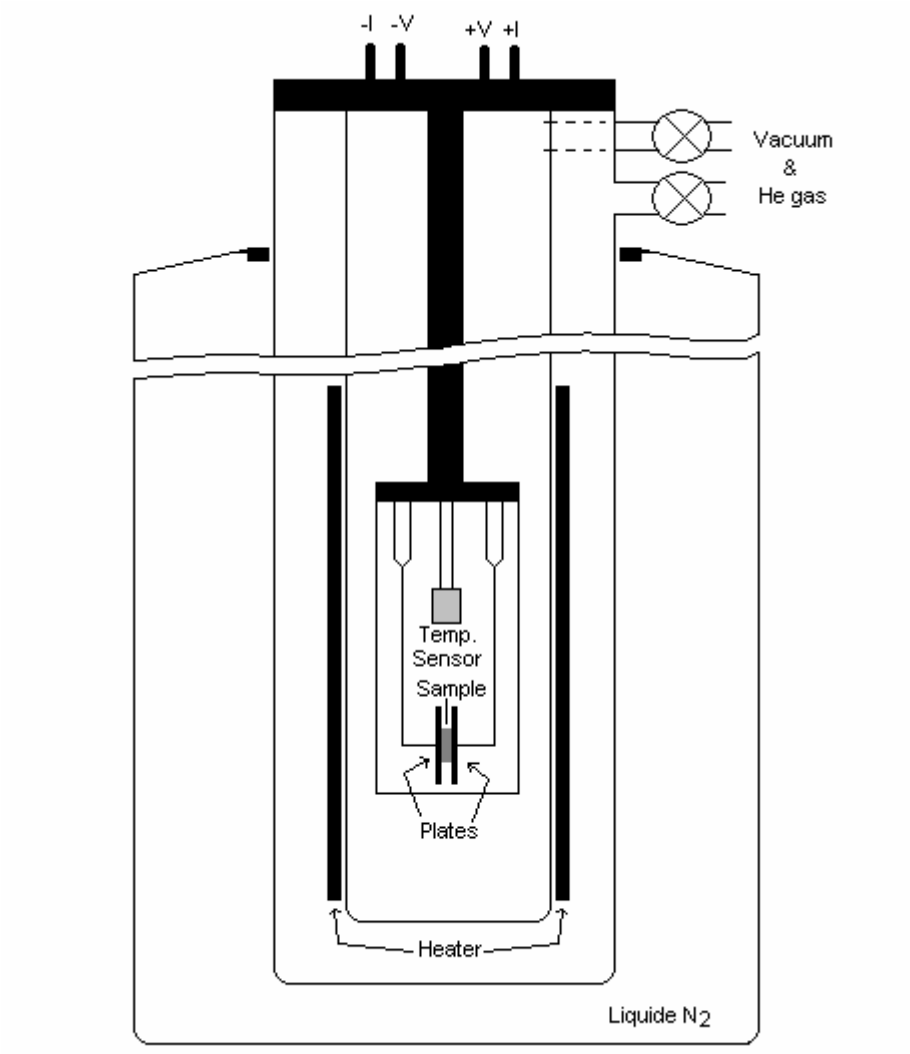

Figure 38 - Bath cryostat used in experiments

Especially at high frequencies, any mutual inductance, interference of the measurement signals, and unwanted residual factors in the connection method related to ordinary termination methods will have significant effects on the measurements.

If the measurement equipment employs a four-terminal pair measurement configuration, two current inputs and two potential inputs, such inconvenient factors can be reduced significantly.

HP 4285A LCR has a four-terminal configuration, high current (Hc), high potential (Hp), low potential (Lp), and low current (Lc) [51]. The measurement principle shown in figure 39, has advantage in both low and high impedance measurements. The outer shield conductors work as the return path for the measurement signal current (they are not grounded). The same current flows through both the center conductor and outer shield conductor (in opposite directions), so no external magnetic fields are generated around the conductors (the magnetic fields produced by the inner and outer currents completely cancel each other). Because the measurement signal current does not develop an inductive magnetic field, test leads do not contribute additional errors due to self or mutual inductance between the individual leads.

Samples were tested with temperatures from room temperature to 120ºC. Cp and Rp were the measured parameters, using two plates' contacts, as showed in the cryostat diagram of figure 38.

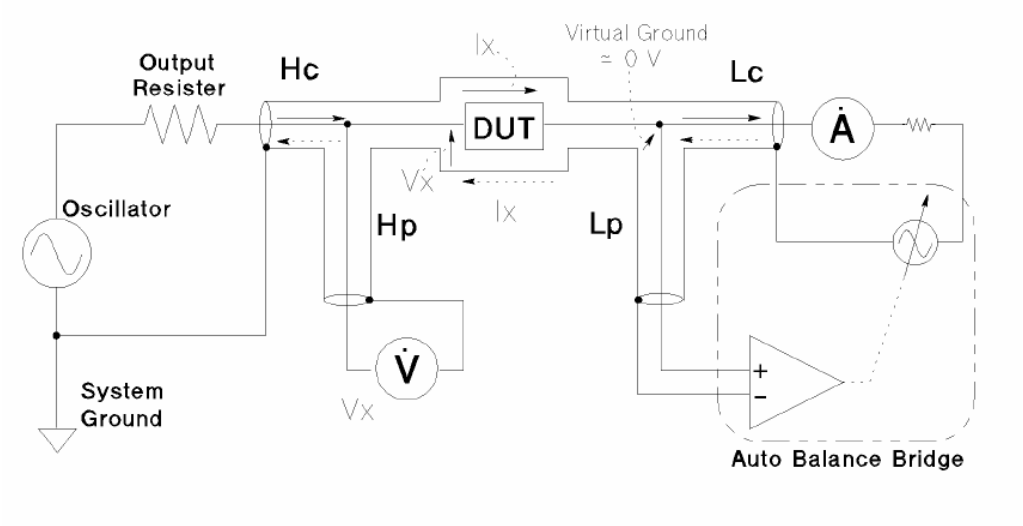

Figure 39 - Four-terminal pair measurement principle [51]

Complementary information was also achieved from DC electrical measurements. For that it was used a 617 Keithley electrometer with an internal voltage source.

Although dielectric measurements depends of a simple theoretical procedure, real samples, like the one represented in figure 36(a), aren't so simple and there accuracies depend mainly of the measurement system and the sample preparation (sample geometry, bad electrical contacts between sample material and electrodes, edge capacities and electrode polarization) [52].

6. Complementary methods

There where also some complementary analyses preformed in some of the studies to further comprehension of films properties.

Tribological properties like wear rates and friction coefficients where preformed by Pin-on-disk system (Plint TE 67HT) with steel disks (Ck45-Din).

It was also used X-ray diffraction (XRD) to determine the structure of crystals or molecules. The technique involves directing a beam of X-rays at a crystalline sample and recording the diffracted X-rays. The diffraction pattern consists of a pattern of spots on the plate, and the crystal structure can be worked out from the positions and intensities of the diffraction spots. X-rays are diffracted by the electrons in the molecules and if molecular crystals of a compound are used, the electron density distribution in the molecule can be determined.

CHAPTER V

FILM CHARACTERIZATION AND DISCUSSION

1. Conventional CVD optimization

The first step of the experimental work was to get ideal deposition conditions for conventional CVD diamond films grown in TEMA's HFCVD reactor. It is important to note that the term "conventional CVD" refers to films deposited, using CVD, under constant flow of CH_4, into the vacuum reactor, throughout the growth process.

To achieve this task, we did a set of depositions onto silicon {100} substrates (5 mm x 5 mm x 0.5 mm). Silicon wafers were chosen especially because of the lattice and thermal expansion resemblance to diamond material. The growth of diamond films onto silicon doesn't present any problems of adhesion, unlike the deposition onto many metals, including copper, steel, etc. [23].

The substrates were abraded with diamond powder (Lands, Super Abrasives, Type LS600T 2-4μm) (New York, NY) prior to film deposition in order to enhance the nucleation density. After the substrates underwent abrasion for 2 minutes using the diamond abrasive, they were ultrasonically cleaned in acetone for 5 minutes to remove any loose abrasive particles.

Prior to the depositions the filament was pre-carbonized to prevent filament poisoning. The conditions employed during filament pre-carbonization were:

Table 4 – Pre-carbonization condition

CH_4 concentration (%)	3
CH_4 flow (sccm)	4.5
H_2 flow (sccm)	150
Filament power (W)	264
Chamber pressure	30
Deposition time (mins)	20

Starting from typical deposition conditions described in the literature, as reported in chapter 1 – substrate temperature ~ 800ºC; filament temperature ~ 2000ºC; deposition pressure ~ 20 Torr; CH_4/H_2 rates ~ 1 to 2 %, considering a hydrogen flow ~ 150 sccm [2,23], we varied a parameter at the time, until the ideal conditions were achieved.

In the next tables we present the different conditions of deposition. In bold we note the parameter that is changed.

a) CH_4/H_2 variation

Table 5 - CH_4/H_2 variation experiments

Sample Reference	Opt01	Opt02	Opt03	Opt04
CH_4/H_2 (%)	**1**	**2**	**3**	**4**
Chamber Pressure (Torr)	20	20	20	20
H_2 flow (sccm)	150	150	150	150
Deposition Time (minutes)	30	30	30	30
Filament power (W)	~ 260	~ 260	~ 260	~ 260
Substrate Temperature (ºC)	~ 800	~ 800	~ 800	~ 800
Filament-Substrate distance (mm)	4	4	4	4

b) Deposition time variation

Table 6 - Deposition time variation experiments

Sample Reference	Opt11	Opt12
CH_4/H_2 (%)	2	2
Chamber Pressure (Torr)	20	20
H_2 flow (sccm)	150	150
Deposition Time (minutes)	**10**	**20**
Filament power (W)	~ 260	~ 260
Substrate Temperature (ºC)	~ 800	~ 800
Filament-Substrate distance (mm)	4	4

c) Chamber pressure variation

Table 7 - Chamber pressure variation experiments

Sample Reference	Opt21	Opt22	Opt23	Opt24	Opt25
CH_4/H_2 (%)	2	2	2	2	2
Chamber Pressure (Torr)	**10**	**20**	**30**	**40**	**50**
H_2 flow (sccm)	150	150	150	150	150
Deposition Time (minutes)	10	10	10	10	10
Filament power (W)	~ 260	~ 260	~ 260	~ 260	~ 260
Substrate Temperature (ºC)	~ 800	~ 800	~ 800	~ 800	~ 800
Filament-Substrate distance (mm)	4	4	4	4	4

d) Filament-substrate distance variation

Table 8 - Filament-substrate distance variation experimements

Sample Reference	Opt26	Opt27	Opt28
CH_4/H_2 (%)	2	2	2
Chamber Pressure (Torr)	30	30	30
H_2 flow (sccm)	150	150	150
Deposition Time (minutes)	30	30	30
Filament power (W)	~ 260	~ 260	~ 260
Substrate Temperature (ºC)	~ 800	~ 800	~ 800
Filament-Substrate distance (mm)	**4**	**6**	**8**

The above samples were mainly characterized using SEM in order to evaluate their morphologies.

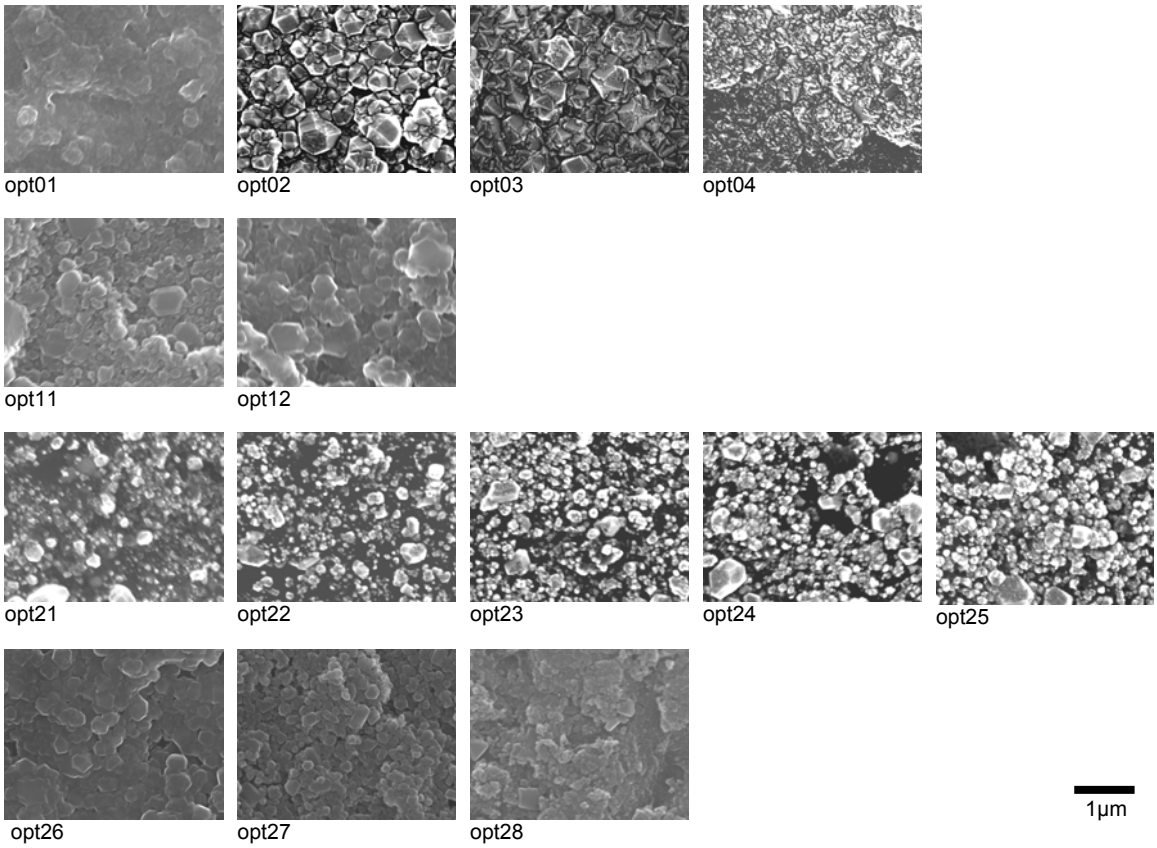

Figure 40 - SEM pictures of optimization experiments

From the set of images presented in figure 40, we can have an idea of "ideal" conditions to grow diamond films. From the first group of experiments, CH_4/H_2 variation, one can say that opt02 and opt03 present well defined crystals. In sample opt01 there is no nucleation at all, and in opt04 it can be observed the incorporation of amorphous carbon and graphite phases to the films.

With deposition time variation experiments, we can see that after 10 minutes of deposition we have already a homogeneous layer of nucleation seeds and even some nice looking crystals. After 20 minutes, the film is almost closed in the surface plane.

When we vary the deposition pressure, it is seen that the nucleation density increases with the pressure, in this discrete number of experiments. We can say that deposition pressure must not be lower than 30 Torr and can be any value between 30 to 50 Torr. Although it was not studied, it is known that with higher deposition pressure the crystal quality is reduced. With all this in view, optimized pressure value must be around 30 Torr.

Finally, varying filament to substrate distance can change two parameters – substrate temperature and/or near substrate atmosphere.

The HFCVD system used does not have any device to measure the filament temperature. The only way to have some control of it is by extrapolation from the applied power although it is not an accurate method.

Analyzing the SEM results, 4 mm of filament-substrate distance presents the better looking crystals, although the 6 mm distance is not bad, so presumably the ideal value is between these two values.

From this set of experiments, we can consider that “ideal” conditions of diamond growth using HFCVD are:

Table 9 – “Ideal” deposition conditions

CH_4/H_2 (%)	2
Chamber Pressure (Torr)	30
H_2 flow (sccm)	150
Filament power (W)	~ 260
Substrate Temperature (ºC)	~ 800
Filament-Substrate distance (mm)	4

It can be stated that after 10 minutes of deposition there is already a good nucleation density and that after 20 minutes the first layer of diamond is made.

2. TMCVD optimization by Taguchi method

Prior to the Taguchi experiments, we performed some experiments to better understand the TMCVD process.

The key feature of the TMCVD process is second order of nucleation, achieved at higher methane flows. One of the projected experiments were to investigate the second order nucleation dependency of the higher pulse.

Samples where prepared as described previously, and deposition was performed for 2 hours, using a conventional method, with 2% of CH_4. After this 2 hours deposition,

sample A continued the deposition with a 3% pulse for 10 minutes, and sample B with a pulse of 4%.

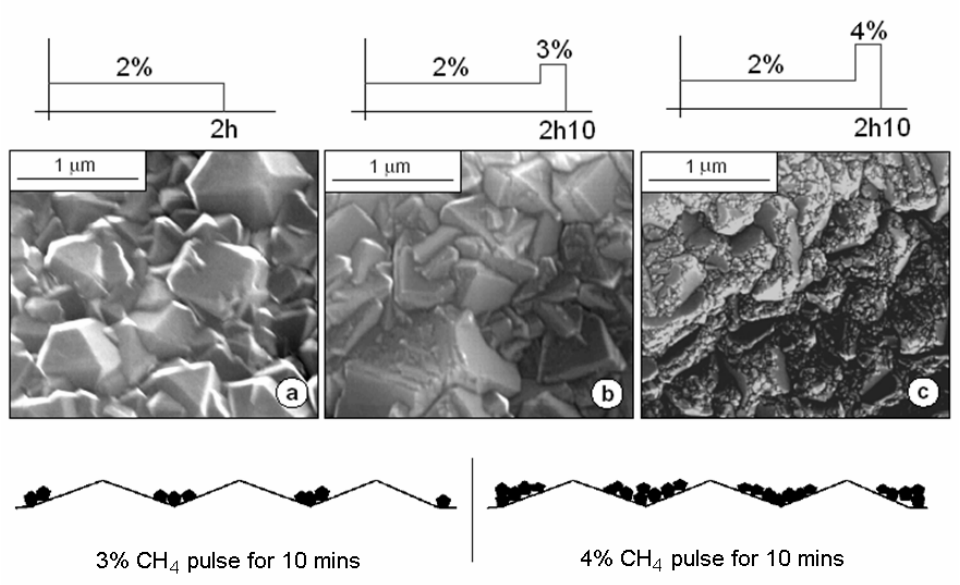

Figure 41 - Films grown by conventional method for 2 hours (a), with a 10 minutes pulse at 3% CH_4 (b) and 4% (c)

Figure 41 displays SEM micrographs showing secondary nucleation occurring after pulsing CH_4 at 3% (b) and 4% (c) for 10 minutes. It is important to note that prior to the methane pulses, diamond deposition was conducted under standard conventional conditions CVD (a) as obtained in previews sub-section, for two hours using the HFCVD system. The SEM images show that secondary nucleation occurs, in both cases, during the CH_4 pulses at 3 and 4%. However, the secondary nucleation density is greater after the CH_4 pulse at 4% than after the 3% pulse. This can be expected, since at higher methane concentrations, carbon-containing radicals are present in the CVD reactor in greater amount, which favor the growth process by initiating diamond nucleation. The average secondary nucleation crystallite size was in the nanometer range. It is evident that the generation of secondary nucleation has lead to the successful filling of the surface irregularities found on the film profile, in between the mainly {111} crystals with these newly formed nano-sized diamond grains. Bottom pictorially scheme, shows the consequence of pulsing methane, at 3 and 4% for 10 minutes, on the production of secondary diamond crystallites on the surface of the microcrystalline diamond film. The surface roughness values of the two samples were measured and it was found that the 10 minute CH_4 pulse at 4% produced a smoother surface, giving rise to a Ra value of 0.25 μm. Whereas, the 10 minute CH_4 pulse at 3% produced a less smooth film surface of Ra value 0.28 μm.

After this preliminary study, we employ the Taguchi method to optimize the time-modulated chemical vapor deposition (TMCVD) process.

The traditional approach used to optimize a process involves changing one parameter at a time whilst keeping the remaining parameters constant. However, in CVD processes, where numerous experimental parameters are involved, the use of the traditional optimization method becomes less significant, since many experiments need

to be performed before arriving at the optimum conditions. Although, the traditional approach can be useful in selecting predominant parameters in many fabrication processes, it is still time and energy consuming. Furthermore, the results obtained from the traditional approach are only valid for fixed experimental conditions and their prediction under other conditions is uncertain. In the 1950s, Taguchi [53] developed a statistical tool for designing-of-experiments (DOE) to meet the above requirements. The Taguchi technique provides an efficient and systematic method to optimize designs for performance, quality and cost [54]. It has been successfully employed in designing reliable, high quality products at relatively low costs [55]. The advantage of employing Taguchi technique has been summarized by Weiser [56]. Primarily, the method requires limited number of experiments to conduct the experimental design. Another important point is that many different variables can be examined simultaneously. This means that predominant parameters can be investigated deeply whereas, secondary parameters can be overlooked. Therefore, time, energy and resources can be saved. Finally, signal-to-noise (S/N) in the Taguchi method can be used to optimize the process and to reduce the process variability.

In this study, we employ the Taguchi method to optimize the TMCVD process. We consider the following five key TMCVD process parameters: (i) high CH_4 flow (HF), (ii) low CH_4 flow (LF), (iii) high-timed modulations (HTm), (iv) low-timed modulation (LTm) and (v) substrate temperature (Temp). Each parameter was varied at the 4 experimental levels. The effect of each of the 5 parameters, varied at 4 experimental levels, on the following factors was investigated: surface roughness (Ra); average grain size; hardness; Full-Width Half Maximum (FWHM); and quality (Q), in terms of diamond-carbon phase purity. The as-grown films were characterized using micro-Raman spectroscopy, surface profilometery, Vickers hardness, and scanning electron microscopy (SEM).

Diamond films were deposited onto silicon {100} substrates (5 x 5 x 0.5mm) using the hot-filament CVD system. The silicon substrates were abraded with diamond powder as described previously.

Table 10 - Experimental conditions employed during diamond deposition using the TMCVD process

Parameter	Film deposition
Pressure (Torr)	30
H2 flow (sccm)	150
CH4 flow (sccm)	0.9 – 9
Substrate Temperature (ºC)	700 – 850
Filament power (W)	168 – 272
Filament-substrate distance (mm)	4
Deposition total time (min)	60

The conditions employed during the growth conditions used during the 16 experiments are shown in table 10.

Design-of-experiments (DOE)

Table 11 shows the key five TMCVD process parameters investigated at the four experimental levels. Since the distinctive feature of the TMCVD process is the timed CH4 modulations, flow of CH4 was timely introduced into the vacuum chamber at high and low modulations. The values used for low CH4 flows, LF, were 0.9, 1.5, 2.25 and 3 sccm, whereas, the high CH4 flows, HF, used were 4.5, 6, 7.5 and 9 sccm. The modulation times used for high CH4 flow (HTm) were 2, 4, 6 and 8 mins. Modulation times of 3, 6, 9 and 12 minutes were used for low CH4 flows (LTm). The four substrate temperatures (Temp) investigated were 700, 750, 800 and 850ºC.

Table 11 - The 5 parameters considered and the 4 experimental levels investigated in this study

	Experimental levels			
Parameter	**1**	**2**	**3**	**4**
HF (sccm)	4.5	6	7.5	9
LF (sccm)	0.9	1.5	2.25	3
HTm (mins)	2	4	6	8
LTm (mins)	3	6	9	12
Temp (ºC)	700	750	800	850

On table 12, it is showed the complete DOE used in this process optimization study. Only 16 experiments were designed, which were sufficient for our case. For each of the 5 parameters and for each experiment, the experimental level (1-4) is shown in table 12. Each level corresponds to a value, as shown in table 11.

Table 12 - The design-of-experiments, DOE, by the Taguchi method for 5 parameters and 4 experimental levels

Experiment	HF	LF	HTm	LTm	Temp.	Total CH4 flow (ml)
1	1	2	3	2	3	180
2	3	4	1	2	2	252
3	2	4	3	3	4	252
4	4	2	1	3	1	412
5	1	3	1	4	4	158
6	3	1	3	4	1	212
7	2	1	1	1	3	176
8	4	3	3	1	2	418
9	1	1	4	3	2	169
10	3	3	2	3	3	240
11	2	3	4	2	1	255
12	4	1	2	2	4	248
13	1	4	4	1	1	248
14	3	2	2	1	4	306
15	2	2	2	4	2	162
16	4	4	4	4	3	324

As previously mentioned, the samples were characterized using several different techniques. The average grain size values were calculated from the SEM micrographs. Surface profilometry was used to measure the surface roughness (Ra) values. The hardness values were obtained using conventional Vickers hardness tester. Finally, Q values were calculated from the Raman spectra. The quality, in terms of diamond phase purity (sp^3 to sp^2 bonding) was assessed. A semi-quantitative measure of the quality of diamond films can be calculated using the equation (14) presented in chapter IV (section 3).

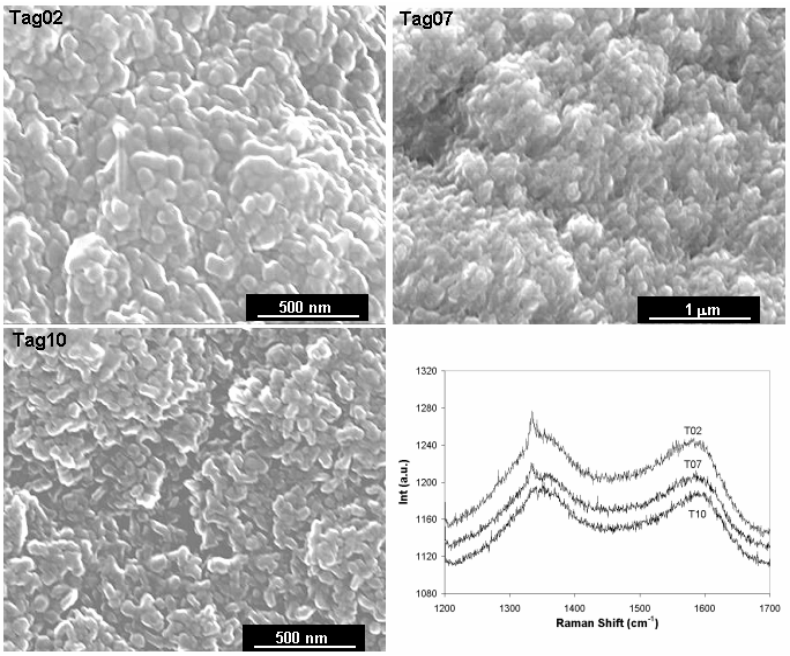

Figure 42 - SEM images and Raman Spectrums of samples Tag02, 07 and 10

Table 13 - Experimental results. Am = amorphous = 1; and ∞ = 1000

Experiment	FWHM (cm^{-1})	Ra (μm)	Grain Size (μm)	Hardness (HV)	Q (%)	Total CH_4 flow (ml)
1	9.9	0.28	0.48	1086	76	180
2	269.1	0.21	0.11	1282	61	252
3	243.9	0.26	0.22	1546	59	252
4	9	0.14	Am.	1168	39	412
5	35.1	0.22	0.25	1479	64	158
6	13.05	0.17	0.64	1057	23	212
7	60.3	0.11	0.19	1466	57	176
8	∞	0.27	Am.	1187	0	418
9	12.15	0.24	0.85	1185	67	169
10	70.2	0.22	0.11	1620	53	240
11	7.2	0.20	0.25	1199	40	255
12	71.1	0.17	0.15	905	51	248
13	∞	0.22	0.16	1428	0	248
14	27.45	0.14	Am.	1773	49	306
15	9.9	0.13	0.49	1187	45	162
16	6.3	0.34	0.17	1178	25	324

Table 13 shows the results of the 16 experiments performed. Table 14 shows the calculated Taguchi results. The table shows a value for each parameter at each level and for the five factors considered. The information in table 12 and table 13 was used to calculate the data presented in table 14. For example, the values shown in table14 for FWHM corresponding to HF at the 4 levels were calculated as follows:

Level 1: 9.9 + 35.1 + 12.15 + 1000 (∞) = 1057.15

Level 2: 243.9 + 60.3 + 7.2 + 9.9 = 321.3

Level 3: 269.1 + 13.05 + 70.2 + 27.45 = 379.80

Level 4: 9 + 1000 + 71.1 + 6.3 = 1086.4

The remaining values shown in the table have been calculated in the same manner as above. When making the calculations it is important to refer to the information given in table 12 in order establish the correct levels in correspondence to the experiments.

Table 14 - Calculated Taguchi results

	Level	HF	LF	HTm	LTm	Temp
FWHM	1	1057.15	156.6	373.5	2087.75	1029.25
	2	321.3	56.25	178.65	357.3	1291.15
	3	379.8	1112.5	1266.85	335.25	146.7
	4	1086.4	1519.3	1025.65	64.35	377.55
Ra	1	0.96	0.69	0.68	0.74	0.73
	2	0.7	0.69	0.66	0.86	0.85
	3	0.74	0.91	0.98	0.86	0.95
	4	0.92	1.03	1	0.86	0.79
Grain size	1	1.74	1.83	1.55	2.35	2.05
	2	1.15	2.97	1.75	0.99	2.45
	3	1.86	1.61	2.34	2.18	0.95
	4	2.32	0.66	1.43	1.55	1.62
Hardness	1	5178	4613	5395	5854	4852
	2	5398	5214	5485	4472	4841
	3	5732	5485	4876	5519	5350
	4	4438	5434	4990	4901	5703
Q	1	207	198	221	106	102
	2	201	209	198	228	173
	3	186	157	158	218	211
	4	115	145	132	157	223

The effect of the five parameters, at the 4 levels, on the 5 factors is graphically shown in figure 43. It is evident that the parameters at all 4 levels have a profound effect on the 5 factors investigated. For a hard, smooth, good quality diamond film, it is required that the FWHM, Ra, average grain size values are small; and hardness, Q values are high. In order to select the optimum conditions, the two best values obtained for each parameter, at all 4 levels, were selected and have been shown on the graphs in figure 43 with a cross sign (+), which appears on top of the selected lines on all the five graphs.

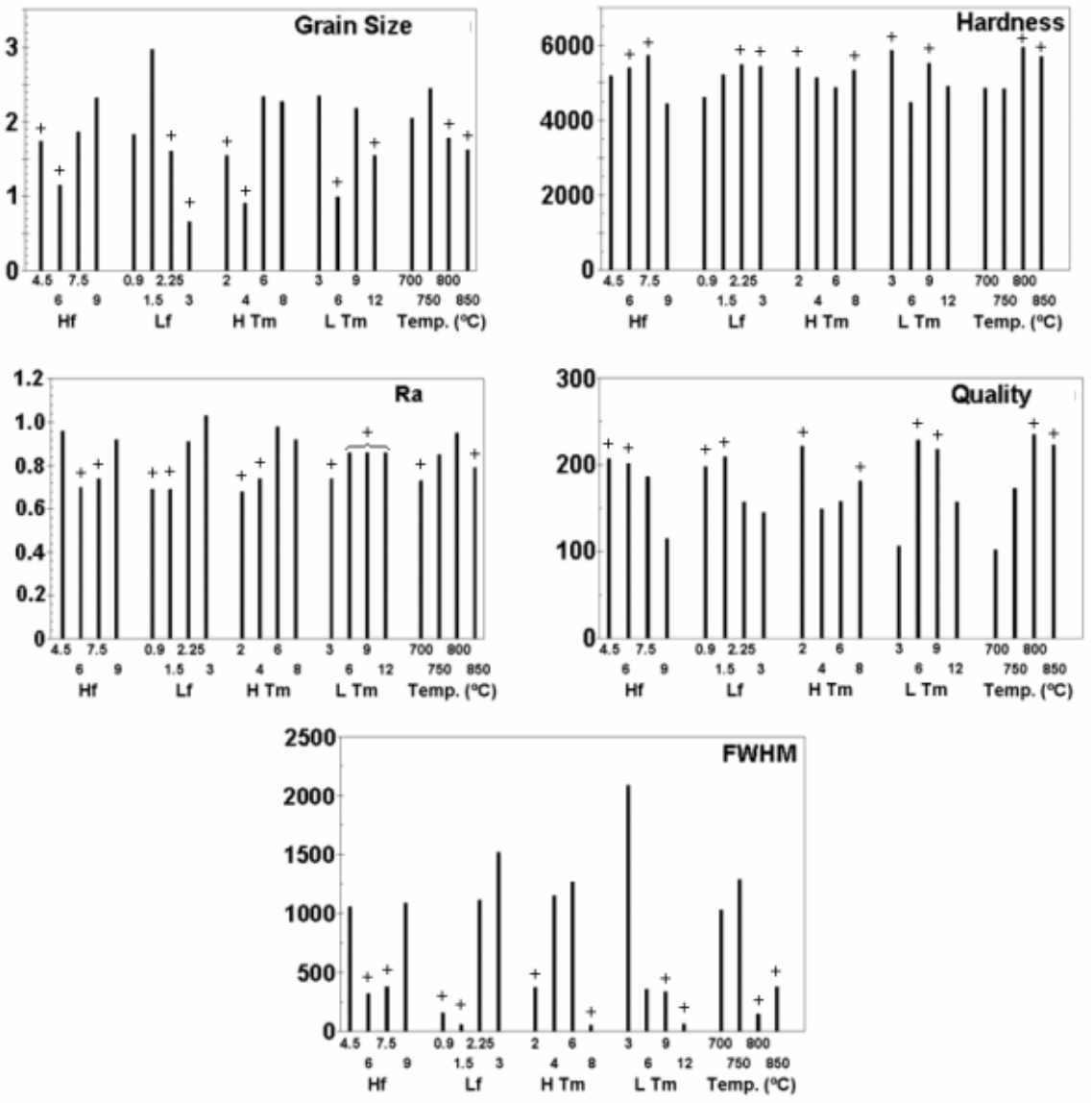

Figure 43 - Graphical representation of the data shown in table 14. The (+) signs on top of the selected lines correspond to those values that we considered in determining the optimum conditions

The selected results have been tabulated and shown in table 15. It can be seen that the optimum values for HF, LF, HTm, LTm and Temp, are 6 sccm, 0.9-1.5 sccm, 2 minutes, 9 minutes and 850ºC, respectively. Figure 44 displays the graph showing the optimized time-modulated CH_4 flows with deposition time. Primarily, CH_4 is introduced into the chamber at 6 sccm for 2 minutes and then the CH_4 flow is reduced to 1.5 sccm and kept constant for 9 minutes. This modulated cycle is then repeated, and it the repetition of such cycles that render the process the name “time-modulated CVD”. It is interesting to note that these optimum conditions have been obtained after only performing 16 experiments using the Taguchi DOE. If the traditional optimization method was used to optimize a process having 5 parameters and 4 levels, a total number of 45 = 1024 experiments would be required for complete optimization. However, using the Taguchi approach to optimize the same process, the number of experiments required is drastically reduced from 1024 to only 16.

Table 15 - Optimized results for the TMCVD process, as obtained from the Taguchi analysis

Factor	HF (sccm)		LF (sccm)		H Tm (mins)		L Tm (mins)		Temp (ºC)	
FWHM	**6**	7.5	**0.9**	**1.5**	**2**	8	**9**	12	800	**850**
Ra	**6**	7.5	**0.9**	**1.5**	**2**	4	3	6/**9**/12	700	**850**
G. Size	4.5	**6**	2.25	3	**2**	4	6	12	800	**850**
Hardness	**6**	7.5	2.25	3	**2**	8	3	**9**	800	**850**
Quality	4.5	**6**	**0.9**	**1.5**	**2**	8	6	**9**	800	**850**
Optimized value	**6**		**0.9, 1.5**		**2**		**9**		**850**	

With respect to the results obtained and the TMCVD process, there are some points that are noteworthy. First, flow rate of CH_4 into the vacuum reactor is a critical parameter in diamond CVD process. Diamond deposition using CVD consists of two stages, namely, (i) nucleation stage and (ii) the film growth stage. It is known that diamond nucleation density increases with CH_4 concentration in the vacuum rector. However, the quality of the deposited films, in terms of diamond-carbon phase purity, deteriorates with CH_4 concentration. In developing the TMCVD process for diamond deposition, the above points were taken into consideration. The higher timed CH_4 modulation is to ensure rapid diamond nucleation to form the first monolayer of the film. The lower CH_4 pulse helps increase the quality of the depositing film and favours columnar growth mode.

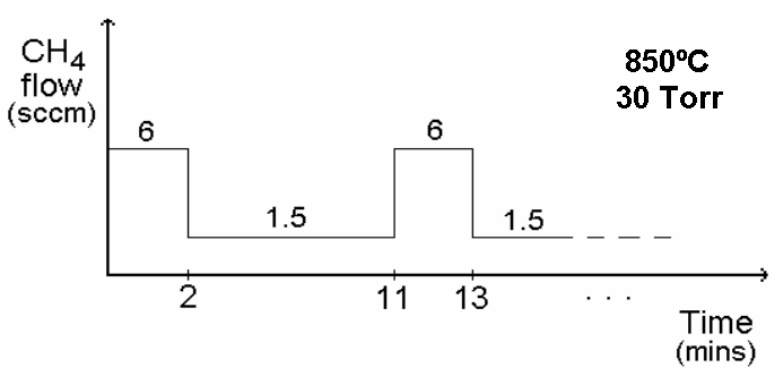

Figure 44 - Optimized timed-CH_4 flows (HF, LF) during the TMCVD process

The generation of secondary diamond nucleation, which is also a key feature of the TMCVD process, is an important factor, which is influenced by three parameters. The three parameters are (i) deposition temperature, (ii) CH_4 content and (iii) pressure. The deposition temperature was kept constant at 30 Torr in all the 16 experiments. It is expected that the rate of secondary nucleation increases with deposition temperature. Furthermore, the secondary nucleation rate increases with CH_4 content, at suitable temperatures. The increase in secondary nucleation can result in the production of a smoother film surface profile by the effective filling of the surface irregularities, during film growth. The generation of nano-sized diamond grains during TMCVD can be held

responsible for improving the hardness of the coating samples. It was found that the films deposited in experiments 4, 8 and 14 were amorphous in nature. This can be attributed to the relatively higher total flow of CH_4 into the vacuum chamber during the complete growth process. The total flow of CH_4 into the deposition reactor for each of the 16 experiments has been shown in table 12.

3. Comparative study between time-modulated and conventional CVD film samples

An important step of this study is to compare conventional films with time-modulated films, so one can evaluate the potential advantage or not of the modulation processes.

For that propose, two main experiments where conducted. The first one consisted of a conventional deposition with 2% CH_4 for 126 minutes and a modulated deposition with pulses of 2 and 3% CH_4, with 8 and 10 minutes of duration, respectively, for a total of 126 minutes. The second experiment was a conventional deposition with 2% CH_4 for 300 minutes and a modulated deposition with CH_4 pulses of 1% for 15 minutes and 3% for 45 minutes, for a total of 300 minutes.

The exact Taguchi optimized values weren't used because your equipment doesn't aloud automatic parameters setup.

3.1. Study 1

In this study, we present results obtained from a comparison study, relating to the deposition of diamond films, using TMCVD and conventional CVD. Polycrystalline diamond films were deposited onto silicon substrates using a HFCVD system.

Film properties, such as surface roughness, crystallinity, growth rate, morphology, micro-hardness, diamond-carbon phase purity and stress were characterized using surface profilometery, SEM, Vickers hardness tester and Raman spectroscopy. The growth mode of the two types of films was assessed using cross-sectional SEM examination.

Diamond films were deposited onto silicon {100} substrates (5×5×0.5 mm). The substrates were abraded with diamond powder (2-4μm) before deposition, to enhance the diamond nucleation density. After the substrates underwent abrasion for 2 minutes using the diamond abrasive, they were ultrasonically cleaned in acetone for 5 minutes to remove any loose abrasive particles.

Prior to the depositions the filament was pre-carburized to prevent filament poisoning, with the conditions presented in table 4. The conditions employed during the growth conditions used during conventional CVD and TMCVD depositions are given in table 16. The TMCVD process pulsed CH_4 at 2 and 3% for different time durations. Figure 45 shows the CH_4 modulations and the duration of each pulse. It is important to note that the TMCVD process finished with the lower CH_4 pulse (2%).

Table 16 - Diamond deposition process parameters employed during diamond growth using Conventional CVD and Time modulated CVD processes

Parameter	Con. CVD	TMCVD
CH_4 Conc. (%)	2	2 and 3
CH_4 Flow rate (sccm)	3	3 and 4.5
H_2 Flow rate (sccm)	150	150
Filament Power (W)	264	264
Substrate Temperature (ºC)	800	800, 780
Deposition Pressure (Torr)	30	30
Deposition Time (mins)	126	126
Filament-Substrate distance (mm)	4	4

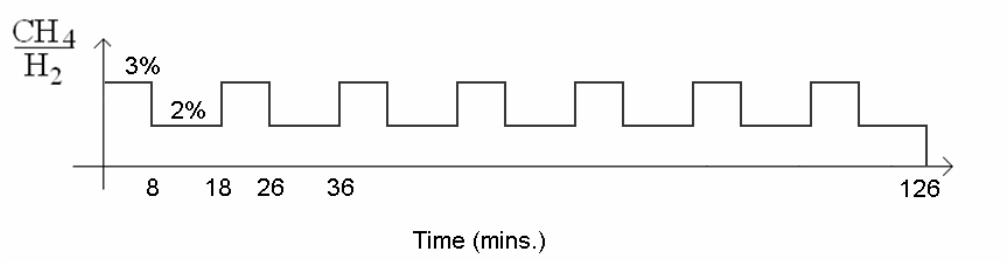

Figure 45 - Progression of the TMCVD process

Figure 46 shows the SEM images of the as-deposited films grown using (a) Conventional CVD and (b) TMCVD processes. The micrographs show the surface morphologies of the two deposited films. It is clear that both films, are polycrystalline in nature, consist of diamond crystals that exhibit predominantly {111} orientation. Figure 47 shows the average grain sizes of the conventional CVD and TMCVD diamond films. The time modulated film, consisted of diamond crystallites that were 0.3 μm in size. Whereas, the conventional CVD diamond film consisted of diamond crystals that displayed average crystallite size of 0.5 μm. This result is as expected since during the TMCVD process the CH_4 flow was modulated, which leads to the generation of secondary nuclei. Generally, the crystallite size of diamond films, grown using conventional CVD methods, increases with the evolution of growth.

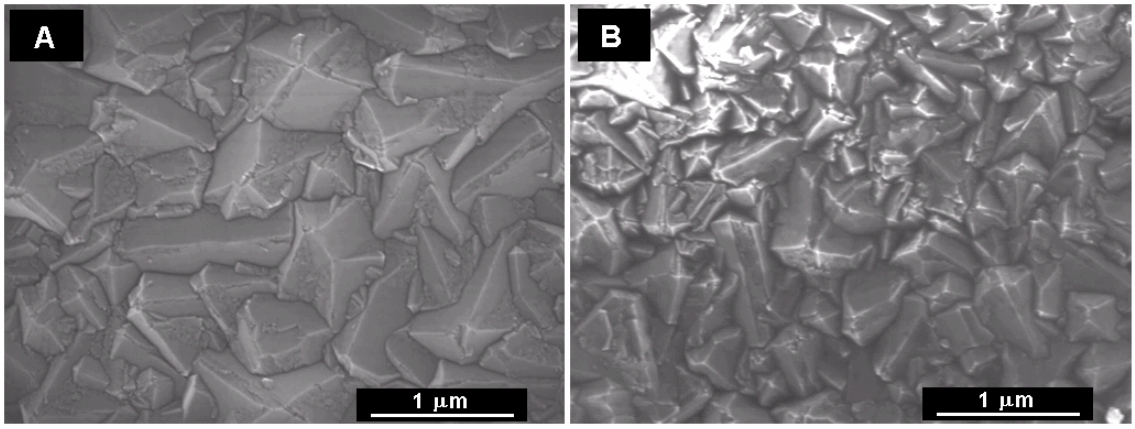

Figure 46 - SEM images of the conventional CVD diamond film (a) and time modulated film (b)

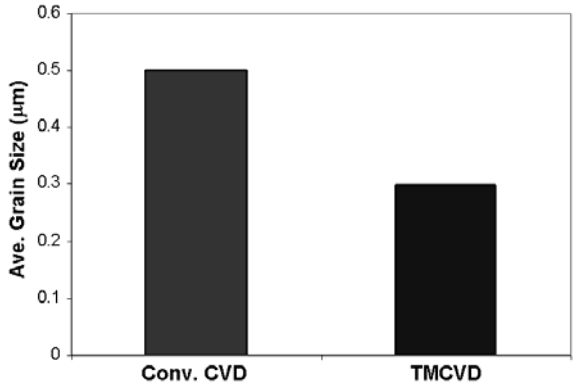

Figure 47 - The average grain size of the two films

Figure 48 shows the graph of Vickers hardness values, Hv, for the two types of diamond films and the bare silicon substrate. Due to the time-modulated film consisting of smaller crystallites, it was found that films grown via TMCVD were harder than similar films grown via conventional CVD. The mean hardness values, Hv, for films grown under constant and modulated CH_4 flow were 1048 and 1424, respectively. It is known that polycrystalline films consisting of small sized crystallites display greater hardness. The hardness value for the silicon substrate was found to be 831 Hv. After the indentations, the samples were examined under an optical microscope for any potential film cracks or coating delamination. It was found that the films did not delaminate and the coatings remained attached to the substrates. This suggests that the adhesion was sufficient to tolerate the indentations during hardness testing. Since silicon is a strong carbide-forming material, diamond coatings bond very strongly to silicon substrates after deposition.

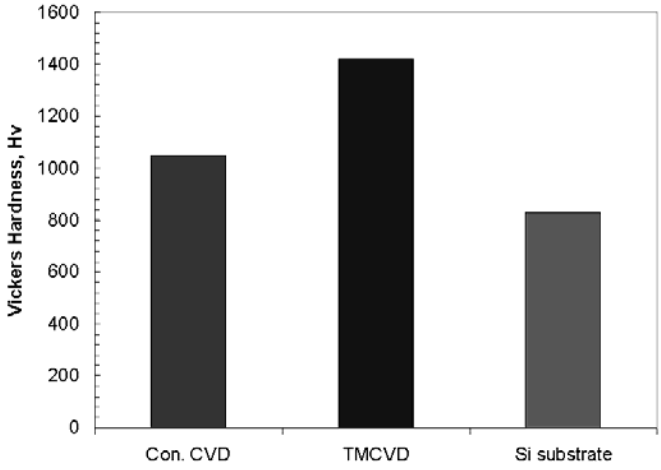

Figure 48 - Graph of Vickers hardness of the films and the silicon substrate (as a reference)

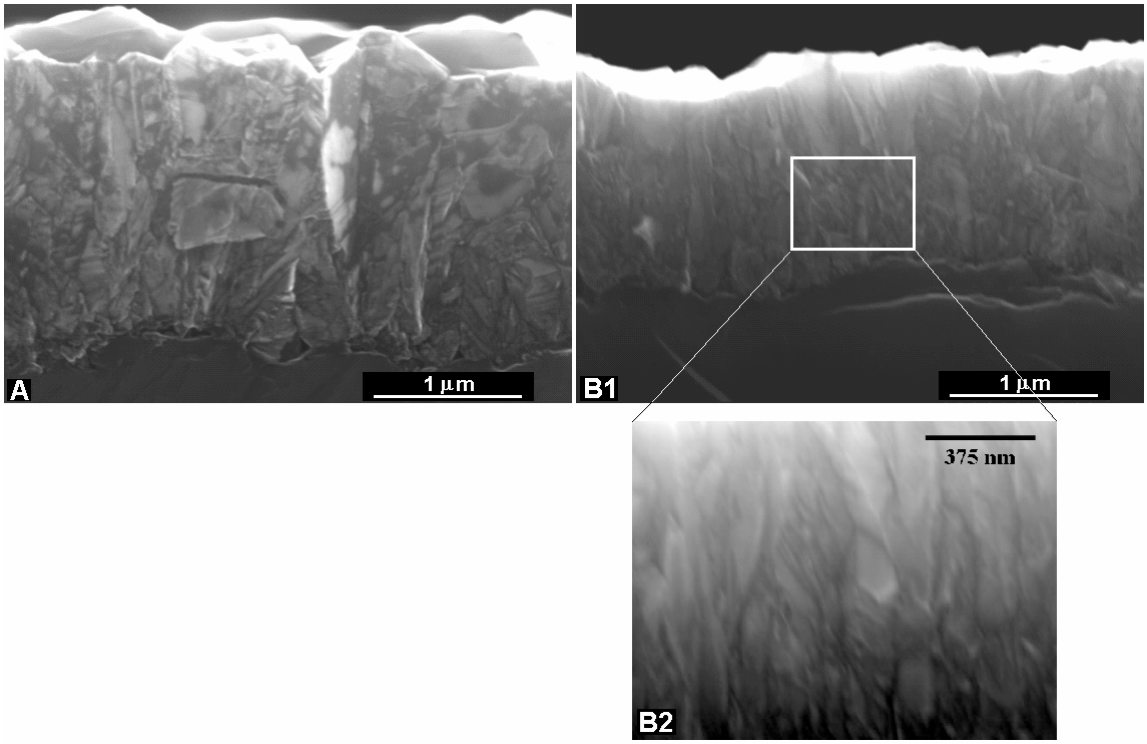

Figure 49 - Cross section SEM images of the films grown using (A) conventional CVD and (B1) TMCVD. A magnified sub-section of the film in (B1) has been shown in (B2)

Figure 49(A) & (B1) displays the SEM images of the cross sections of the films shown in figure 46(A) & (B), respectively. It is indicative from figure 49(A) that the conventional CVD diamond film displays a columnar structure, since during deposition the columnar growth is the dominant growth mode. On the contrary, the cross section of the time modulated film, as shown in figure 49(B1), displays a somewhat different growth mode from the film deposited under constant CH_4 flow. A section of the film has been magnified and shown in figure 49(B2) for closer examination of the film growth mode along the cross section. It is visible that the growth mode of the time modulated film is not the typical columnar type. Instead the cross section consists of many coarse diamond grains that are closely packed together. Diamond nucleation occurs first in both the TMCVD and conventional CVD processes. However, with the TMCVD process, diamond nucleates more rapidly as a result of high CH_4 pulse at the beginning. The high CH_4 pulse ensures that the diamond grains nucleate quicker to form the first diamond layer. The second stage, where CH_4 content is reduced to 2%, the diamond crystals are allowed to grow for 10 minutes. This step enables the crystals to grow with columnar growth characteristics. The film surface starts to become rough, as expected. The third stage involves increasing the CH_4 concentration back to 3%. This enables further secondary nucleation of diamond grains to occur in between the existing diamond crystals, where the surface energy is lower. As a comparison, much less secondary nucleation occurs when the CH_4 flow is kept constant throughout the deposition process. The distinctive feature of TMCVD is that it promotes secondary nucleation to occur onto the existing grains in order to fill up surface irregularities, like the proposed model of figure 16, in chapter II. The final stage of the TMCVD process ends with a lower methane concentration, 2%. This means hydrogen ions will be

present in greater amount in the plasma and these will be responsible for etching the non-diamond phases to produce a good quality diamond film.

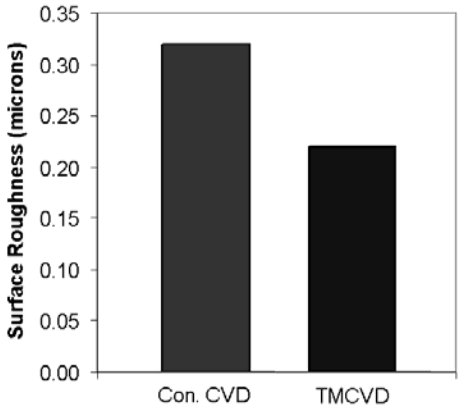

Figure 50 - Surface roughness values of conventional and time modulated diamond films

Figure 50 shows the graph of average surface roughness values of the films grown using conventional and time modulated CVD processes. The average Ra value for the conventional diamond film was 0.32 µm, whereas, for the time modulated film the value was 0.20 µm. The key point to note is that the time modulated film displayed a smoother surface than the film grown under constant CH_4 flow.

Figure 51 shows the Raman spectra of diamond films deposited using (a) conventional CVD and (b) TMCVD processes. The spectra display the characteristic Raman diamond peak positioned at 1334 cm^{-1}. In addition, a broad band, at around 1555 cm^{-1}, appeared on both of the spectrums. These broad bands indicate the presence of amorphous carbon phases in the films and act as film impurities. In earlier investigation, it was found that the quality of the diamond films, as indicated by the intensity of the Raman diamond peak, improves with film thickness [25]. In our case, the average film thickness of the coatings studied was: TMCVD, 1.4 µm; and conventional CVD, 1.8 µm. Therefore, the quality of the conventional film should be slightly better than the time modulated film. Furthermore, increased CH_4 concentrations lead to the incorporation of impurities, such as graphitic and amorphous phases, into the films which degrades the global quality of the deposited films. It is important to note that during the TMCVD process the total flow of CH_4 (in mass), 331.5 mg, is much higher than the total CH_4 flow, 271.2 mg, used in the conventional CVD process.

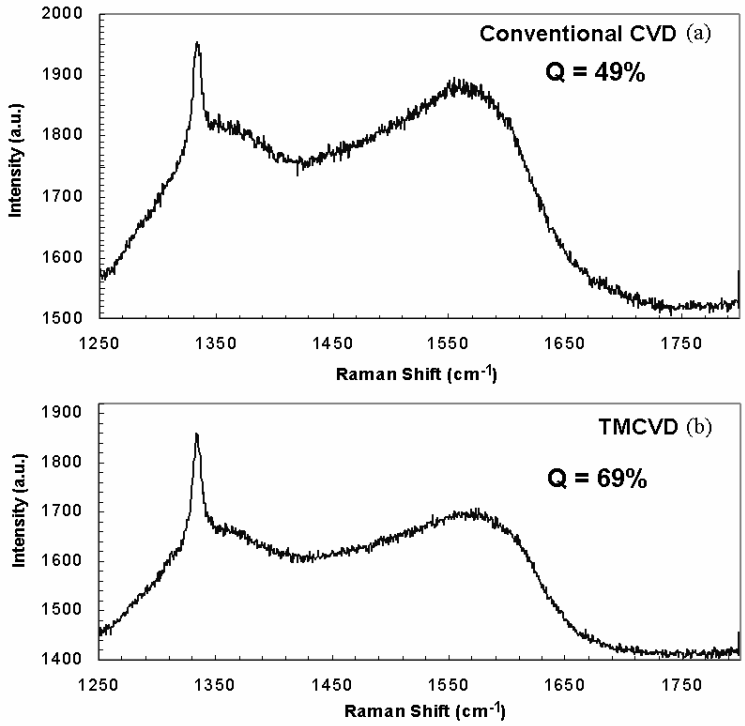

Figure 51 - Raman spectra of the films grown using (a) conventional CVD and (b) TMCVD

The data used to construct the Raman spectra, shown in figure 51, was used to calculate the Q values using equation (14). The values for the quality factor, Q, corresponding to the films grown using conventional CVD and TMCVD were calculated to be 48% and 69% respectively. The Q value for the time-modulated film is much closer to the ideal value of 100%, as compared to the Q value for the conventional CVD film. Therefore, this implies that the time modulated film is better in quality.

The Raman spectra obtained were used to characterize the film stress. Using equation 17, the film stress was calculated and it was found that both films were under compressive stress at a value of –1.13GPa.

The growth rate was calculated from the film thickness determined by figure 49. A growth rate of 0.9μm/hr was obtained using constant CH_4 flow. The time modulated film grown at a rate of 0.7μm/hr. Although, it is known that growth rates increase with methane concentration, in the present case using the HFCVD system, the TMCVD process employs greater CH_4 flow than conventional CVD. Our results show that the growth rate of films deposited using constant CH_4 flow is slightly higher than similar films grown using timed CH_4 modulations.

The substrate temperature is a key parameter, which governs the growth rate in diamond CVD. Since the TMCVD process pulsed CH_4 during film growth, it was necessary to monitor the change in the substrate temperature during the pulse cycles. It was observed that the substrate temperature decreased with CH_4 concentration. In explaining the observed trend, it needs to be considered that the dissociation of CH_4 by the hot filament absorbs energy (heat) from the filament and is considered as a cooling process. In our case the filament power was kept constant, therefore, less heat can be expected to radiate to the substrate. In addition, only a small percentage of the

thermally dissociated CH species reach the substrate and transfer kinetic energy to the substrate. It is known that the deposition of diamond films increases with substrate temperature [57].

In explaining the obtained results in figure 50, it should be considered that by changing the CH_4 concentration, this can potentially alter the relative growth rates of the {100} and {111} facets and consequently this can influence the surface profile and the morphology of the deposited diamond film. In addition to the CH_4 concentration influencing the growth rate of {100} and {111} facets, it should be noted that substrate temperature is another parameter that can significantly alter the facet growth rates. Since there are variations in the substrate temperature with CH_4 concentration and as both these parameters influence facet growth rates.

3.2. Study 2

The silicon samples were of the same kind as the previous samples, and were prepared in the same way.

The conditions employed during the growth of conventional CVD and TMCVD depositions are given in table17. The TMCVD process pulsed CH_4 at 1 and 3% for different time durations.

Table 17 - Diamond deposition process parameters employed during diamond growth using Conventional and Time modulated CVD processes

Parameter	Con. CVD	TMCVD
CH_4 Conc. (%)	2	1 and 3
CH_4 Flow rate (sccm)	3	1.5 and 4.5
H_2 Flow rate (sccm)	150	150
Filament Power (W)	264	264
Substrate Temperature (^{0}C)	~800	~800
Deposition Pressure (Torr)	30	30
Deposition Time (mins)	300	300
Filament-Substrate distance (mm)	4	4

In figure 52, the CH_4 modulations and the duration of each pulse are shown.

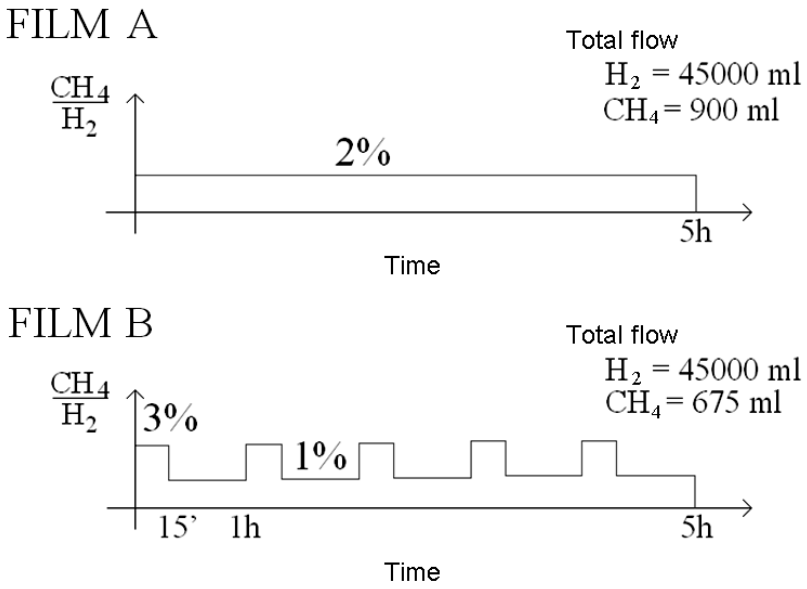

Figure 52 - Deposition gas modulation of the two deposit films

Figure 53 shows the SEM images of the as-deposited films grown using (a) Conventional CVD and (b) TMCVD. The micrographs show the surface morphologies of the two deposited films. It is clear that both films, polycrystalline in nature, consist of diamond crystals that exhibit predominantly {111} orientation. The time modulated film consisted of diamond crystallites that were 1.27μm in size. Whereas, the conventional CVD diamond film consisted of diamond crystals that displayed average crystallite size of 1.53 μm. This result is as expected since during the TMCVD process the CH_4 flow was modulated, which leads to the generation of secondary nuclei. Generally, the crystallite size of diamond films, grown using conventional CVD methods, increases with the evolution of growth, as remarked previously.

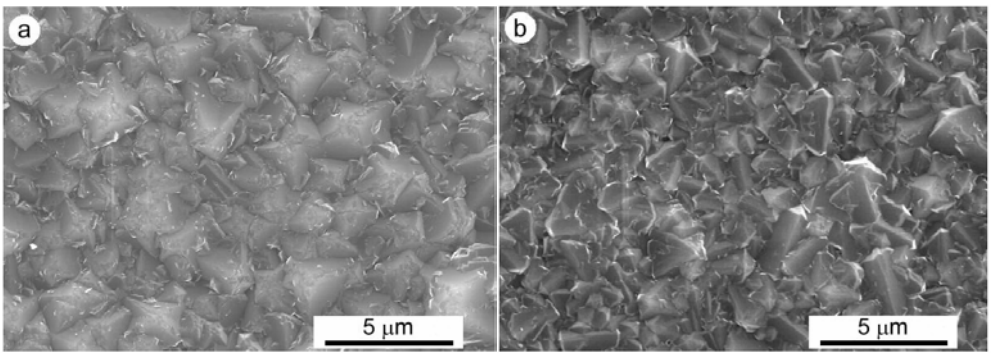

Figure 53 - SEM of the as-deposited films grown using (a) Conventional CVD and (b) TMCVD processes

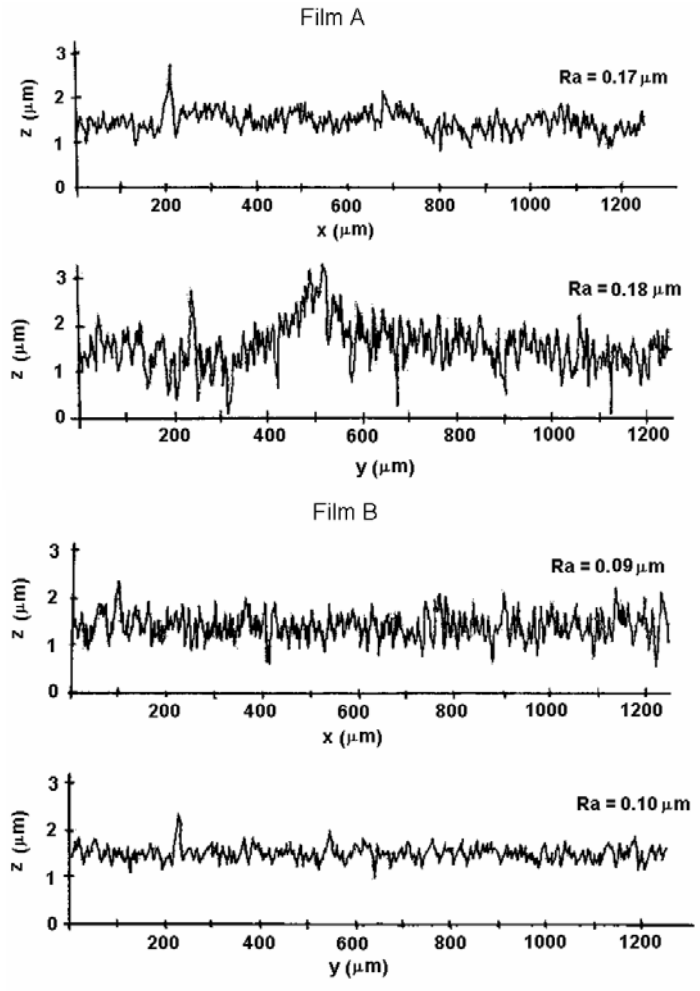

Figure 54 - Roughness of film A and B in two perpendicular directions

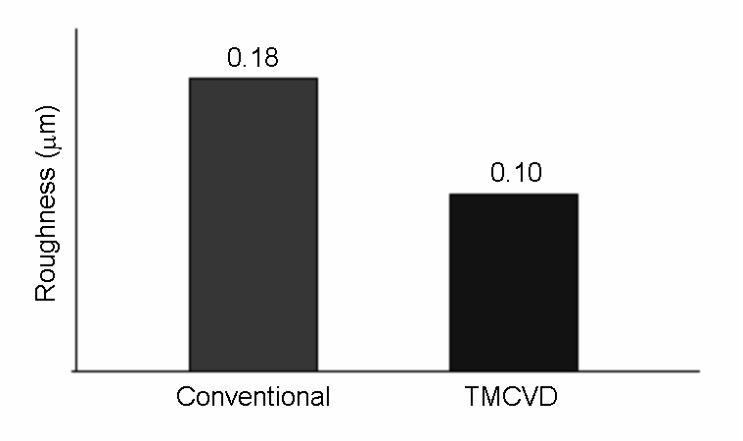

Figure 55 - Average roughness of the two deposit films

Figure 55 shows the graph of average surface roughness values of the films grown using conventional and time modulated CVD processes. The average Ra value for the conventional diamond film was 0.18 μm, whereas, for the time modulated film the value

was 0.10 μm. The key point to note is that the time modulated film displayed a smoother surface than the film grown under constant CH_4 flow.

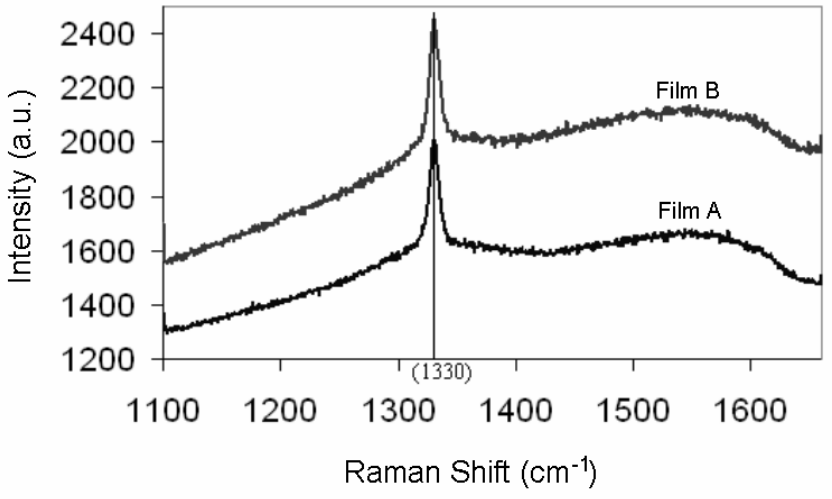

Figure 56 - Raman spectrum of the conventional and modulated film

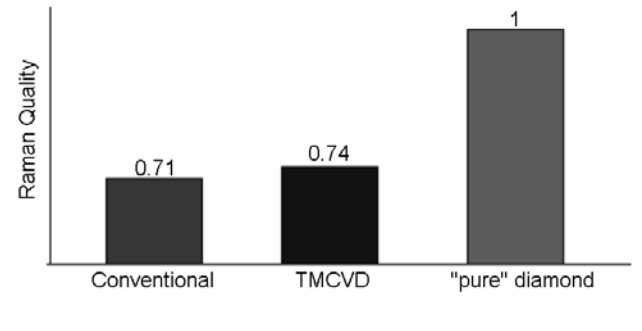

Figure 57 - Raman quality of the two deposit films and theoretical pure diamond

Figure 56 shows the Raman spectra of diamond films deposited using (a) conventional CVD and (b) TMCVD processes. The spectra display the characteristic Raman diamond peak positioned at 1330 cm^{-1}. In addition, a broad band, at around 1550 cm^{-1}, appeared on both of the spectrums, indicating the presence of amorphous carbon phases in the films and act as film impurities.

The main goal of this second study was to observe essentially the behavior the surface final roughness of a longer deposit film. It was demonstrated that the TMCVD is much smother then the conventional diamond film.

The Q value for the time-modulated film is, like in the previous study, higher in the modulated films then in the conventional CVD film. Therefore, this implies that the time modulated film is better in quality.

4. The role of substrate temperature during diamond film growth using TMCVD

The process of dynamic film growth using CH_4 modulations constitutes an interesting concept in CVD diamond technology. However, the TMCVD process is not yet fully

understood, for example, the mechanisms involved during film growth remain un-investigated. In this section, we present the results relating to the effects of substrate temperature, during CH_4 pulses, on the properties of diamond films grown using TMCVD.

Diamond films were deposited onto silicon {100} substrates, as used before. The substrates were prepared using the same method as described previously.

In this investigation, two types of samples were prepared, namely, sample A and sample B. The conditions employed during film growth were: hydrogen flow, 150 sccm; pressure, 30 Torr; growth time, 126 mins; filament-substrate distance, 4mm. The TMCVD process pulsed CH_4 throughout the growth process. The substrate temperature was measured using a K-type thermocouple.

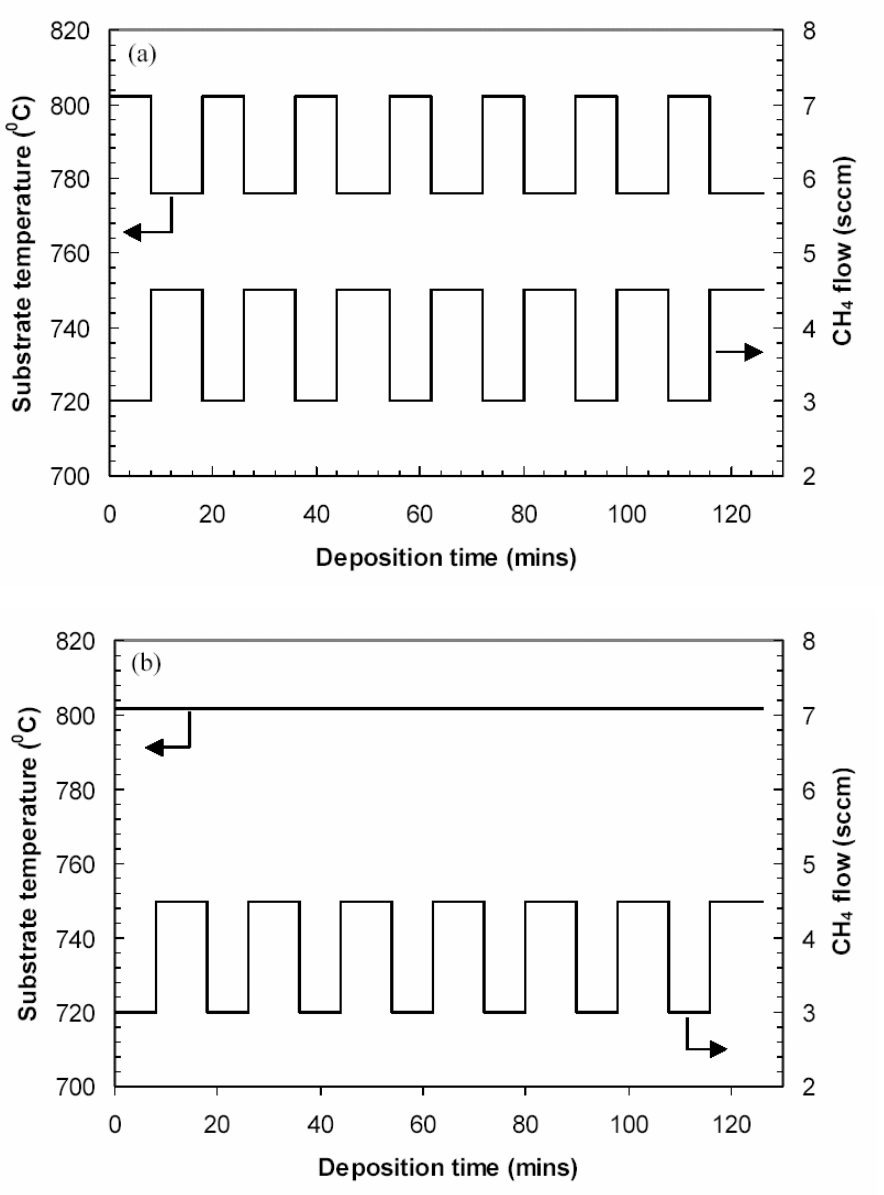

Figure 58 - Graph showing the variations in substrate temperature and CH_4 flow during sample A (a) and sample B (b) preparation using the TMCVD process

Figure 58 shows the variations in substrate temperature and CH_4 flow during sample A (a) and sample B (b) preparation using the TMCVD process. It is important to note that during sample B preparation, although the CH_4 flow was modulated, the substrate temperature was maintained constant throughout the growth process. It may be of interest to note that the substrate temperature was kept constant during the high/low CH_4 pulse cycles merely by adjusting the filament power accordingly. The temperature of the silicon substrates at 3 and 4.5 sccm CH_4 flow was noted to be 802ºC and 776ºC, respectively. The fluctuations in substrate temperature, resulting from the CH_4 pulses during TMCVD, can significantly alter the diamond film growth process.

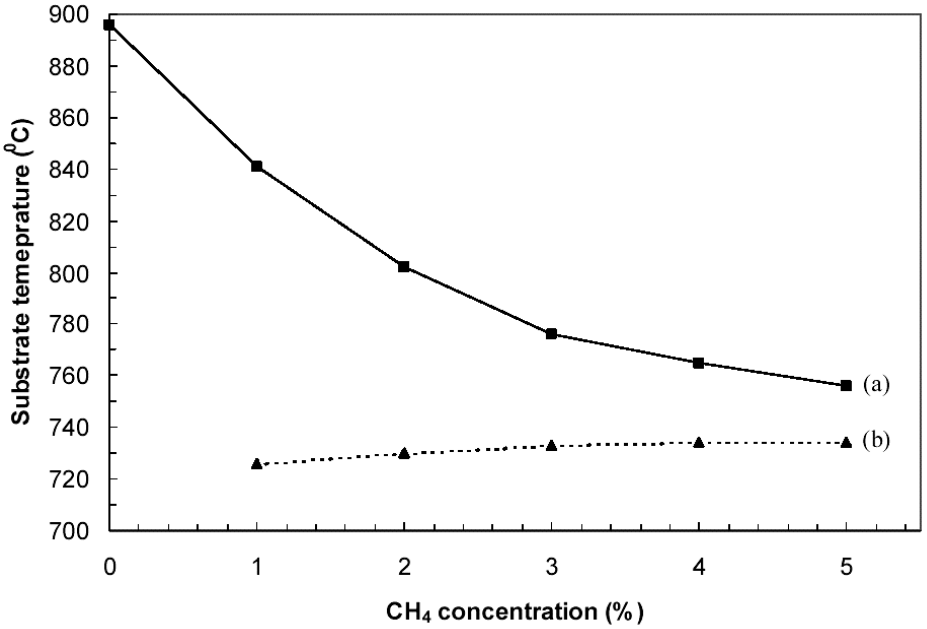

Figure 59 - Graph showing the relationships between substrate temperature and CH_4 concentration under standard diamond CVD conditions (a) and during no hydrogen flow (only CH_4) (b)

Figure 59(a) displays the graph relating substrate temperature to CH_4 concentration under typical diamond CVD growth conditions. Generally, the substrate temperature decreased with increasing CH_4 concentration. It should be noted that the observed temperature trend was obtained in the presence of two gases, namely, CH_4 and hydrogen, present in the reactor chamber during film growth. Since the TMCVD process pulses CH_4 at 3% and 2% concentrations, the fluctuation in the substrate temperature, from 776 to 802ºC, respectively, needs to be considered, as it is a critical factor influencing film growth during diamond CVD. In order to investigate the independent affect of CH_4 on substrate temperature, only CH_4, without any hydrogen, was introduced into the vacuum chamber. It is clear from figure 59(b) that the substrate temperature remains almost constant with varying CH_4 flow. Therefore, it can be stated that CH_4 flow has no significant affect on the substrate temperature. However, once excess of hydrogen ions are present in the CVD reactor then the resulting H_2/CH_4 plasma plays a critical role in governing the substrate temperature.

There are three main factors that can contribute to the substrate temperature changes observed during CH_4 pulses, namely, (i) gas species thermal motion, (ii) chemical

reactions between carbon-containing species and hydrogen, and (iii) the carbon-phase transitions. It is important to realize that generally during diamond CVD, these three factors come into play simultaneously. The mean-free-path (MFP) of the gas species is known to be proportional to both temperature and pressure. In our case, the pressure was kept constant at 30 Torr. However, since the substrate temperature fluctuates during CH_4 pulse cycles, this will alter the MFP of the reactive gas species present in the CVD reactor. But once the temperature is fixed the MFP remains constant. The deposition of diamond using CVD involves a number of complex chemical reactions occurring in the gas phase. The direction of the key reactions depends very much on two parameters, namely, temperature and pressure. Such reactions are accompanied by heat absorption (resulting in decreasing the substrate temperature) and heat release (resulting in increasing the substrate temperature). Generally, once the reaction is favored and proceeds towards the positive direction, then it can be expected that heat is released (exothermic reaction). Therefore, this could lead to increasing the substrate temperature as long as the preferred reactions are dominating. The other main factor, carbon-phase transition, occurring during diamond CVD also has a significant influence on the growth properties of diamond films. During diamond CVD, sp^3 carbon bonds appear under metastable conditions. The transition from sp^2 bond to sp^3 and/or from sp bond to sp^3 requires large amount of localized energy (not under thermal equilibrium). This phenomenon can potentially lead to decreasing the substrate temperature especially since there are less atomic hydrogen ions present in the hot-filament CVD reactor, as compared to microwave plasma CVD, which can force the key diamond CVD reactions in the positive direction. In our case, it is most likely that factor (iii) is having a greater impact, compared to factors (i) and (ii), on the substrate temperature.

Figure 60 displays the SEM micrographs showing the morphologies of samples A (a) and B (b). The image of sample B (b) has been magnified and shown as a separate image. The corresponding Raman spectra for samples A and B is also shown. Due to the growth phenomena observed in TMCVD, the surface of the deposited film is smooth. Both films displayed good uniformity and coverage. The morphology of sample B is different from that of sample A. From the two samples, sample B consisted of smaller sized diamond crystallites (~ 50-100 nm). Possibly more secondary nucleation occurs during sample B preparation than in sample A. This could again be due to the "substrate temperature effect". Secondary nucleation is mainly dependant on three factors in diamond CVD, namely, CH_4 concentration, pressure and substrate temperature. Since the overall CH_4 flow in sample B deposition was greater than in sample A, it can be expected that greater number of secondary diamond nuclei will deposit in sample B. It is worth noting that the effects of pressure will not dominate since this parameter was fixed throughout the CH_4 and temperature fluctuations.

Raman spectroscopy showed that the film quality, in terms of diamond-carbon phase purity, of sample A was better than sample B. Although, there is a very slight broad band emerging at around 1580 cm^{-1} on the sample A spectrum, the intensity of the characteristic Raman diamond peak was greater than sample B. The Raman spectrum for sample B displays a diamond-peak and shows no other non-diamond carbon phases. It is worth noting that throughout the two growth processes, during the production of sample B, hydrogen ions were produced and present in the reactor in

greater amount. This is due to the maintenance of the higher substrate temperature, 802ºC, during the film growth process. Whereas, during sample A deposition, the substrate temperature fluctuated at two values, 776 and 802ºC, for 10 and 8 minutes, respectively. It is known that at elevated temperatures hydrogen ions are generated more efficiently. As a result of the increased concentration of hydrogen ions present in the CVD reactor during sample B preparation, it can be expected that greater degree of non-diamond carbon phase etching occurs since hydrogen ions etch preferentially graphitic and amorphous carbon phases than diamond phase. However, since the secondary nucleation density is greater in sample B during each CH_4 pulse cycle, it can be expected that more grain boundaries exist in the film sample and possibly twinning occurs. This effect can be held responsible for the relatively lower sample B film quality.

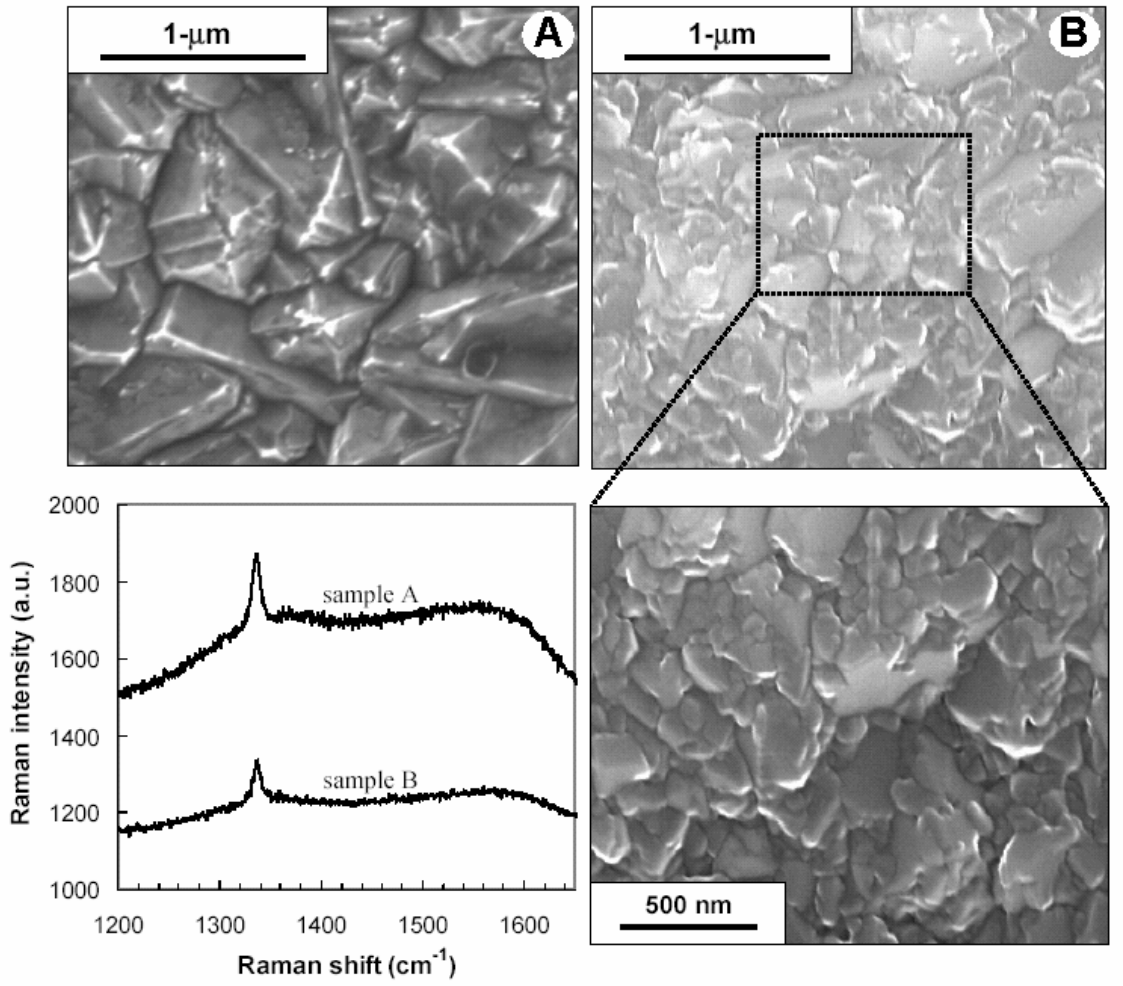

Figure 60 - SEM micrographs showing the morphologies of samples A (a) and B (b). The corresponding Raman spectra for samples A and B is also shown

It was found that samples A and B were deposited at growth rates of 0.70 and 0.77μm/hr, respectively. The constant substrate temperature can be held responsible for the increased growth rate in sample B. The higher substrate temperature (802ºC) observed during sample B deposition, compared to 776ºC noted in sample A formation, at a 3% CH_4 pulse enabled greater production of carbon-containing species, which favor diamond growth. Therefore, it can be expected that the growth rate is higher. It is

generally the case that increased substrate temperatures increase the growth rates [57]. The relatively increased secondary nucleation occurring onto the existing diamond crystals, in sample B, during each pulse cycle has enabled the filling up of the surface irregularities. Therefore, the resultant film displays a smoother surface. It was found that the surface roughness values (Ra) for samples A and B were 0.20 and 0.15μm, respectively.

5. Electrical behavior of deposit diamond films in {100} silicon wafers

In this study, we investigate the electrical properties, namely the complex conductivity, $\sigma^*(\omega,T)$ of diamond films deposited under different CH_4 flow rates and deposition time. The Cp-Rp model was employed to study the electrical properties in a range of controlled temperatures varying from 15ºC to 120ºC and frequencies between 75 kHz and 30 MHz. As a support, DC measurements of I-U was preformed.

The as-deposited film samples were characterized for diamond carbon phase purity using micro-Raman spectroscopy. In addition, the crystallinity, surface morphology and cross sectional analysis was performed using SEM.

The polycrystalline diamond films were deposit in the HFCVD system onto silicon {100} substrates (5.0 x 5.0 x 0.5mm). The substrates were abraded with diamond powder prior to film deposition in order to enhance the nucleation density and were ultrasonically cleaned in acetone in order to remove any loose abrasive particles.

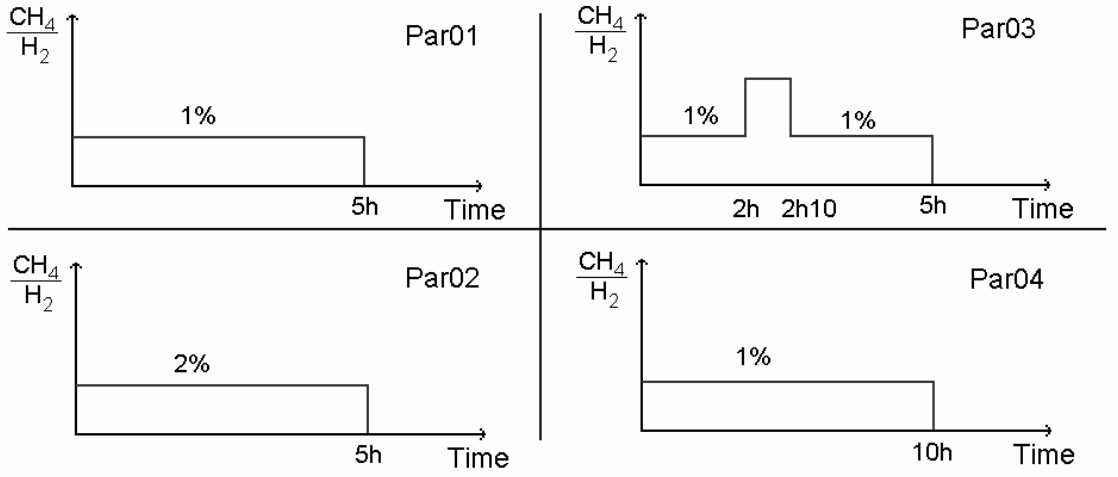

Figure 61 - CH_4 flows employed during preparing samples Par01 to Par04. The different concentrations of CH_4 in the CVD reactor, during film growth, and the total deposition times are evident from the graphs

Figure 61 displays the different CH_4 flows employed during the deposition of samples Par01, Par02, Par03 and Par04. Samples Par01, Par02 and Par04 were prepared, in the CVD vacuum chamber, under constant flows of CH_4. However, the concentration of the CH_4 gas in the vacuum reactor, during film deposition, while preparing the samples Par01, Par02 and Par04 was 1%, 2% and 1%, respectively. It should be noted that the deposition time for preparing samples Par01, Par02 and Par03 was 5

hours, whereas, the deposition time for preparing sample Par04 was 10 hours. The preparation of sample Par03 involved the intermediate modulated CH_4 step, where the CH_4 flow was maintained at 1.5 sccm for the first 2 hours, subsequently the CH_4 flow was modulated to 3 sccm for 10 minutes and then again lowered to 1.5 sccm. Sample Par05 represents a bare silicon wafer, similar to the ones used as substrates for the diamond deposition, but without any film coatings. Table 18 shows the complete deposition parameters.

Table 18 - Conditions employed during filament pre-carburization and film depositions

Parameter	Filament pre-carburization	Film deposition
Pressure (Torr)	30	30
H_2 flow (sccm)	150	150
CH_4 flow (sccm)	4.5	1.5(1%)–4.5(3%)
Substrate Temperature (ºC)	-	~800
Filament power (W)	280	~250
Filament-substrate distance (mm)	-	4
Deposition total time (hours)	0.5	5–10

To measure the electrical properties, the sample geometry used consisted of the parallel plate capacitor arrangement, in a Rp-Cp configuration. Typically, the samples displayed a thickness of approx. 0.5 mm and a surface area of approx. 25 mm2. For the a.c. measurements a HP 4285A LCR impedance meter was used, with the sample placed in a cryostat (figure 38), in order to obtain a temperature controlled between 15ºC and 120 ºC, with an accuracy better than 0.1 ºC. Figure 62 illustrates the set-up used during measuring the electrical properties of the film samples.

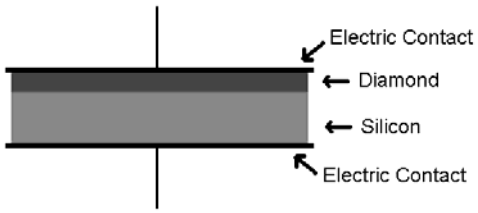

Figure 62 - Schematic of experimental set up employed for the characterization of the electrical properties of the deposited film samples

For sinusoidal electrical fields, the complex permittivity ε*, and the electrical complex conductivity σ*, are related to each other by equation (39) (chapter IV). It is usual to express the real part of the electrical conductivity as the empirical relation [58]:

$$\sigma'(\omega) = \sigma_0 + A\omega^s \qquad (42)$$

where σ_0 is the d.c conductivity, A is the pre-exponential factor and s is a exponent between 0 and 1. In the low frequency side a plateau value is obtained, which can be extrapolated to the d.c. conductivity σ_0, for $\omega \rightarrow 0$. This fact reflects that at low frequencies the outer electric field forces the charge carriers to drift over large distances when compared with the separation of the between neighboring sites. With

the increasing frequency the main displacement of the charges is reduced, thus, the frequency dependence of the conductivity reflects the effective topology of the conducting plates at a certain temperature [59].

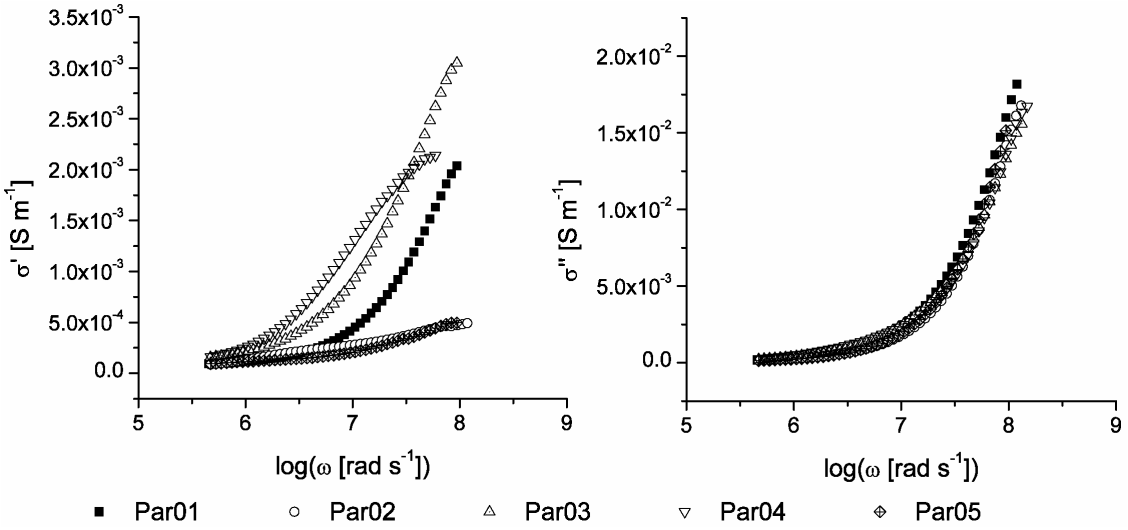

Figure 63 - Real and imaginary conductivities shown by samples Par01-05 at room temperature

In figure 63, we can observe the real and imaginary parts of the complex conductivity, at room temperature, for the 5 samples. For the imaginary part, the differences between the 5 samples are not significant, but they are important for the real part. The values for silicon substrate (Par05) and sample Par02 are similar. It is possible that the higher CH_4 flow employed in sample Par02 preparation induces a larger presence of amorphous carbon, which can be confirmed by the Raman spectra, as is shown in figure 64. From the Lorentzian disconvolution we can have an idea of the different scattering sources. In all the deposited samples one can find mainly polycrystalline diamond and amorphous carbon/graphite. However, sample Par02 displayed relatively intense graphite bands centered at 1615 cm^{-1}, the 1332 cm^{-1} diamond peak and a rather broad band at 1327 cm^{-1}, normally attributed to hexagonal diamond crystals. As a result, this can enable the formation of a thin conducting film, which does not affect the electrical complex conductivity of the original silicon substrate.

Although, samples Par01 and Par04 were deposited using 1% CH_4/H_2 mixture, but for different deposition times, sample Par04 consisted of relatively large sized diamond crystallites. In addition, sample Par04 displayed a small presence of amorphous carbon phase, as can be observed from the Raman spectrum, shown in figure 64. The Raman spectrum for sample Par01 displayed the diamond characteristic peak centered at 1332 cm^{-1} and also signaled the presence of D and G bands of microcrystalline graphite, peaks centered at 1354 cm^{-1} and 1576 cm^{-1}. Sample Par04 displayed the diamond peak centered at 1332 cm^{-1} and also small traces of graphite from the peaks centered at 1368 cm^{-1} and 1580 cm^{-1}. Grain boundaries are more important in this case, which explains the higher conductivity.

Sample Par03 was prepared by the partial employed TMCVD process. Typically, the TMCVD process continuously time modulates CH_4 flow throughout the film deposition

process. In this investigation, we have employed only one timed CH_4 modulation, as an intermediate growth step.

In sample Par03, small sized diamond crystallites were obtained, with two-layer morphology, with higher grain boundaries and consequently higher electrical conductivity. In sample Par03, the Raman spectrum displayed the diamond peak at 1333 cm^{-1}, some diamond precursors at 1338 cm^{-1} and some amorphous carbon at 1478 and 1594 cm^{-1}.

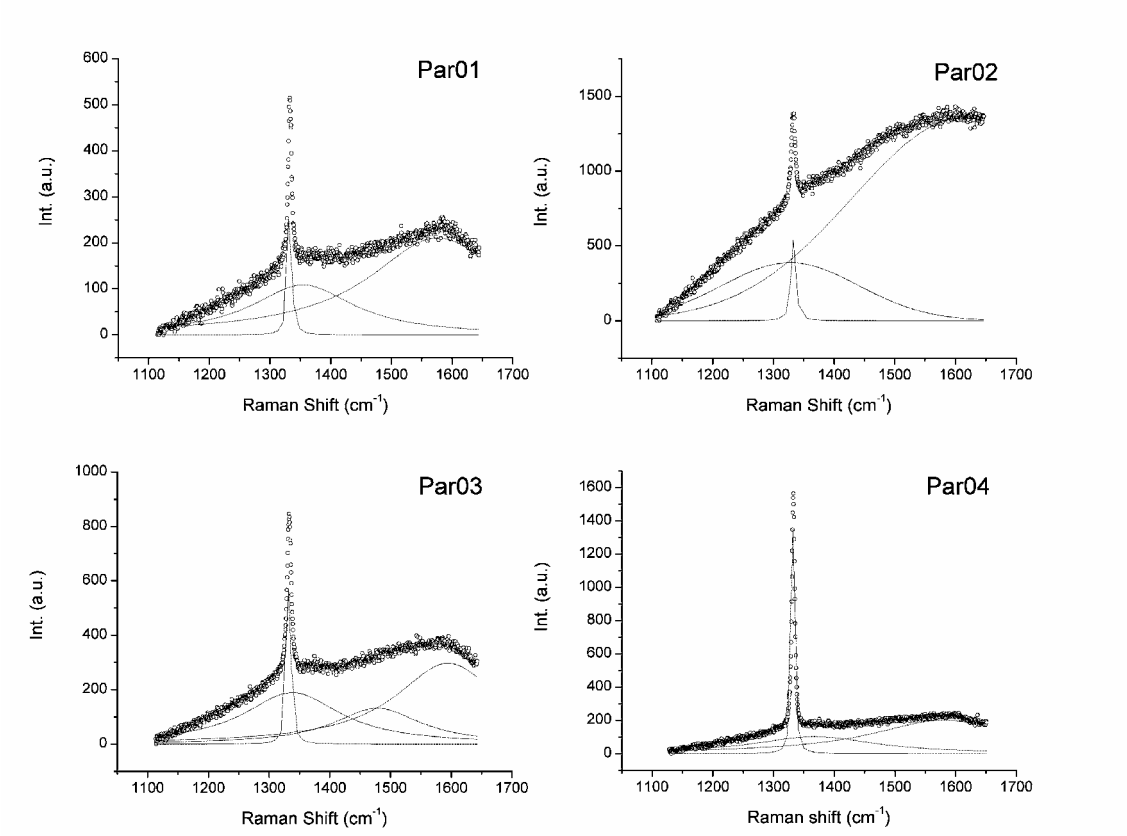

Figure 64 - Raman spectra with the signal disconvolution for samples Par01, Par02, Par03 and Par04

In order to further assess the quality of the deposited films, a semi-quantitative method previously presented in equation (14), was used to measure the 'quality factor', Q. Concerning our samples, sample Par04 displayed the highest quality factor value at 0.96 and sample Par02 displayed the lowest Q value at 0.48. Samples Par01 and Par03 displayed Q values of 0.79 and 0.83, respectively.

In the present case, the following factors can contribute to the quality of the film samples: (i) total CH_4 flow into the reactor during film deposition: (ii) the average crystallite size of the diamond films; and (iii) the film thickness. Obviously, the total CH_4 flow employed during the preparation of samples Par01-Par04 is different in each case. The Q value obtained for sample Par02 could be expected, since the methane flow into the reactor is relatively higher. As previously shown, higher CH_4 concentration in the CVD reactor, consequently deteriorates the film quality, in terms of diamond carbon phase purity.

Table 19 - Calculated parameters σ_0 and s. Equation (42) was used to perform the calculations

Sample	σ_0 (S m^{-1})	s
Par01	1.1×10^{-4}	0.59
Par03	1.6×10^{-4}	0.85
Par04	1.5×10^{-4}	0.77

Table 19 presents the results obtained with DC measurements, which are comparable with the low frequency conductivity, and the 's' exponent for the different samples, which are consistent with the above explanation. The universality of the observed behavior is confirmed by the calculated correlation factors.

For all the samples, an ohmic behavior was observed in DC electric properties analyses.

Figure 65 shows the complex conductivity of three samples, Par01, Par03 and Par04, at different temperatures. The comportment is described by equation (42). It is observed that the influence of the temperature is more important for Par01, the most resistive of the three films, corresponding to higher activations energies. The observed non-linearity in figure 66 is an indication of temperature dependent activation energy. These energies are estimated for different temperatures and samples, which are shown in figure 67. The more conducting sample, Par04, has the smallest activation energy, and the higher energy is calculated for Par01, the more resistive sample. This is evidence that the thermal activation energy plays a critical role in the conducting processes of these materials.

Figure 68 displays the SEM micrographs of samples Par01 to Par04. All the four samples displayed excellent film uniformity. It is also clear that sample Par04 consisted of larger sized diamond grains. From the enclosed zoomed images, one can notice that the films are polycrystalline in nature, with {111} predominant crystal orientation. Cross-section SEM micrographs (not shown) gave information about the film thickness values of the films. The average film thinness value for samples Par01, Par02 and Par03 was 2 μm, whereas, the average film thickness of sample Par04 was 3.5 μm.

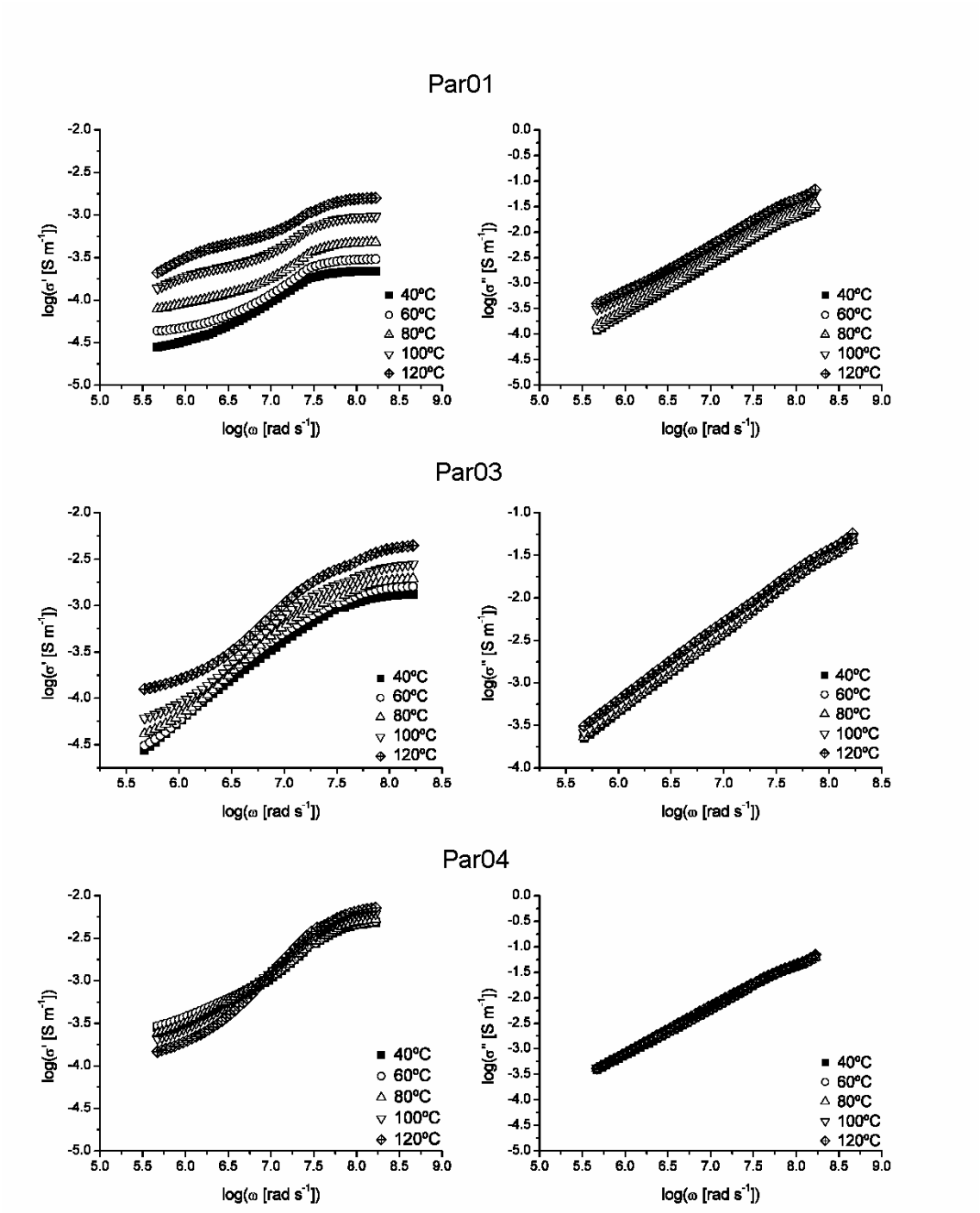

Figure 65 - Real and imaginary conductivities of Par01, Par03 and Par04 at different temperatures

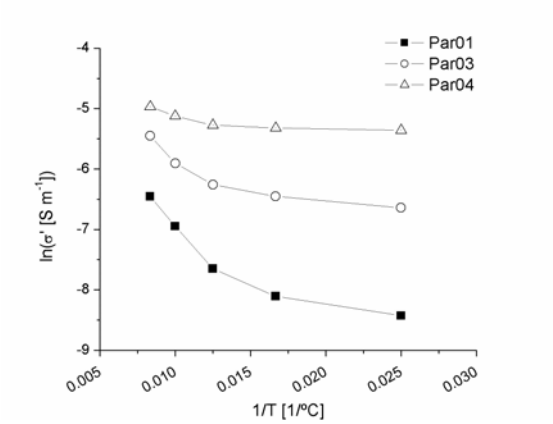

Figure 66 - ln σ´ versus 1/T of Par01, 03 and 04 at 21.1 MHz

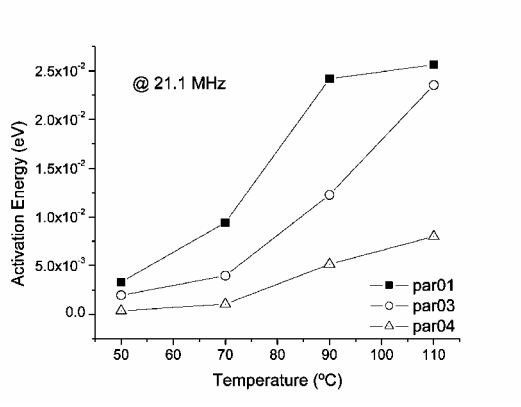

Figure 67 - Activation Energy of Par01, 03 and 04 at 21.1 MHz

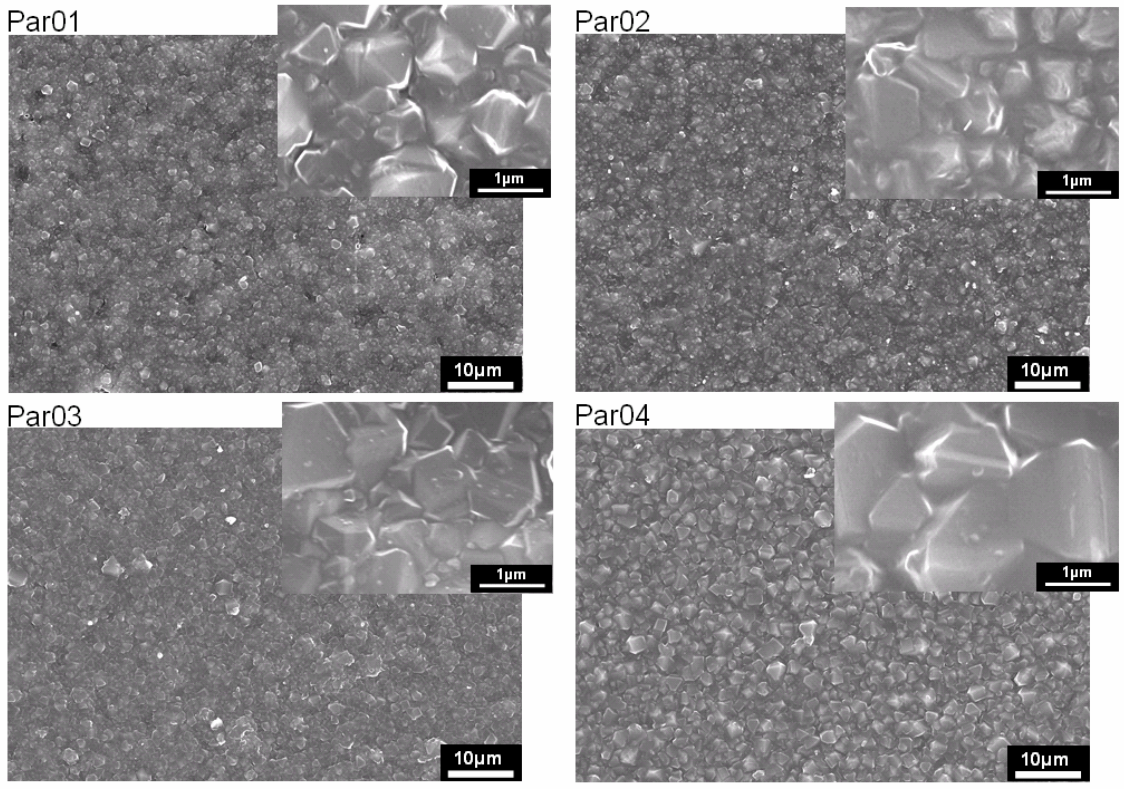

Figure 68 - SEM micrographs of samples Par01, Par02, Par03 and Par04

6. Applications

It has been preformed some, not fully developed, applications of the newly developed coating process, namely surface engineering of small dental tools and heart valves components.

6.1. Surface engineering of WC-Co used in dental tools

The degree of difficulty involved in depositing diamond onto WC–Co substrates increases with increasing cobalt concentration. In addition, it is easier to deposit diamond onto larger grained WC than onto smaller grained WC. Cemented WC–Co consisting of 10% cobalt and micrometer to sub-micrometer WC grains are typically used in the manufacture of dental tools and micro-drills. There are few reports in the literature regarding diamond growth onto this 'grade' of hard metal. In addition, very few workers have investigated diamond deposition onto dental burrs in any great detail. Borges et al. [60] employed a dc arc jet reactor to deposit diamond coatings onto dental burrs. Airoldi et al. [61] deposited diamond films onto dental burrs using a hot filament CVD system, where the system configuration was such that two filaments were employed and the dental burrs were placed on a rotary substrate holder between the two filaments. The burrs were rotated during film growth in order to obtain uniform film coatings. H. Sein et al. [62] have recently modified a conventional hot filament CVD system to deposit thick diamond coatings onto small tools such as dental burrs and micro-drills. The modification was such that the filament was placed vertically in the deposition chamber and the burrs were inserted concentrically within the coils of the filament. It may be of interest to note that this system can be operated in the time modulated mode for more precise control and reproducibility.

The major difficulties facing diamond deposition onto WC–Co tools are low diamond nucleation density and poor coating adhesion. The main culprit preventing successful diamond deposition onto WC–Co is cobalt, the binder material. The cobalt binder suppresses diamond nucleation and causes deterioration of film adhesion [63]. Many researchers have employed a range of different surface pretreatment methods to etch out effectively the surface cobalt and prepare the surface for subsequent diamond growth [64-68]. A broad range of cutting tool applications become accessible if adherent diamond films can be deposited onto WC– Co. Therefore, a detailed study of diamond nucleation and adhesion onto WC–Co used in dental burrs is highly relevant and timely.

This investigation studies diamond nucleation and deposition onto 10%Co, micrometer grain WC substrates. In order to assess the coating adhesion and obtain a better understanding of coating – substrate interactions, diamond coatings were deposited onto flat cemented WC–Co substrates, of comparable grade to the WC–Co used in dental burrs.

The hot filament CVD system was used in the conventional and in the modified form to deposit diamond coatings onto flat WC–Co substrates and dental burrs, respectively. The dental burrs and flat WC–Co substrates contained 10% cobalt and the WC grain size was in the range 0.8 –1 μm. The dental burrs were 20 mm in length (10 mm, burr

head (WC–Co), 10 mm (Fe/Cr) burr shaft) and 1 mm in diameter. Prior to diamond deposition, the substrates were ultrasonically cleaned in acetone for 10 min in order to remove any loose residues. It is known that the poor adhesion of deposited diamond films onto cemented carbide tools can lead to catastrophic failure of the coating during metal cutting [69]. The substrates, after being ultrasonically cleaned in acetone, were chemically etched in Murakami solution (10g $K_3(Fe(CN)_6)$+10g KOH+100mL of water), containing diamond powder for seeding effects, for 15 min in an ultrasonic bath followed by a rinse in distilled water. The substrates were then etched for 60s in HNO_3(10%)+H_2O_2(90%) in an ultrasonic bath. Finally, the substrates/burrs were cleaned in ultrasonically deionized water for 3 min. The deposition conditions employed during diamond CVD onto dental burrs and flat WC–Co substrates are shown in table 20. The performance of the diamond coated and conventional diamond particle imbedded burrs was tested using drilling procedures into extracted human teeth. Holes were drilled, at 30 000 rev.min^{-1} rotational speeds, into the teeth using a sequence of 50 drilling tests.

Table 20 - Film growth conditions employed during diamond CVD onto dental burs and flat cemented WC-Co substrates

Parameter	Dental Burs	Flat WC-Co
Filament-substrate distance (mm)	4.5	4
Pressure (Torr)	20	30
Methane concentration (%)	1	2
Hydrogen concentration (%)	99	98
Deposition time (hours)	14	0.5, 2

The as grown diamond films were characterized for morphology and crystallinity using SEM. In addition, a Raman spectroscopy was used to characterize the deposited diamond films for diamond carbon phase purity. The coating adhesion was assessed using an indentation method employing a Rockwell C indenter. Indentation loads of 300 and 500 N were imposed on the coated samples to characterize the coating adhesion strength.

6.1.1. Study on flat cemented WC–Co substrates

Figure 69 shows: (a) the nucleation of diamond crystallites on flat WC–Co substrate after 30 min deposition; (b) the morphology of as grown film deposited for 2 h onto flat WC substrate under standard deposition conditions; and (c) the Raman spectrum for the film shown in 1b. The SEM micrograph figure 69(a) shows the diamond crystals (lighter in color) nucleating on top of the WC grains. It was found that under the conditions employed in this study, 30 min was not sufficient to form the first diamond layer on the cemented WC–Co substrate. This can be expected, since diamond nucleation and growth onto WC–Co is rather difficult. However, the chemical pre-treatment used in this was effective in etching out the cobalt from the near surface region of the substrate. The morphology of as grown film, deposited for 2 h under the conditions outlined in table 20, is shown in figure 69(b). It was found that the diamond

film deposited onto WC–Co was polycrystalline in nature and the coating displayed good film coverage and uniformity.

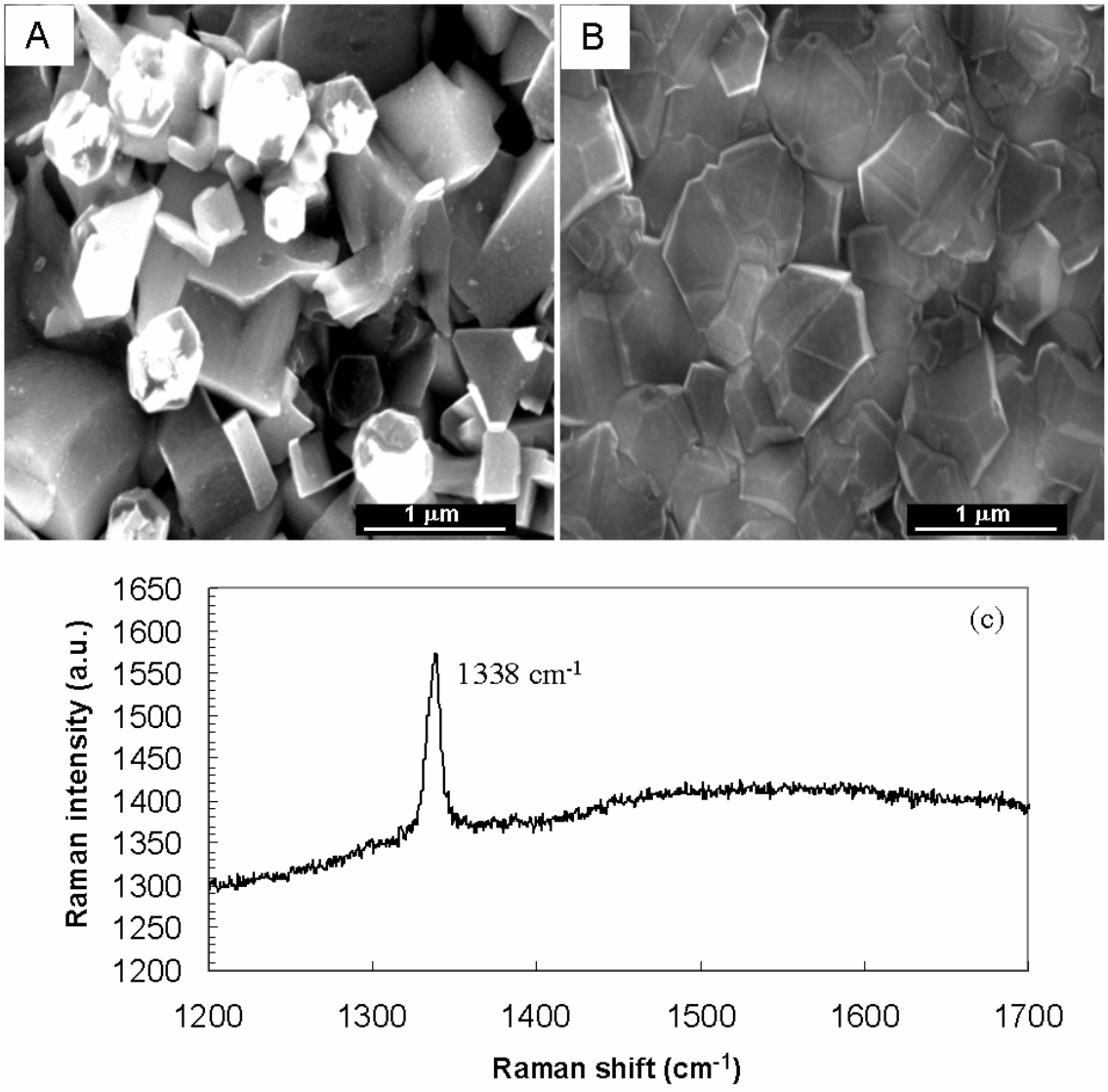

Figure 69 - SEM images showing the nucleation of diamond crystallites on flat WC-Co substrate after 30 minutes of deposition (a); the morphology of the as-grown film deposited for 2 hours onto the flat WC substrate under standard deposition conditions (b); and (c) the Raman spectrum for the film shown in 1(b)

The film was found to be approx. 0.8–1μm in thickness. The average crystallite size of the diamond grains measured from SEM micrographs was found to be smaller then 1 μm. SEM analysis showed a continuous film and there were no voids present in the film coating. This suggests that the cobalt was kept suppressed during film growth on the WC substrate, therefore, the diffusion rate of Co to the surface can be expected to be low. In order to assess the quality of the film grown, as shown in figure 69(b), in terms of diamond carbon phase purity, Raman spectroscopy was used. A fairly intense peak, centered at 1338 cm^{-1}, was clearly evident on the Raman spectrum. This peak signals the existence of fairly good quality diamond. No other major peaks were observed on the spectrum, other than the characteristic Raman diamond peak. From

the positioning of the peak on the spectrum the film is believed to be under compressive stress. This is due to the large difference in the thermal expansion coefficient values for WC–Co substrate and diamond coating deposited onto it. However, the film can accommodate these stresses without debonding from the substrate. Though Ager and Drory investigations, we can calculate the stress value (23.4GPa) in compression.

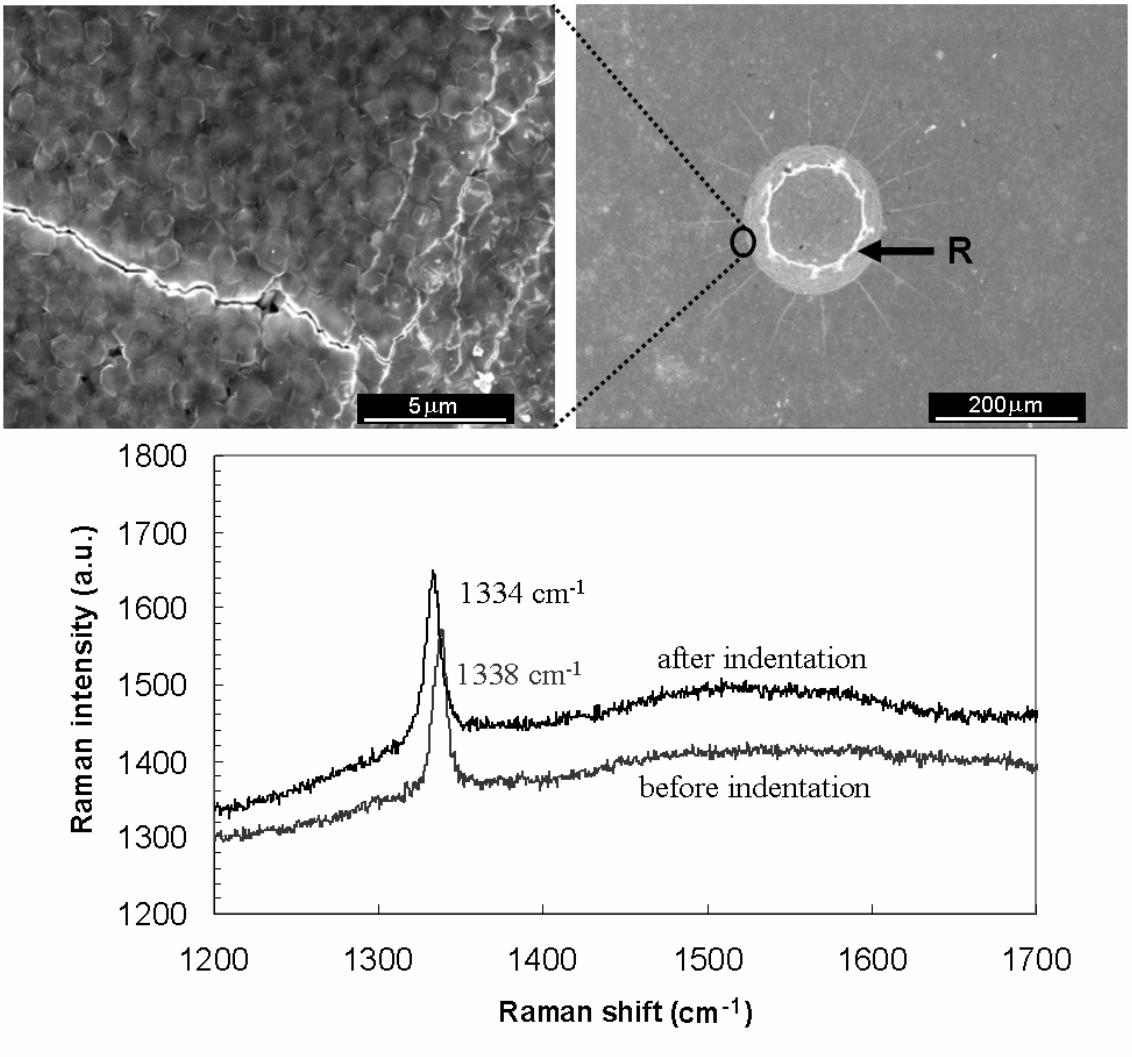

Figure 70 - SEM image of the indented diamond-coated flat WC-Co substrate and the Raman spectra showing the positioning of the Raman diamond peaks before and after the 300N load indentation. A close up view of one of the film lateral cracks is also shown in a separate SEM micrograph

Figure 70 shows a SEM image of the indented diamond coated flat WC–Co substrate and Raman spectra showing the positioning of the Raman diamond peaks before and after the 300 N load indentation. The positions taken for Raman analysis on the coating were as follows: before indentation, well outside the indentation region (in the as grown state); after indentation, at point ‘R’ marked on the SEM image. It is clear that a 300 N load imposed on the diamond coated WC–Co substrate inflicted damage to the sample.

The SEM shown in figure 70 resembles a 'sun shining'. It is clear that some lateral cracking has occurred, which corresponds to the 'rays' of the sun on the SEM micrograph image. A section of the lateral crack on the coating was closely examined using SEM and a magnified image is shown in figure 70. It can be seen that the polycrystalline diamond film has cracked, mainly along the film grain boundaries. The lighter regions forming the circumference to the indentation mark represent parts of the coating that have experienced some localized film cracking. Although the coating remains attached to the substrate, even after localized film cracking, the coating deforms to the shape of the indenter. This is due to the plastic deformation processes occurring on the substrate during indentation loading. The lateral cracks could have two possible causes. First, the external stresses imposed onto the coated sample during indentation loading may well force the film to crack in order to dissipate stress and/or energy. Second, the underlying substrate could fail and cause film cracking during plastic deformation at the substrate. However, the result of the 300 N load indentation enables us to deduce that the coating adhesion can tolerate a 300 N load indentation and the critical load required to delaminate the film from the substrate is >300 N. It is at the critical load value that debonding occurs at the film/substrate interface. The Raman spectra show that prior to indentation, the Raman diamond peak was centered at 1338 cm^{-1}, i.e. in the as grown state.

The stress in the film prior to the 300 N load indentation was calculated to be 23.4GPa, in compression. However, after indentation, the Raman diamond peak shifted from 1338 cm^{-1} to 1334 cm^{-1}. The shift in the Raman peak suggests that the film becomes slightly less stressed, 21.13GPa, and debonds slightly from the substrate. A completely stress free diamond film displays an intense peak centered at 1332 cm^{-1}. Therefore, after indentation, the interface between the film coating and the substrate slightly weakens. However, the coating adhesion is strong enough to withstand the stresses without delaminating in both cases, before and after indentation.

In order to determine the critical load necessary for film delamination, it was necessary to perform another indentation, but at a higher load of 500 N.

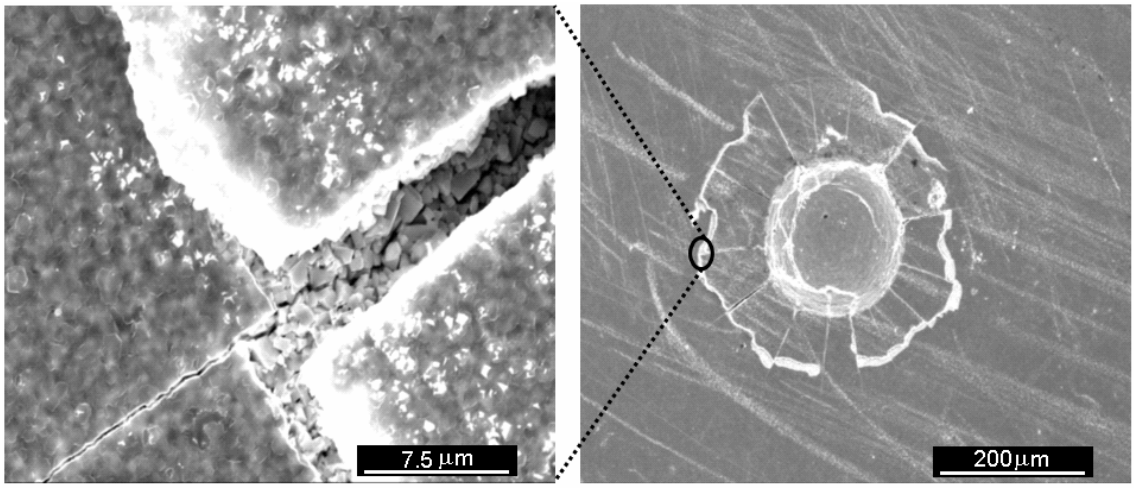

Figure 71 - SEM image of the indented diamond-coated sample after a 500 N load indentation. A magnified view of the outermost region, from the indentation mark, of one of the lateral cracks is also shown

Figure 71 shows an SEM image of a sample after a 500 N load indentation. It is observed that the coating has cracked and lifted off from the substrate at the outer regions of the lateral cracks/sun rays. At regions where the coating has lifted from the substrate the film behaved similarly to a stress free, free standing film. However, it was noted that the coating at and around the indentation mark remained attached to the substrate. However, around the indentation mark the film had experienced severe and extensive cracking. A magnified view of the outermost region, from the indentation mark, of one of the lateral cracks is shown in figure 71. The lift-off and detachment of the film from the substrate is clearly evident in the SEM image. In addition, it can be seen that the underlying substrate has undergone lateral cracking. Therefore, possibly the substrate initially cracks laterally during indentation loading and as a result of the cracking a mechanical stress is applied to the inner surface of the coating. Due to the mechanical stress imposed on the coating and the dissipation of energy resulting from the cracking processes, the region of the film covering the crack length also cracks and follows the substrate radial crack lines.

The lateral cracking of the cemented WC–Co substrate is due to the fracture toughness of the material, which usually increases with cobalt concentration in the tungsten carbide.

Summarizing, from the two indentations performed at 300 and 500 N load, it is not possible to determine exactly the precise critical load value required to delaminate the film coating from the WC–Co substrate. However, it can be stated that the critical load value lies between 300 and 500 N.

6.1.2. Study on cemented WC–Co burs

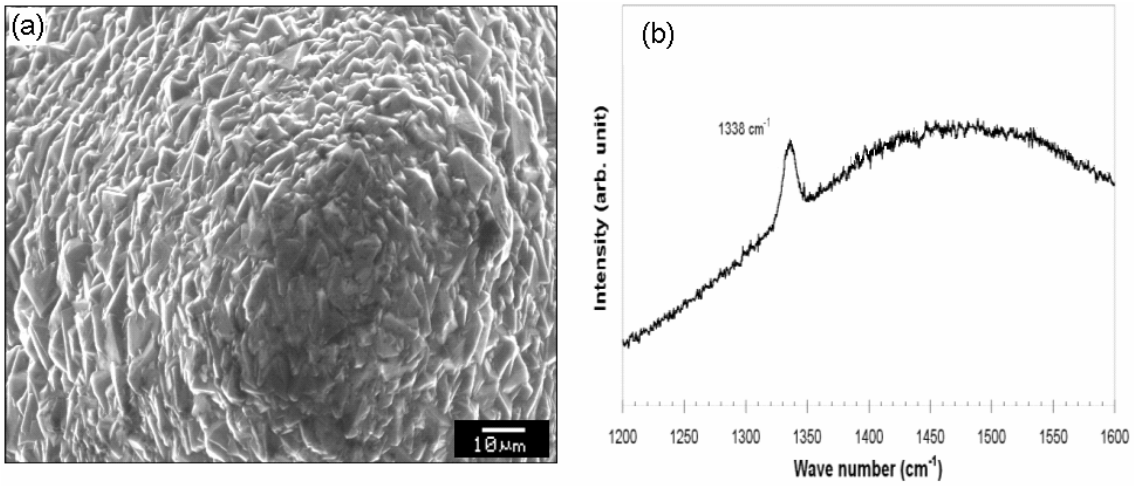

Figure 72 - SEM image showing the tip of the diamond-coated dental bur. The corresponding Raman spectrum is also shown

Figure 72 shows an SEM micrograph of the as grown diamond film deposited onto a cemented WC–Co dental burr and the corresponding Raman spectrum for the film.

The SEM image, displaying the top end view, shows the tip of the diamond coated bur. This SEM image clearly displays the unique ability of CVD to coat extremely complex shaped components uniformly. As expected, the deposited film is polycrystalline in

nature. The film consisted of diamond grains that exhibited predominantly {111} crystal orientation, which is the preferred and most effective crystal orientation for cutting tool applications. The average size of the crystals was found to be in the range 1–5 μm.

The Raman spectrum of the as grown film displayed a diamond peak that was centered at 1338 cm^{-1}. In addition, a broad band centered at around 1500 cm^{-1} was also present on the spectrum. This broad band signals the presence of amorphous carbon in the deposited film covering the dental bur. The stress in the film covering the dental burr was calculated to be 23.4GPa, in compression.

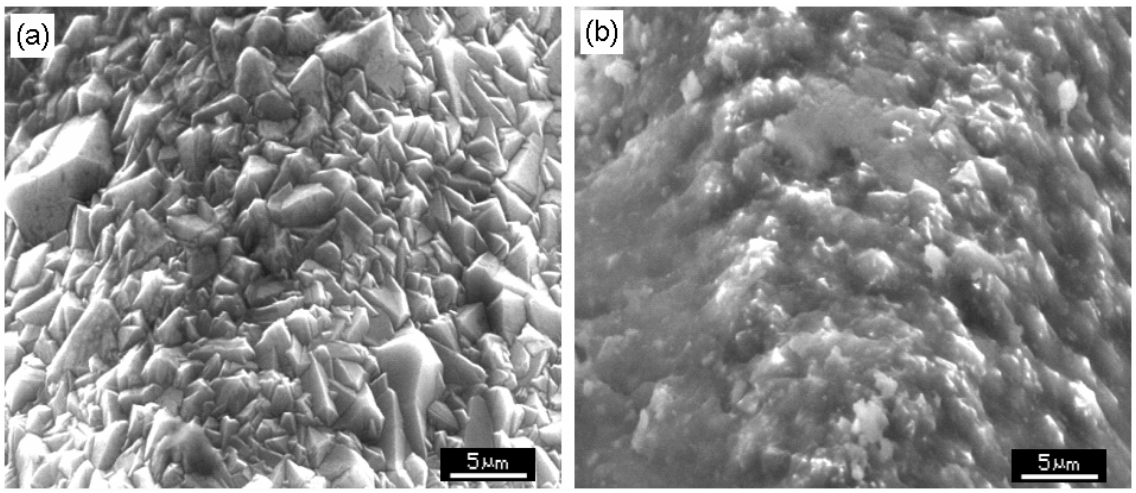

Figure 73 - SEM micrographs of the diamond-coated dental bur before (a) and after (b) the drilling of 500 holes into human teeth

Figure 73 shows SEM micrographs of diamond coated WC–Co dental burrs before (a) and after (b) performance testing. After every 10 drilling operations, the geometry, i.e. sharpness and diameter, of the burr was inspected using an optical microscope. Generally, a good cutting tool produces accurate cutting with very little loss of material from the cutting edges.

It was found that the CVD diamond coated dental burrs did not degrade in performance, even after 500 holes were drilled. The polydiamond crystals remained completely intact on the burr after 500 holes were drilled at 30 000 $rev.min^{-1}$, into human teeth. It can be seen on the SEM image in figure 73(b) that the diamond particles are intact and also that dentine from the wisdom teeth is also present on the bur. However, after washing the bur, the dentine was removed and the polycrystalline diamond coating was clearly visible and remained undamaged. In comparison, conventional diamond imbedded burrs revealed that most of the imbedded diamond particles were dislodged from their cavities after drilling 500 holes under similar conditions.

These results show the promise of CVD as a viable alternative technology to conventional diamond dental burrs. However, there is still considerable work to be done on scaling up the technology in order to coat multiple components economically.

6.2. Deposition of nanocrystalline diamond onto artificial heart valves

Heart disease is one of the most common causes of death in the world today, particularly in the western countries. The failure of heart valves accounts for about 25-30 % of heart problems that occur today. Faulty heart valves need to be replaced by artificial ones using sophisticated and sometimes risky surgery. However, once a heart valve has been replaced with an artificial one there should be no need to replace it again and it should last at least as long as the life of the patient. Therefore, any technique that can increase the operating life of heart valves is highly desirable and valuable. Currently, pyrolytic-carbon (PyC) is used for the manufacture of mechanical heart valves.

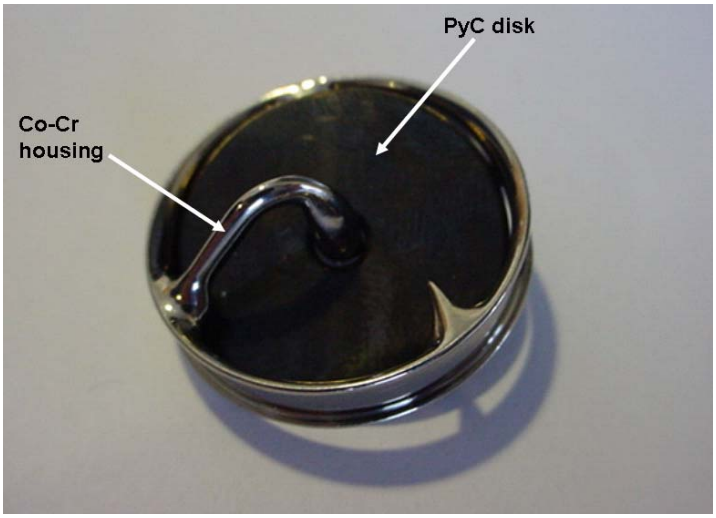

Figure 74 - A typical leaflet mechanical heart valve, from Medtronic, USA

Figure 74 shows a typical PyC leaflet heart valve. Although, PyC is widely used for heart valve purposes, it is not the ideal material. In its processed form, PyC is a ceramic-like material and like ceramics, it is subject to brittleness. Therefore, if a crack appears, the material, like glass, has very little resistance to the growth/propagation of the crack and may fail under loads. In addition, its blood compatibility is not ideal for prolonged clinical use. As a result, thrombosis often occurs in patients who must continue to take anti-coagulation drugs on a regular basis [70]. The anti-coagulation therapy can give rise to some serious side effects, such as birth defects. It is therefore extremely urgent that new materials, which have better surface characteristics, blood compatibility, improved wear properties, better availability and higher resistance towards breaking are developed. In artificial heart valve applications, a principal requirement is that the surface should essentially display a smooth surface, since surface roughness causes turbulence in the blood, which leads to the integrity of the red cells being damaged causing bacteria to adhere, and blood coagulation and clots. A possible method to increase the degree of PyC thrombo-resistance is by alloying the material with silicon [71].

Although, research on the surface engineering of mechanical heart valves has been limited and restricted, a number of researchers have attempted to develop

biocompatible coatings, which could potentially be used for artificial heart valve purposes. For example, carbon nitride (CN) thin films have been investigated for biocompatibility and their properties strongly suggest their potentials for use in various surgical implants [72]. Generally, both the bio- and haemo- compatibilities of DLC coatings have been extensively investigated and widely reported in the open literature [73]. Jones et al. [74] deposited DLC coatings, consisting of multilayers of TiC and TiN, onto titanium substrates and characterized the coatings for haemocompatibility, thrombogenicity and interactions with rabbit blood platelets. It was found that DLC produced no haemolytic effect, platelet activation or tendency towards thrombus formation. Furthermore, the platelet spreading correlated with the surface energy of the coatings. Thomson et al. [75] and Dion et al. [76] have also investigated DLC coatings and characterized their biological properties.

It is worth considering that titanium and its alloys have been used in biomedical implants for many years now and therefore it is sensible to look at the surface treatment of titanium alloys for producing superior surface characteristics, which could be ideal for heart valves. It should be noted that titanium alloys are not brittle like PyC.

A large number of research scientists have deposited Ti-based coatings, using energized vapor-assisted deposition methods, and studied their potentials for use in biomedical areas, such as heart valves or stents. Yang et al [77] deposited Ti-O thin films using plasma immersion ion implantation technique and characterized the anti-coagulant property employing in-vivo methods. They found that the Ti-O film coatings exhibited better thrombo-resistant properties than low-temperature isotropic carbon (LTIC), in long-term implantation. Chen et al [78] deposited TiO coatings doped with Ta, using magnetron sputtering and thermal oxidation procedures, and studied the antithrombogenic and haemocompatibility of $Ti(Ta^{+5})O_2$ thin films. The blood compatibility was measured in-vitro using blood clotting and platelet adhesion measurements. The films were found to exhibit attractive blood compatibility exceeding that of LTIC. Leng et al [79] investigated the biomedical properties of tantalum nitride (TaN) thin films. They demonstrated that the blood compatibility of TaN films was superior to other common biocompatible coatings, such as TiN, Ta and LTIC. Potential heart valve duplex coatings, consisting of layers of TiO and TiN, have been deposited onto biomedical Ti-alloy by Leng et al. [80] and their blood compatibility and mechanical properties have been characterized. The TiO layer was designed to improve the blood compatibility, whereas, TiN was deposited to improve the mechanical properties of the TiO/TiN duplex coatings. They found that the duplex coatings displayed (i) better blood compatibility than LTIC; (ii) greater micro-hardness; and (iii) improved wear resistant than Ti6Al4V alloys. It has been reported that the TiO coatings display superior blood compatibility then LTIC [81].

From the above, it is clear that reasonable effort has been made to address the common concerns facing artificial heart valves. A broad range of biological coatings, including CN, DLC, TiC, TiN, TiO, TaN, TiO/TiN, have been deposited, using a number of different methods, with the aim to improve the characteristics, both in terms of blood compatibility and mechanical behavior, of surfaces for potential biomedical use.

However, there have been no reports, to the author's knowledge, of the use of NCD coatings in the surface engineering of artificial heart valves.

In this study, we characterize the mechanical and micro-structural properties of artificial heart valve disks (HVD) made of PyC and the preparation of freestanding nanocrystalline diamond films (FSND) using TMCVD process.

6.2.1. Characterization of mechanical and micro-structural properties of artificial heart valve disks

Leaflet HVD made of PyC (Medtronic, USA) were used in this investigation. The diameter measurements of the HVD were: outer diameter- 15mm, inner diameter- 3 mm. The mechanical strength of PyC, cobalt chrome (Co-Cr) and biomedical titanium alloy (Ti6Al4V) was assessed using conventional indentation test methods employing a Brinell indenter. The indentation loads applied to the samples were maintained imposed for 30 seconds before withdrawing the indenter tip. The diameter values of the indented samples were measured using an optical microscope. Conventional pin-on-disk technique was used to measure wear rates and the coefficient of friction values of PyC. The pin-on-disk experiments were performed at 38ºC and at a speed of 239 $rev.min^{-1}$. The maximum distance covered by the revolving sample during testing was 4000 meters. The wear rate and the coefficient of friction values were recorded automatically by the computer during testing.

A number of indentations at different loads were performed onto PyC, CoCr and Ti6Al4V substrates. Figure 75 displays the graph showing the relationship between indentation load and indentation diameter for three different biomaterials. The PyC deformed to a greater extent and broke at a much lower load compared to CoCr and Ti6Al4V. Both CoCr and Ti6Al4V are widely used biomaterials in artificial hip-joint applications. It is one possibility that these materials can be considered for use in artificial heart valves. It was noted that Ti6Al4V displayed greater resistance to deformation than CoCr at all indentation loads. The PyC snapped in between the indentation load range ~ 51-63 N.

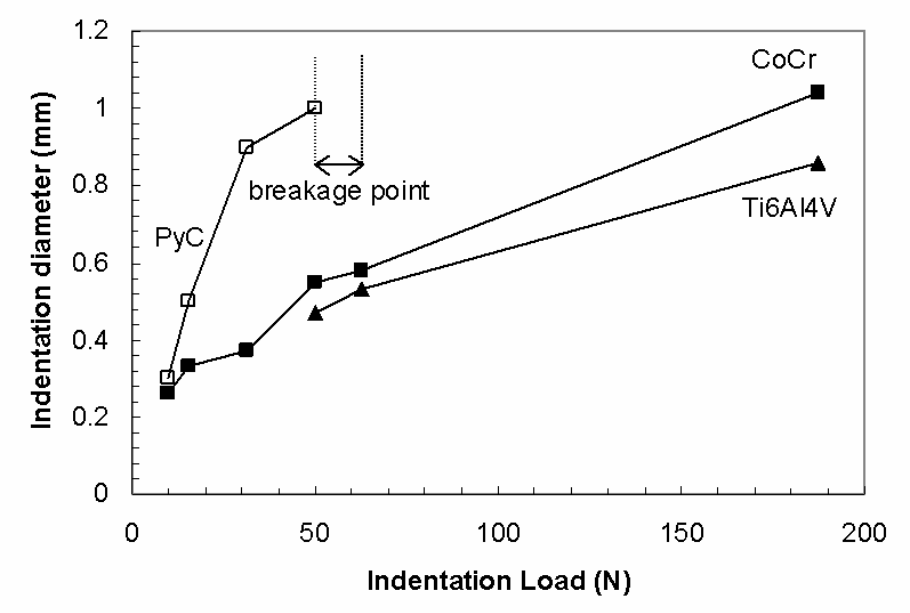

Figure 75 - Graph showing the relationship between indentation load and indentation diameter for three different biomaterials

PyC has a unique property, unlike true ceramics; it is comparatively ductile. Thus, if a sharp, hard object is pressed into the material, it can respond by deforming locally in order to accommodate the object elastically. Once the object is removed/withdrawn, there may be (unlike for a ceramic) no residual depression, and little or no micro-cracking surrounding the site. It is this intrinsic, atomic microstructure-derived resistance to externally imposed crack nucleation that permits such an otherwise brittle material to be used in the human body. However, despite this tendency of PyC to resist micro-crack nucleation/propagation, cracks can and do occur. PyC belongs to a carbon family called “turbostratic”. It consists of a network of carbon atoms covalently bonded together, similar to the bonding in graphite, in planes. However, the planes in graphite are much more ordered than in the PyC structure, where the planes are disordered. The disorder in the planes introduces additional beneficial characteristics in PyC compared to graphite.

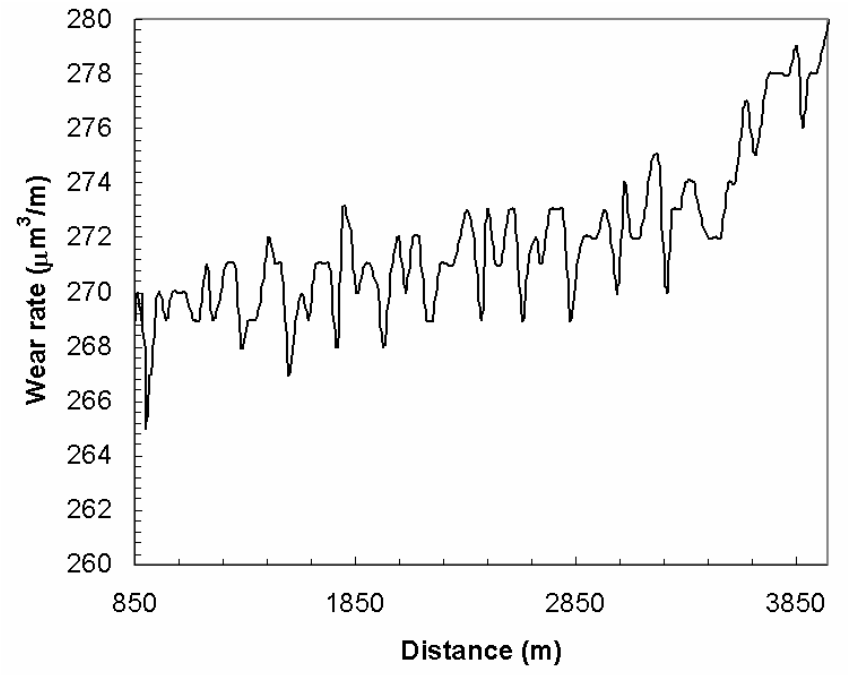

Figure 76 - Graph showing the wear rate of PyC with distance

Figure 76 represents the graph showing the wear rate of PyC with distance, as obtained from the pin-on-disk test method. Generally, it was noted that the wear rate increased steadily with distance. It is expected that the material undergoes abrasive wear during the pin-on-disk testing. Figure 77 shows the coefficient of friction values for PyC observed during pin-on-disk testing. The values for the coefficient of friction generally increased steadily with distance. The observed increase in the coefficient of friction values with was noted to be from approximately 0.16 to 0.21.

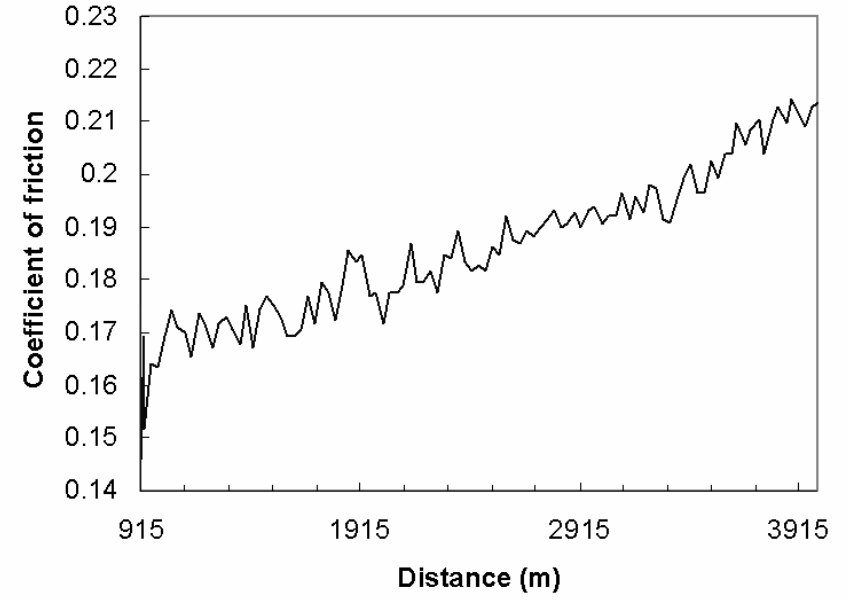

Figure 77 - Graph showing the coefficient of friction values for PyC observed during pin-on-disk testing

6.2.2. Freestanding nanocrystalline diamond films (FSND) used as HVD

In this section, it is described the deposition of FSND to possible replacement of artificial heart valves. Replacing conventional HVD with FSND can potentially overcome the strength limitations in PyC, since diamond is the hardest known material.

The FSND films, in the shape of HVD, were deposited onto HVD using the TMCVD process. The growth conditions employed during film deposition were as follows: hydrogen flow, 150 sccm; methane (CH_4) concentration, 3 and 2 %; (CH_4) modulations, 3% (5 mins), 2% (10 mins); pressure, 30 Torr; deposition time, ~ 1 hour. Three FSND film samples, A1, A2 and A3, were prepared at 650, 700 and 850ºC, respectively.

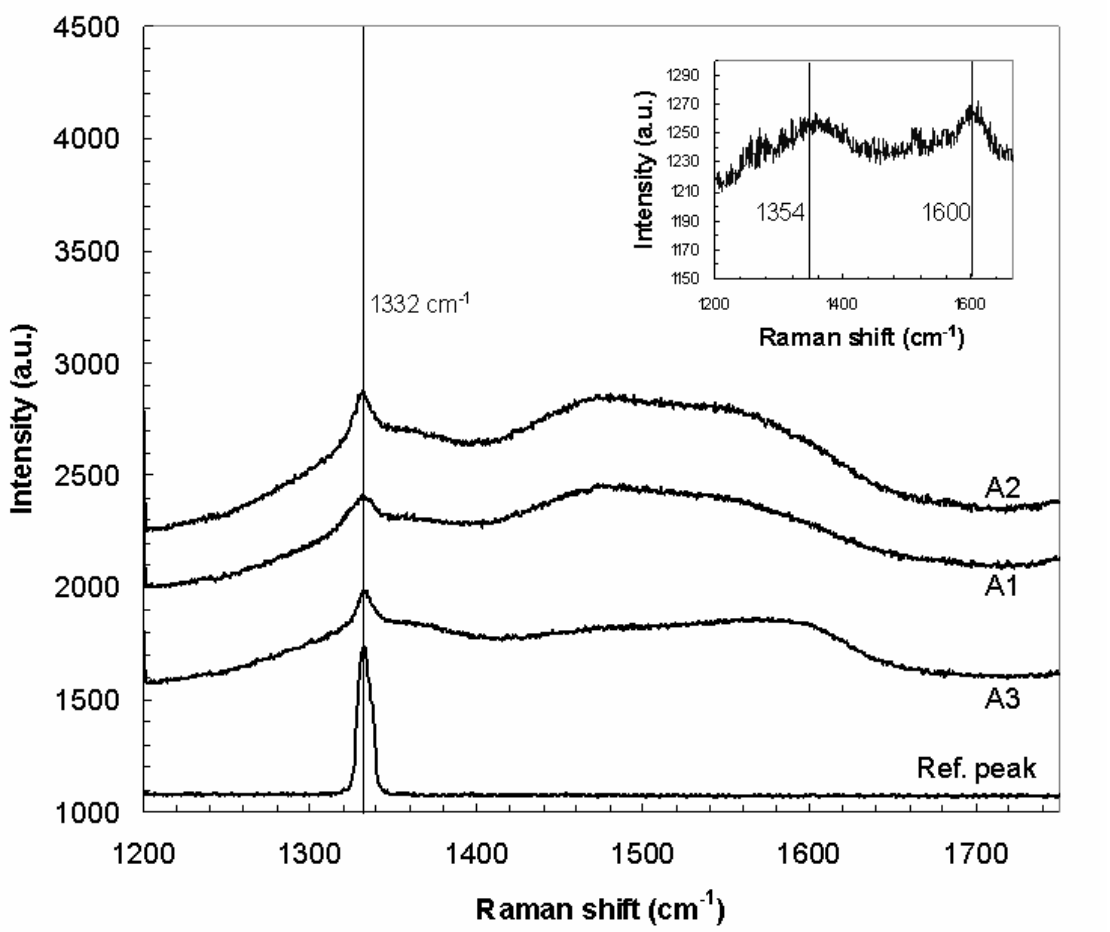

Figure 78 - Raman spectra for samples A1, A2 and A3. The inset represents the Raman spectrum for PyC

Figure 78 shows the Raman spectra for samples A1, A2 and A3. In addition, the reference diamond peak is also shown. For all the samples, the diamond peaks were centered at 1332 cm^{-1}, which characterizes the presence of diamond-sp^3 bonding in the samples. In addition, with all the samples, A1, A2 and A3, a broad shoulder, centered at approximately 1500 cm^{-1}, was observed on the Raman spectra. These broad bands represent the non-diamond carbon phases consisting of carbon-carbon bonding where the bonds are mainly in sp^2 hybridization. Since the position of the Raman diamond peaks are centered at 1332 cm^{-1}, this suggests that the film samples are stress-free.

Generally, freestanding diamond films, which are detached from the substrates, are free from stress. Direct diamond CVD onto PyC, a material analogous to graphite, in terms of microstructure, produces films that display poor coating adhesion [86]. This can be an advantage when considering preparing freestanding diamond films. Generally, freestanding diamond films are prepared by depositing coatings onto weak carbide-forming materials, such as molybdenum and the resultant films are mechanically peeled off from the substrates. Also, freestanding diamond films can be prepared by depositing diamond onto a strong carbide-forming material, such as silicon, and then chemically etching out the substrate material from the film coating. The inset in figure 78 shows the Raman spectrum of un-coated PyC. The two peaks centered at around 1354 and 1600 cm^{-1} represent the D- and G- bands of graphite. This again justifies the likeness of PyC and graphite in terms of microstructure and signals it is difficult to identify the PyC form using conventional Raman spectroscopy.

Table 21 - Details about samples A1, A2 and A3, in terms of film color and film quality

Sample	Film color	Quality factor, Q
A1	light grey	0.30
A2	light grey	0.40
A3	dark grey	0.50

Table 21 gives details about samples A1, A2 and A3, in terms of film color and Raman film quality. The Q values for samples A1, A2 and A3 were calculated to be 0.3, 0.4 and 0.5, respectively. The results show that sample A3 displayed better film quality. It is important to note that the ratio of sp^3 to sp^2 bonding in a diamond-based coating, including DLC, is critical in effecting the blood compatibility of the material [87]. The difference in the quality factor values for the three samples can be attributed to the substrate temperature effect.

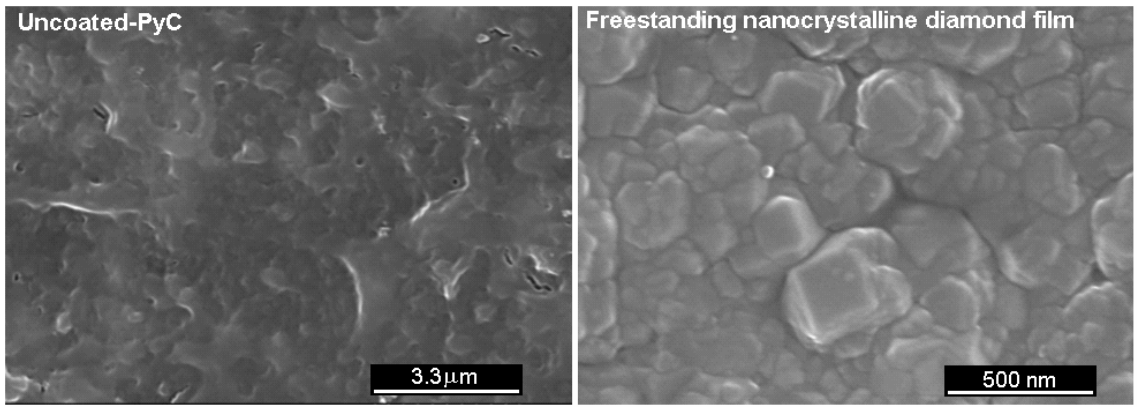

Figure 79 - SEM micrographs for bare PyC and a FSND deposited at 850^0C using the TMCVD process

Figure 79 shows the SEM micrographs for bare PyC-HVD and a FSND deposited at 850ºC using the TMCVD process. The FSND film was very uniform and it was

deposited in the shape of the HVD. The average crystallite size of the FSND sample was approximately 100nm. As stated previously, surface roughness is a crucial parameter. It is possible to control the surface smoothness of the film coating by adjusting, accordingly, the timed CH_4 modulations, this being the distinctive advantage of the TMCVD process over conventional diamond CVD processes employing CH_4 and hydrogen as the process gases.

Much work must be done before FSND can effectively replace PyC disk, namely compare the mechanical and micro-structural properties of the FSND with the PyC material. Although, this preliminary results give good indication on that possibility.

CHAPTER VI

CONCLUSIONS

Polycrystalline diamond films have been deposited onto several types of substrates using manly two processes, known as conventional CVD and TMCVD.

All the results presented seem to be coherent with the proposed model of mechanism for the TMCVD process. Diamond nucleation occurs first in both the TMCVD and conventional CVD processes. However, with the TMCVD process, diamond nucleates more rapidly as a result of high CH_4 pulse at the beginning. The high CH_4 pulse ensures that the diamond grains nucleate quicker to form the first diamond layer. The second stage, where CH_4 content is reduced, the diamond crystals are allowed to grow. This step enables the crystals to grow with columnar growth characteristics. The film surface starts to become rough, as expected. The third stage involves increasing the CH_4 concentration. This enables further secondary nucleation of diamond grains to occur in between the existing diamond crystals, where the surface energy is lower. As a comparison, much less secondary nucleation occurs when the CH_4 flow is kept constant throughout the deposition process.

The distinctive feature of TMCVD is in fact, that it promotes secondary nucleation to occur onto the existing grains in order to fill up surface irregularities. The final stage of the TMCVD process should end with a lower methane concentration. This means hydrogen ions will be present in greater amount in the plasma and these will be responsible for etching the non-diamond phases to produce a good quality diamond film.

It was found that the TMCVD process enabled the production of smoother, harder, and better quality diamond films. The timed-modulations of CH_4 pulses were found to be very effective in producing films that consisted of smaller crystallite size, which may permit one to consider the possibility of depositing nano-scale polycrystalline diamond films, walking through the twenty first century technological trend.

Diamond TMCVD process, as diamond conventional CVD coating, still haves needs of further investigation, in order to fully understand nucleation and growth conditions, opening the possibility to achieve the final optimized deposition conditions to a particular application.

One of the components that need improved investigation is the complete role that hydrogen plays in the deposition chamber. Further work must be done in order to increase the films growth rate, opening new application field.

GLOSSARY

Diamond (C-C)

The cubic high density crystalline form of carbon four fold (tetrahedrally) coordinated, forming a covalent bonded aliphatic pure sp^3 hybridized network. Shows a characteristic Raman peak at 1332 cm^{-1}. [28]

Diamond Films

Thin coatings of single phase, cubic, polycrystalline high density carbon (diamond). Structure is mostly composed of particles of distinct diamond (cubooctahedral) morphology. Films must be identifiable as diamond by both their X-ray (or electron) diffraction pattern and the characteristic Raman frequency at 1332 cm^{-1}. [28]

Diamond Like Carbon (DLC)

A thermodynamically metastable amorphous form of carbon, of interest due to its wide range of applications and relative ease of synthesis. [28]

epitaxy (epitaxial growth)

(Crystallography) the growth of crystals on a crystalline substrate that determines their orientation. [88]

Growth of a layer of one substance on a single crystal of another, such that the crystal structure in the layer is the same as that in the substrate. It is used in making semiconductor devices. [89]

Nanodiamond or Nano crystalline diamond (NCD)

Diamond of particle size considerably less than one micron, often only fifty to hundreds of Angstrom. [28]

REFERENCES

[1] American Museum of Natural History – Diamonds
http://www.amnh.org/exhibitions/diamonds/

[2] Karl E. Spears, John P. Dismukes, “Synthetic diamond: emerging CVD science and technology”, Wiley Inter-Science, 1994

[3] H. Yabuhara, M. Ciappa and W. Fichtner, Microelectronics Releability 41 (2001) 1459-1463

[4] E. V. Koposova, S. E. Myasnikova, V. V. Parshin and S. N. lasov, Diamond and Related Materials, 11 (2002) 1485–1490

[5] P. Bergonzo, A. Brambilla, D. Tromson, C. Mer, B. Guizard, R. D. Marshall and F. Foulon, Nuclear Instruments and Methods in Physics Research A, 476 (2002) 694–700

[6] H. K. Tonshoff, H. Hillmann-Apmann and J. Asche, Diamond and Related Materials, 11 (2002) 736–741

[7] T. Le Huu, M. Schmitt, D. Paulmier, A. G. Mamalis and A. Grabchenko, Wear, 225–229 (1999) 843–847

[8] J. Cifre, M. C. Polo, G. Sinchez, A. Lousa and J. Esteve, Diamond and Related Materials, 4 (1995) 798-801

[9] N. A. Morrison, I. C. Drummond, C. Garth, P. John, D. K. Milne, G. P. Smith, M. G. Jubber and J. I. B. Wilson, Diamond and Related Materials, 5 (1996) 1118-1126

[10] W. Ahmed, H. Sein, N. Ali , J. Gracio and R. Woodwards, Diamond and Related Materials, 12 (2003) 1300–1306

[11] Y. Kousar, N. Ali, V. F. Neto and J. Grácio, Diamond and Related Materials, in press

[12] Charles Kittel and Herbert Kroemer, “Thermal Physics”, W. H. Freeman and Company (1980)

[13] Federick Reif, “Fundamentals of Statistical and Thermal Physics”, McGraw-Hill International Editions, Physics Series (1985)

[14] Ivan V. Markov, “Crystal Growth for Beginners – Fundamentals of Nucleation, Crystal Growth and Epitaxy”, World Scientific (1995)

[15] F. P. Bundy, J. Geophys. Res. 85 (B12) (1980) 6930

[16] Lawrence S. Pan and Don R. Kania, “Diamond: Electronic properties and applications”, Kluwer Academic Publishers, 1995

[17] MRS Bulletin - Diamond Films: Recent Developments, 23-9, September 1998

[18] Luiz Pereira, “Propriedades optoelectrónicas de diamante crescido a partir da fase gasosa” (PhD Thesis), Universidade de Aveiro, 2000

[19] C. Wild, P. Koidl, W. Mfiuer-Sebert, H. Walcher, R. Kohl, N. Herres and R. Locher, R. Samlenski and R. Brenn, Diamond and Related Materials, 2 (1993) 158-168

[20] R. Haubner and B. Lux, Diamond and Related Materials, 2 (1993) 1277-1294

[21] P. Mehta Menon, A. Edwards, C. S. Feigerle, R. W. Shaw, D. W. Coffey, L. Heatherly, R. E. Claisuing, L. Robinson, D. C. Glasgow, Diamond and Related Materials 8 (1999) 101-109

[22] S. Shin, N. M. Hwang, D. Kim, Diamond and Related Materials, 11 (2002) 1337-1343

[23] Qi Hua Fan, “Diamond Growth on Metals” (PhD Thesis), University of Aveiro, 1998

[24] Q. H. Fan, N. Ali, Y. Kousar, W. Ahmed and J. Gracio, J. Mater. Res., Vol. 17, No. 7, Jul 2002

[25] N. Ali, Q. H. Fan, W. Ahmed and J. Gracio, Thin Solid Films 420–421 (2002) 155–160
[26] John E. Field, “The properties of diamond”, Academic Press, 1979
[27] John E. Field, “The properties of natural and synthetic diamond”, Academic Press, 1992
[28] Mark A. Prelas, Galina Popovici and Louis K. Bigelow, “Handbook of industrial diamonds and diamond films”, Marcel Dekker, Inc, 1998
[29] N. Savvides and T. J. Bell, Thin Solid Films, 228 (1993) 289-292
[30] C. V. Cooper and C. P. Beetz, Jr., Surface and Coatings Technology, 47 (1991) 375-387
[31] F. Szuecs, M. Werner, R. S. Sussmann, C. S. J. Picklesand H. J. Fecht, J. Appl. Phys., Vol. 86, No. 11 (1999) 6010-6017
[32] S. Nath and J. I. B Wilson, Diamond and related Materials, 5 (1996) 65
[33] C. Jany, A. Tardieu, A. Gicquel, P. Bergonzo and F. Foulon, Diamond and Related Materials, 9 (2000) 1086
[34] H. W. Xin, Z. M. Zhang, X. Ling, Z. L. Xi, H. S. Shen, Y. B. Dai and Y. Z. Wan, Diamond and related Materials, 11 (2002) 228
[35] H. D. Zhang, G. C. Chen, C. M. Li, W. Z. Tang and F. X. Lu, Surface and Coating Technology, 166 (2003) 101
[36] R. Hessmer, M. Schreck, S. Geier, B. Stritzker, Diamond and Related Materials 2 (1994) 776
[37] A. Ibarra, M. González, R. Vila, J. Mollá, Diamond and Related Material, 6 (1997) 856
[38] Alan T. Collins, Ceramics International, 22 (1996) 321
[39] M. Cannaerts, M. Nesladek ,K. Haenen, L. De Schepper, L. M. Stals and C. Van Haesendonck, Diamond and Related Materials, 11 (2002) 212
[40] T. Sugino, Y. Muto, K. Karasutani and J. S. Kobashi, Diamond and Related Materials, 2 (1993) 803
[41] Ian M. Watt, “The principles and practice of electron microscopy” Cambridge University Press, 1997
[42] M. J. Wilson, “Clay Mineralogy: Spectroscopic and Chemical Determinative Methods”, Chapman & Hall, 1995
[43] Robert W. Cahn, “Concise encyclopedia of materials characterization”, Pergamon Press, 1993
[44] John R. Ferraro, “Introductory Raman spectroscopy”, Academic Press, 1994
[45] Bernhard Schrader, “Infrared and Raman spectroscopy : methods and applications”, VCH, 1995
[46] N. Ali, V. F. Neto, and J. Grácio, Journal Material Research, Vol. 18, No. 2 (2003)
[47] Q. H. Fan, E. Pereira and J. Grácio, Journal of Materials Science, 34 (1999) 1353 – 1365
[48] João Paulo Davim, José Joaquim Grácio, “Tecnologias dos Materiais Metálicos” Universidade Aberta, 1999
[49] L. M. Cadillon, “Propriedades Eléctricas de vidros com alguns iões de Terras Raras” (PhD Thesis), Universidade de Aveiro, 1995
[50] A.K. Jonscher, “Dielectric Relaxation in solids”, Chelsea Dielectric Press, London. 1983
[51] HP Agilent 4285A Precision LCR meter – operation manual, January 2001
[52] Gerhard Schaumburg, Dielectrics Newsletter, Nov. 1997
[53] G. Taguchi, “System of Experimental Design”, Vol. 1 & 2, Unipub-Kraus/ASI, New York/Dearborn, MI, 1988
[54] G. Taguchi, “Introduction to Quality Engineering: Designing Quality into Products and Processes”, Unipub-Kraus/ASI, New York/Dearborn, MI, 1987
[55] R. Unal, E. B. Dean, Annual Conference of the International Society of Parametric Analysts, (1991) 132–141
[56] M. W. Weiser, K. B. Fong, American Ceramic Society Bull. 73 (1994) 83–86

[57] Y. Hayashi, W. Drawl and R. Messier, Japanese J. Applied Physics, Vol. 31 (1992) L194
[58] A. K. Jonscher, Nature, 267 (1977) 673
[59] F. Kremer, Dielectric Newsletter, (1999) 1
[60] C. M. Borges, P. Mange, M. Dent, E. Pfender, D. Ring, J. Heberlein, J. of Prosthetic Dentistry, July 1999, 75
[61] V. J. T. Airoldi, J. R. Moro, E. J. Corat, E. C. Goulart, A. P. Silva and N. F. Leite, Surface Engineering and Technology, 108-109 (1998) 438
[62] H. Sein, W. Ahmed and C. Rego, Diamond and Related Materials, 11 (2002) 731
[63] I. Endler, K. Bartsch, A. Leonhardt, H. J. Scheibe, H. Ziegele, I. Fuchs, Ch. Raatz, Diamond and Related Materials, 8 (1999) 834-839
[64] W. Tang, Q. Wang, S. Wang and F. Lu, Diamond and Related Materials, 10 (2001) 1701
[65] G. Straffelini, P. Scardi, A. Molinari and R. Polini, Wear, 249 (2001) 461
[66] S. Kamiya, H. Takahashi, R. Polini, P. D'Antonio and E. Traversa, Diamond and Related Materials, 10 (2001) 787
[67] R. Haubner, A. Kopf and B. Lux, Diamond and Related Materials, 11 (2002) 556
[68] M. Alam, D. E. Peebles, D. R. Tallant, Thin Solid Films, 300 (1997) 164
[69] M. B. Gusev, V.G. Babaev, V. V. Khvostov, G. M. Lopez Ludena, A. Yu. Brebadze, I. Y. Koyashin, A. E. Alexenko, Diamond and Related Materials, 6 (1997) 89-94
[70] K. Barton, A. Campbell, J. A. Chinn, C. D. Griffin, D. H-Anderson, K. Klein, M. A. Moore and C. Zapanta, Biomedical Engineering Society (BMES) Bulletin, Vol. 25, No. 1 (2001) 3
[71] S. L. Goodman, K. S. Tweden and R. M. Albrecht, J. Biomedical Materials Research, Vol. 32 (1996) 249-258
[72] F. Z. Cui and D. J. Li, Surface and Coatings Technology, 131 (2000) 481-487
[73] J. McLaughlin, B. Meenan, P. Maguire, N. Jamieson, Diamond and Related Materials, 8 (1996) 486-491
[74] M. I. Jones, I. R. McColl, D. M. Grant, K. G. Parker and T. L. Parker, Diamond and Related Materials, 8 (1999) 457-462
[75] A. Thomson, F. G. Law, N. Rushton, J. Franks, Biomaterials, 12 (1) (1991) 37
[76] I. Dion, C. H. Roquey, E. Baudet, B. Basse, N. More, Biomedical Mater. Eng., 3 (1993) 51
[77] P. Yang, N. Huang, Y. X. Leng, J. Y. Chen, H. Sun, J. Wang, F. Chen and P. K. Chu, Surface and Coatings Technology, 156 (2002) 284-288
[78] J. Y. Chen, Y. X. Leng, X. B. Tian, L. P. Wang, N. Huang, P. K. Chu an P. Yang, Biomaterials, 23 (2002) 2545-2552
[79] Y. X. Leng, H. Sun, P. Yang, J. Y. Chen, J. Wang, G. J. Wan, N. Huang, X. B. Tian, L. P. Wang and P. K. Chu, Thin Solid Films, 398-399 (2001) 471-475
[80] Y. X. Leng, P. Yang, J. Y. Chen, H. Sun, J. Wang, G. J. Wang, N. Huang, X. B. Tian and P. K. Chu, Surface and Coatings Technology, 138 (2001) 296-300
[81] J. Li, Biomaterials, 14 (1993) 229
[82] C. L. Fan, D. Ciardullo, J. Paladino and W. Huebner, Journal Material Res., 17 (6) (2002) 1520
[83] Y. G. Yan, S. R. Chaudhuri and A. Sarkar, Journal American Ceramic Soc., 79(4) (1996) 1061
[84] J. Yang, S. Mei, J. M. F. Ferreira, Journal European Ceramic Soc., in press
[85] C. J. Brinker, and G. W. Scherer, Sol-Gel Science: The Physics and Chemistry of Sol-Gel Processing, Academic Press, San Diego, CA, 1990
[86] M. N. Ashfold, P. W. May, C. A. Rego and N. M. Everitt, Chemical Society Reviews, (1994) 23
[87] J. Y. Chen, L. P. Wang, K. Y. Fu, N. Huang, Y. Leng, Y. X. Leng, P. Yang, J. Wang, G. J. Wan, H. Sun, X. B. Tian and P. K. Chu, Surface and Coatings Technology, 156 (2002) 289

[88] The Concise Oxford Dictionary. Ed. Judy Pearsall. Oxford University Press, 2001. Oxford Reference Online. Oxford University Press (http://www.oxfordreference.com)
[89] A Dictionary of Physics. Ed. Alan Isaacs. Oxford University Press, 2000. Oxford Reference Online. Oxford University Press (http://www.oxfordreference.com)